INVESTIGATION OF THE TIP CLEARANCE FLOW INSIDE AND AT THE EXIT OF A COMPRESSOR ROTOR PASSAGE

A. PANDYA AND B. LAKSHMINARAYANA

NASA GRANT NSG 3212
NATIONAL AERONAUTICS & SPACE ADMINISTRATION
LEWIS RESEARCH CENTER

TURBOMACHINERY LABORATORY
DEPARTMENT OF AEROSPACE ENGINEERING
THE PENNSYLVANIA STATE UNIVERSITY
UNIVERSITY PARK, PA 16802

MAY 1982

INVESTIGATION OF THE TIP CLEARANCE FLOW INSIDE AND AT THE EXIT OF A COMPRESSOR ROTOR PASSAGE

A. Pandya and B. Lakshminarayana

NASA Grant NSG 3212

National Aeronautics & Space Administration

Lewis Research Center

Turbomachinery Laboratory
Department of Aerospace Engineering
The Pennsylvania State University
University Park, PA 16802

May 1982

ABSTRACT

This thesis reports an experimental study of the nature of the tip clearance flow in a moderately loaded compressor rotor. Unlike previous studies related to the tip leakage flow, the measurements reported here were taken inside the clearance between the annulus-wall casing and the rotor blade tip. These measurements were obtained using a stationary two-sensor hot-wire probe in combination with an ensemble averaging technique. The flowfield was surveyed at various radial locations and at ten axial locations, four of which were inside the blade passage in the clearance region and the remaining six outside the passage. Variations of the mean flow properties in the tangential and the radial directions at various axial locations were derived from the data. Variation of the leakage velocity at different axial stations and the annulus-wall boundary layer profiles from passage-averaged mean velocities were also estimated. Turbulence intensity profiles at the locations identical to those for the mean flow properties estimation were also derived from the data. The experiments were repeated at a different flow coefficient and reduced rotational speed in order to study the effect of the rotor speed and the blade loading on the leakage flow. The results indicate that there exists a region of strong interaction of the leakage flow with the annulus-wall boundary layer at the half-chord location. The turbulence intensity profiles indicate that the leakage flow travels up to half the blade passage before rolling up at the design condition. The rotor exit flow is found to be uniform beyond 3/4 blade chord downstream of the rotor trailing edge at the design condition.

The leakage flow velocity at the off-design condition is lower than that at the design condition. The former is caused by reduced rotor speed and reduced blade l oading. A fairly regular behavior of the flow at the half-chord locati on is observed. Also, the lower leakage velocity does not destroy the wake structure completely as observed in the velocity profiles at the design condition. A characteristic wake profile is observed even at 60 percent chord downstream of the rotor trailing edge.

TABLE OF CONTENTS

TABLE OF CONTENTS (Continued)

LIST OF TABLES

LIST OF FIGURES

LIST OF FIGURES (Continued)

LIST OF FIGURES (Continued)

LIST OF FIGURES (Continued)

LIST OF FIGURES (Continued)

NOMENCLATURE

C_{L_o}	Camber expressed as design lift coefficient of an isolated air foil
C_p	Pressure coefficient
L.E.	Leading edge
P.S.	Pressure surface
R	Radius ratio (r/r_{tip}), R = 1 at tip, R = 0.5 at hub
$\overline{R}$	Distance from the annulus wall in the radial direction normalized by clearance at the L.E.
$\overline{r}$	Distance from the annulus wall normalized by (i) clearance at L.E. for rotor inlet flow, (ii) local clearance for flow inside the passage, and (iii) clearance at T.E. for rotor exit flow
S	Blade spacing
S.S.	Suction surface
T	Turbulence intensity, normalized by local maximum mean total velocity $[\overline{(w^2)}/(W_z^2 + V_\theta^2)_{max}]^{1/2}$
T.E.	Trailing edge
$\overline{T}$	Passage averaged turbulence intensity normalized by local maximum mean total velocity
U	Rotational velocity Ω x radius
V	Mean velocity in stationary frame of reference
$\overline{V}$	Passage averaged velocity in stationary frame of reference
W'	Total velocity in relative frame of reference (W' = W + w)
W	Mean velocity in relative frame of reference
w	Fluctuations in the velocity about the mean velocity
$\overline{W}$	Velocity in relative frame of reference normalized by U_{tip}
W_N	Leakage velocity, normalized by U_{tip}

W_{N_o} W_N at the inlet of the rotor normalized by U_{tip}

$\bar{Y}$ Distance from the fixed line 0.0 in the tangential direction normalized by the blade spacing (Figure 2.9)

z Axial coordinate direction corresponding to the axis of the compressor

Z Axial distance from the rotor blade leading edge normalized by the axial chord (Figure 2.9)

β Relative flow angle

Ω Rotational speed r.p.m.

θ Tangential direction

ϕ Mass averaged flow coefficient

ρ Fluid density

τ Distance from the annulus wall in radial direction

$\bar{\eta}$ Rotor efficiency (Euler) = $\bar{\psi}/\bar{\psi}_{Euler}$

$\bar{\psi}$ Mass averaged stagnation pressure rise coefficient incident normalized by $1/2\ \rho\ U^2_{tip}$

Subscripts

max,MAX Maximum value in the passage

tip Value at the tip of the rotor blade

z Value in axial direction

θ Value in tangential direction

r Value in radial direction

wz Value sensed by the wire in the direction normal to z

ACKNOWLEDGEMENTS

This work was supported by the National Aeronautics and Space Administration through contract No. NSG3212, with P. M. Sockol as the Project Monitor.

The authors wish to thank J. Fett olf and G. Kane for their aid in experimental set-up and instrumentation. The help from J. Portelli in analog to digital conversion of the signal was invaluable.

CHAPTER I

INTRODUCTION

1.1 Problem Relevance

The design of energy efficient engines has received considerable attention in recent years. Important gains in efficiency can be made by minimizing the aerodynamic losses in various components of the engine, especially in the compressor rotor which is one of the least efficient components in the engine. Even marginal gains in efficiency through reduction of these losses could substantially reduce the fuel requirement for the engine. It is well-known that the end-wall flow losses comprise a substantial proportion of the total losses, and a significant fraction of the end-wall losses is attributed to the tip leakage flow and its interaction with the secondary flow, blade boundary layer, annulus-wall boundary layer and the scraping vortex. Further improvements in design, performance and prediction of the flowfield in this region demand a better understanding of the complex flow structure which results from these interactions in the vicinity of the annulus-wall.

Experimental investigations related to the tip leakage flow have been limited to flowfield measurements in straight cascades with tip clearance [1,2,3]. These studies, however, do not yield any information regarding the effect of rotation and curvature on the tip leakage flow. On the other hand, flow visualization experiments [4,5,6] provide only qualitative information regarding the flow. There have also been attempts to derive some information on leakage flow indirectly via flowfield measurements downstream of the rotor [7,8] and inside

the passage near the tip region [9,10]. Due to limitations imposed by measurement techniques, no measurements were made in these studies beyond 96 percent of the blade span and inside the clearance region. Thus, the need to study the flow in close proximity of the annulus-wall and inside the tip clearance region becomes evident.

1.2 Objectives and Scope of the Investigation

The present investigation was carried out with the following objectives:

(1) To measure the flow in the tip clearance region of a compressor rotor with special emphasis on the leakage flow development in the tip clearance region and at the exit of the rotor. Figure 1.1 shows the region of flowfield measurements. (This figure also shows the region of measurement reported in references [9,10]).

(2) To develop a technique to measure the flowfield in the clearance region with a two-sensor hot-wire probe.

(3) To obtain the mean properties and the turbulence properties of the flowfield in this region.

(4) To understand the effect of rotation and blade loading on the leakage flow development and decay in the end-wall region.

It is important to note that with a two-sensor hot-wire probe, only the axial and the tangential components of the flowfield properties are obtained. Near the end-wall the streamlines are expected to be almost parallel to the wall, and hence the radial velocity should be very small. But the turbulence intensity in the radial direction would introduce an error in the calculation of the axial and turbulence

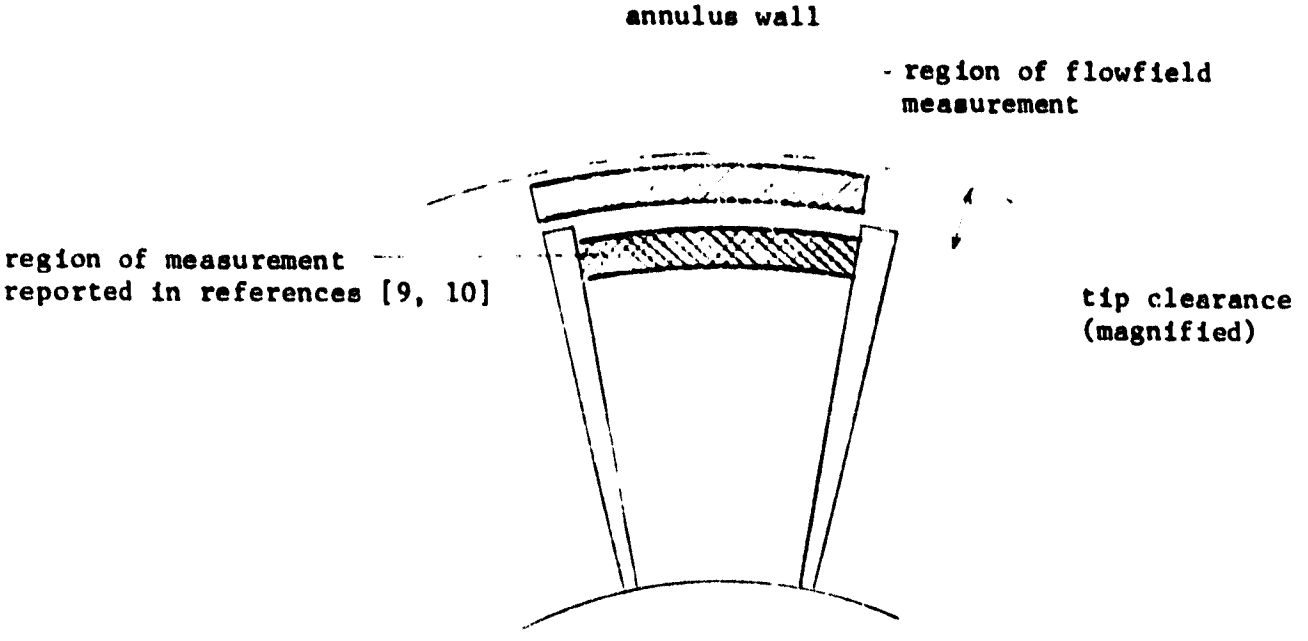

Figure 1.1 Schematic of the End-Wall Region in Compressor Rotor

intensities.* Therefore, the turbulence intensities reported in this thesis should be considered only qualitative in nature. However, in view of the fact that no flowfield measurements are available in this region, the levels of the turbulence intensities (though not the actual magnitude reported in the thesis) do provide important information regarding the nature of interaction among the various flow structures present in the annulus-wall region.

1.3 Previous Related Work

The flow which passes through the clearance area between the blade tip and the annulus wall is termed the tip leakage flow. One of the factors causing the tip leakage flow is the direct flow through the clearance space which remains undeflected by the blading and therefore is not available for doing work. Its magnitude depends upon the clearance height and the thickness and the profile of the annulus wall boundary layer. The second factor contributing to the tip leakage flow is the indirect flow due to the pressure difference between suction and pressure surfaces.

The interaction of the tip leakage flow and the main flow in the blade passage has prompted many investigators to study its effect on the pressure diatribution, induced drag, outlet angles and separation on the blade surfaces. An intensive survey of the available literature has been carried out by Lakshminarayana and Horlock [11] and by Reeder [12]. A brief account of the important studies in this field is presented in the following two subsections.

---

*Discussion on the error involved in the present investigation is included in Appendix A.

1.3.1 Analytical Investigations

The tip clearance flow model developed by Rains [13] estimates the leakage flow velocity. This model is based on the assumption that the leakage flow, resulting from the pressure difference over the rotor, occurs in an annulus of height equal to the clearance height. However, this analysis does not take into account the perturbation in the flow at various spanwise locations and clearance to chord ratio. Vavra [14] uses Rains' analysis. To estimate the drag coefficient due to clearance, Vavra assumes the loss to be equal to the flux of kinetic energy associated with the leakage flow normal to the blade and uses the fact that the pressure distribution about a compressor blade is approximately triangular in shape.

For a perfect fluid the flow through a tip clearance can be considered equivalent to the flow through a slotted wing with the wall represented by the plane of symmetry through the slot. The flow through a slotted wing has been studied by many investigators with the assumption of the lifting line theory where the circulation is shed from the trailing edge as it drops to zero at the edges of the slot. Betz [15] has calculated the minimum induced drag of a cascade of lifting lines with tip clearance. This analysis, however, is applicable only to fans where the tip clearance is large and the blade aspect ratio is high.

Based upon the theory developed by Betz, a modified lifting line approach has been proposed by Lakshminarayana [3]. This model assumes that the lift is uniform all along the span of the blade and only part of the bound vortex at the tip is shed off. The blade

pressure distributions and the induced drag predicted from this model agree with his measurements. A more realistic flow model is presented in the same study where the effect of solid body rotation in the viscous core of the leakage vortex is considered.

Wu and Wu [16] carried out an order of magnitude analysis which reduces the basic equations to a set of simplified equations for both low and high Reynolds number. The analysis is based on a steady relative flow of a viscous incompressible fluid. Expressions for determination of the distributions of pressure and velocity in the clearance space and the mass flow across the tip clearance space were determined.

A pressure balancing model is described by Niida et al. [17] for estimating the flow rate through the clearance in an annular sector. A parameter--effective blade thickness--is introduced to account for the shape of the tip of the blade. This analysis for viscous fluid flows assumes that the flow is two-dimensional. Couette-Poiseuille flow velocity distribution is assumed in the annulus sector.

1.3.2 Experimental Investigations

The experimental investigations related to the tip leakage flow fall under the following categories:

(1) Flowfield measurements in straight cascades

(2) Measurements with a single isolated blade

(3) Flow visualization studies

(4) Efficiency measurements on the compressor as a function of tip clearance

(5) Flowfield measurements outside the clearance region

Flowfield measurements in straight cascades with tip clearance have been reported by Dean [1], Lakshminarayana and Horlock [2] and Lakshminarayana [3]. As mentioned earlier, it is not possible to get any information regarding the effect of rotation from these cascade tests. Rotation has an appreciable influence on the magnitude of the leakage flow.

In the experimental study by Gearhart [18] a single blade with an endless belt to simulate the moving-wall effect was used. Boyce et al. [19] have used a single blade and a rotating disk to study the flow in the clearance region with several kinds of casing treatments. The flow was visualized by injecting globules of neutral density in the flow. The globules were a mixture of dibutyl-phthalate and kerosine colored black for better visualization. Streamline patterns were obtained from the movies taken at a very high speed. Qualitative results from the flow visualization indicate the following:

(1) The flow near the wall is mainly in the tangential direction.

(2) The radial velocity is of an order of magnitude smaller than the tangential velocity.

(3) The flow is essentially laminar.

In the flow visualization study reported by Booth et al. [5], a water-table cascade with die injection was used to visualize the flow. The velocity and the direction of the leakage flow were determined from the high speed photographs of the movement of dye clusters. The experimental observations suggested the following:

(1) The leakage flow stream tubes appeared to be straight.

(2) Application of the Bernaulli equation seemed to predict the local leakage velocity well.

(3) The flow angles observed could be closely predicted (assuming the conservation of the tangential velocity).

Based on the above observations, Booth et al. have suggested a simple leakage flow model similar to the model developed by Rains [13]. The leakage flow velocities calculated using this model agree well with the experiments except at the leading edge and the trailing edge where 3-D effects are greatest.

Several authors have reported efficiency measurements on compressors as a function of tip clearance. Fickert [21] reported that the peak efficiency dropped 3 percent when the radial clearance was increased from .020 inches to .040 inches.

Lakshminarayana et al. [9,10] have reported the flowfield measurements inside the rotor passage as shown in Figure 1.1. Even though these studies do not provide information regarding the leakage flow inside the clearance region, they are extremely valuable in understanding the nature of interaction of the tip leakage flow as it moves radially downwards after leaving the clearance passage with the main flow.

CHAPTER II

EXPERIMENTAL SET-UP, INSTRUMENTATION AND PROCEDURE

The primary objective of the experimental program was to obtain information about the leakage flow inside the clearance region and the rotor inlet and exit flows in the end-wall region. The experiments were conducted on the axial flow compressor facility located in the turbomachinery laboratory at The Pennsylvania State University. The following sections include the relevant information about the compressor facility, instrumentation and the experimental procedure.

2.1 Axial Flow Compressor Facility

A detailed description of the compressor facility with data transmission system for relative flow measurements in the rotor blade passage is given by Lakshminarayana [20]. A brief description of the facility and its operating characteristics are included in this section.

Figure 2.1 shows the compressor facility. The figure does not show the 3m x 1.5m x 3m wire-mesh enclosure coated with 3.1mm thick foam which provides dust free entry of the flow to the aerodynamically designed inlet. The nose-cone and the inlet are followed by inlet guide vane which consists of 43 blades.

The rotor consisting of 21 blades is designed by Smith [21] and is followed by the stator row with 25 blades. The rotor is driven by a 37.29 kw (50 h.p.) variable speed motor through a belt and pulley system. The motor is driven by an eddy current drive and "Dynamic Adjusto Speed" control system. The speed of the motor can be varied from 175 to 1695 r.p.m. with accurate and precise control.

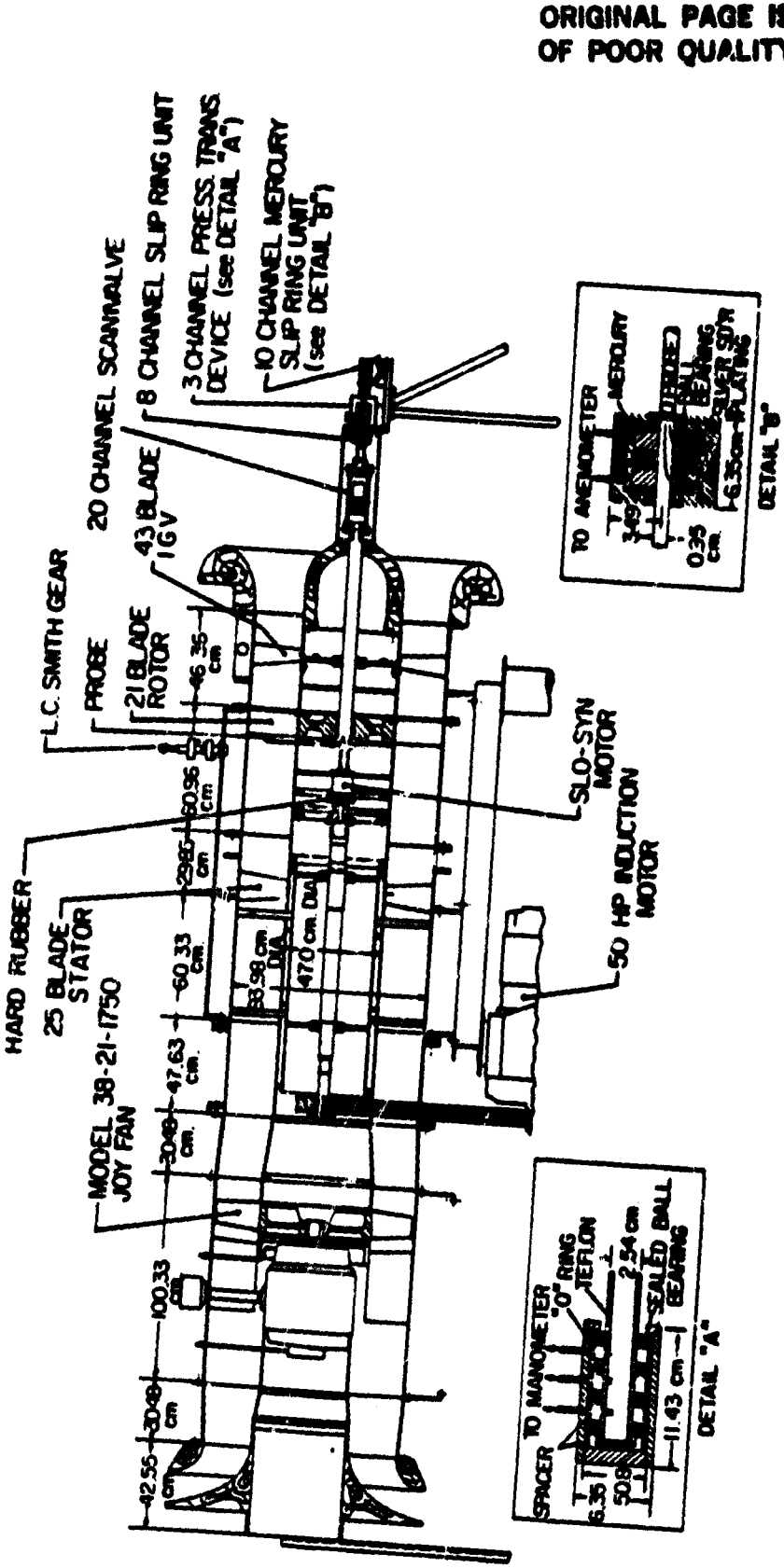

Figure 2.1 PSU Axial-Flow Compressor Facility and Data Transmission Systems

An axial flow fan which enables the operation of the compressor at different flow coefficients follows the drive system. At the rear end of the facility, an aerodynamically designed throttle, which is lined with noise attenuating lining, provides an additional control over the stage operating characteristics.

Table 2.1 lists some of the important parameters of the compressor facility. Good peak efficiencies are exhibited by the rotor. The performance curve of the compressor is given in Figure 2.7. Figures 2.3 and 2.4 show the distribution of static pressure on the blade surface at $\phi = 0.55$ and $\phi = 0.60$, respectively. These measurements were made by N. Sitaram. The characteristics of the flow entering the compressor rotor are shown in Figure 2.5. It shows the mean velocity and the turbulence intensity profiles upstream of the rotor.

The casing of the compressor rotor has a 25cm x 15cm lucite window. Besides providing an easy access to the rotor blades and the hub for relative flow measurement instrumentation, it has provision for measurements with a stationary probe. It has holes at specific axial locations for inserting the probe into the flow. On two of its sides, aluminum guides on which the probe traversing mechanism can slide are provided. The probe traversing mechanism is described in the next section.

2.2 Probe Traversing Mechanism

Figure 2.6b shows the probe traversing mechanism used in these experiments. It is a simple mechanical device with a traverse accuracy of 1/1000 inch. It consists of a steel block which has provision to hold probes of various diameters. This block can slide

Table 2.1

Important Parameters of the Compressor Facility

Rotor	
Hub/tip ratio	0.5
Outer diameter of the rotor	0.9398 m
Rotor Blade Element at the Tip (Modified NASA 65 Series)	
Chord	15.41 cms
Spacing	14.12 cms
Thickness t/c	0.051
Stagger angle	45.0°
C_{Lo}	1.32
Blade inlet angle	63.6°
Air inlet angle	57.2°
Blade outlet angle	42.0
Air outlet angle	51.4
Rotor Drive Motor	
Power	37.3 kw (50 h.p.)
R.P.M.	175-1095
Auxiliary Fan	
Diameter	0.9562 m
Maximum pressure rise	12.7 cms of H_2O at 18 m^3/sec (38,000 cfm) volume flow rate

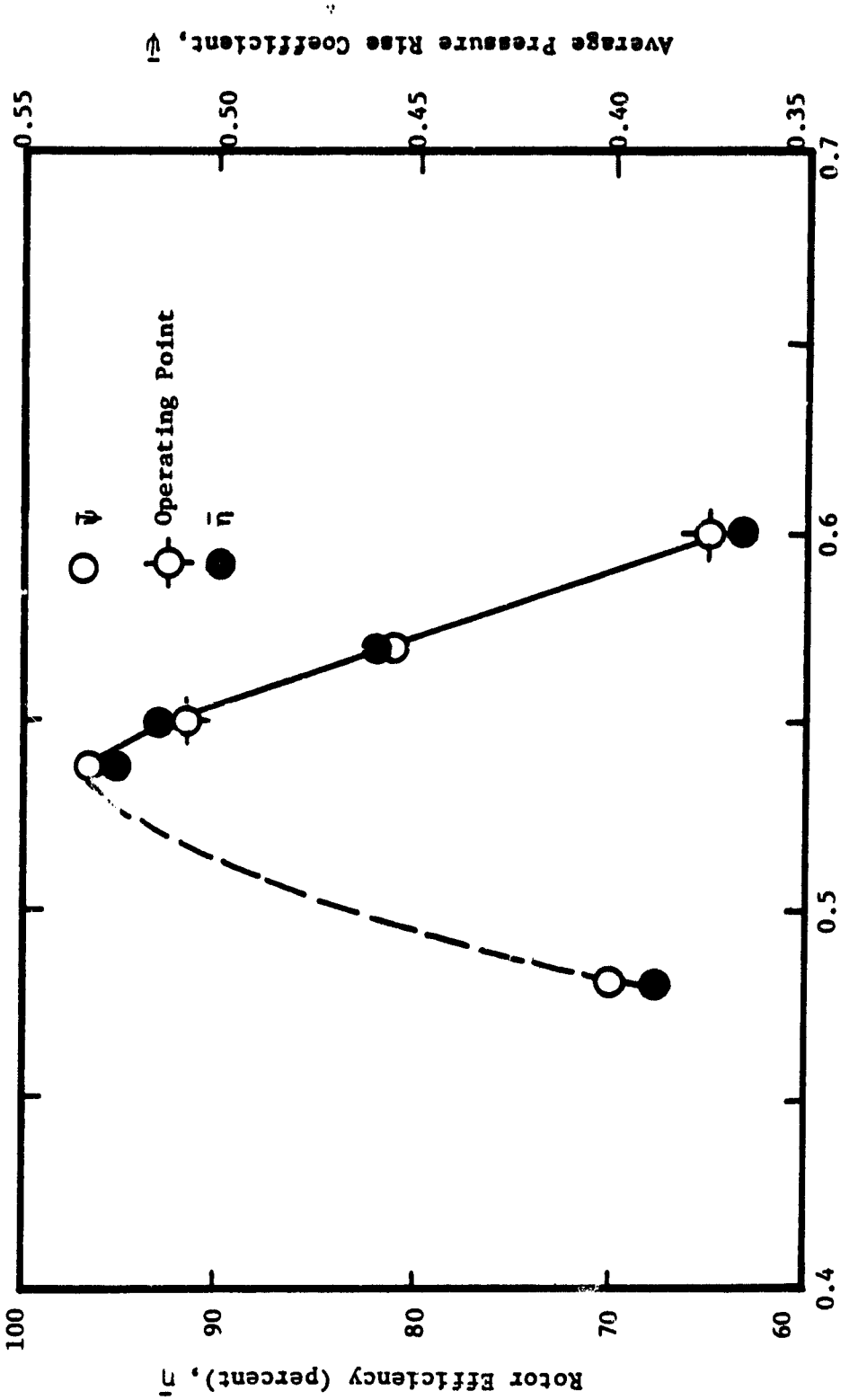

Figure 2.2 Performance Curve of the PSU Axial-Flow Compressor

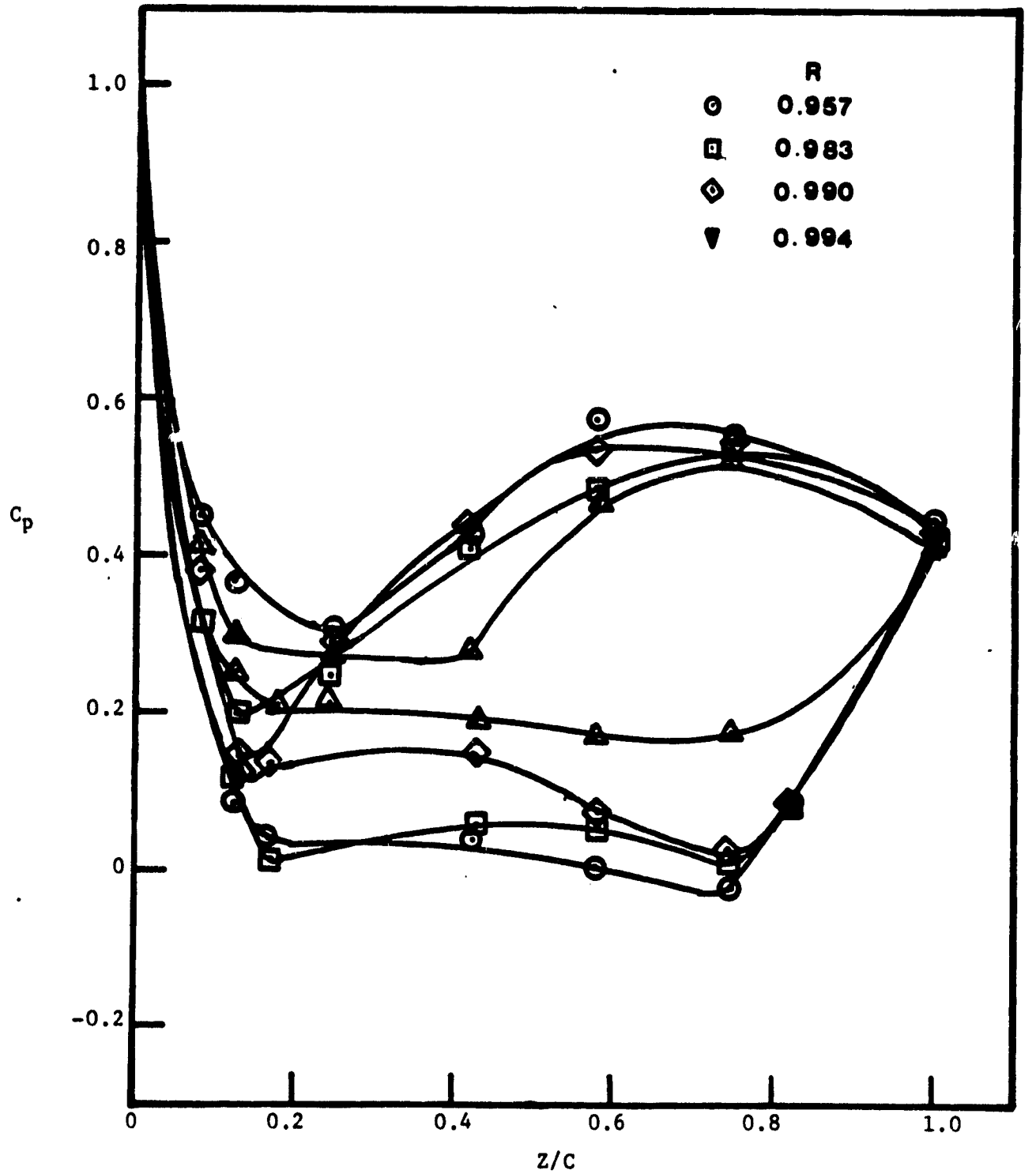

Figure 2.3 Static Pressure Distribution on the Blade Surface at $\phi = 0.55$

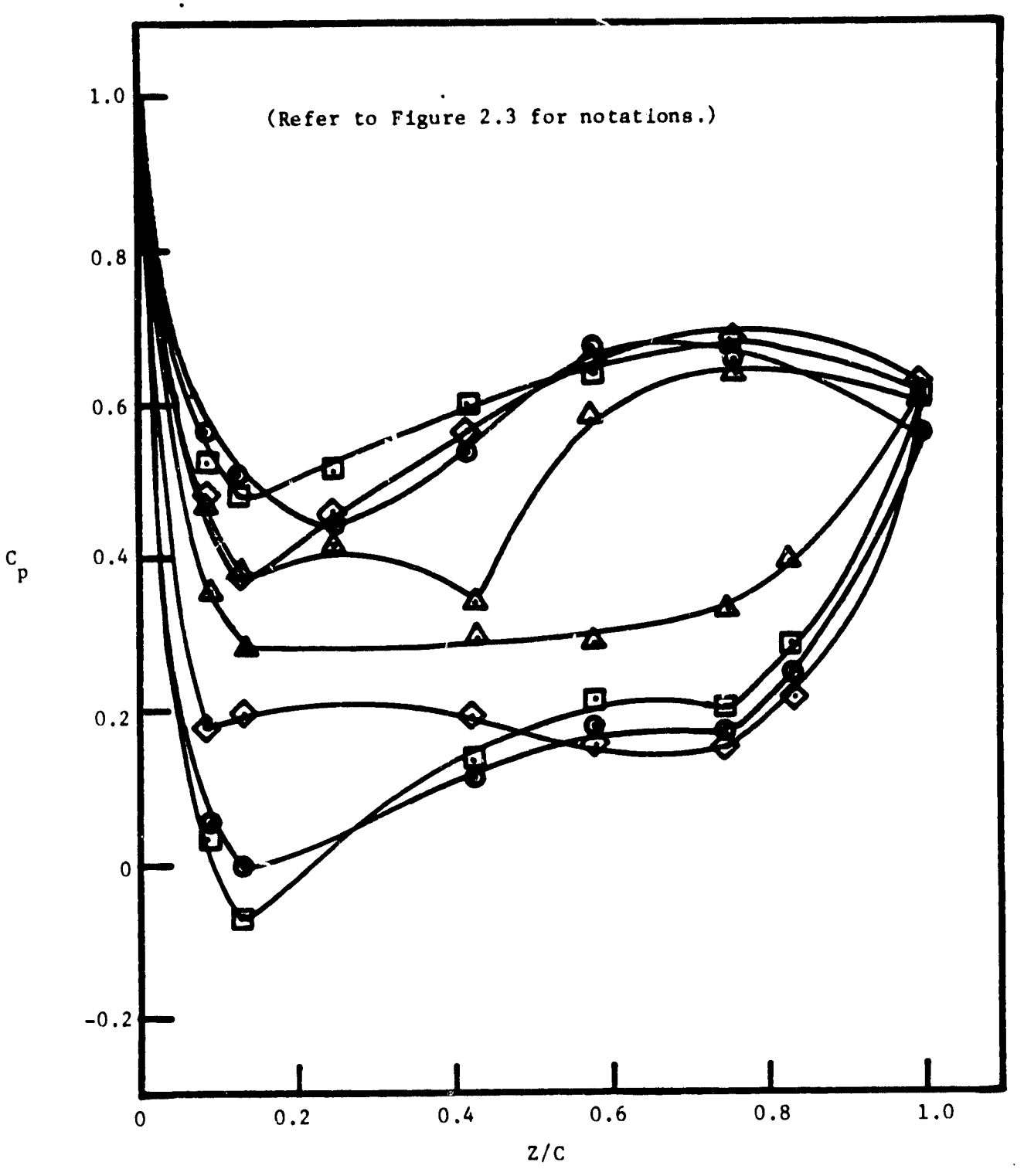

Figure 2.4 Static Pressure Distribution on the Blade Surface at $\phi = 0.60$

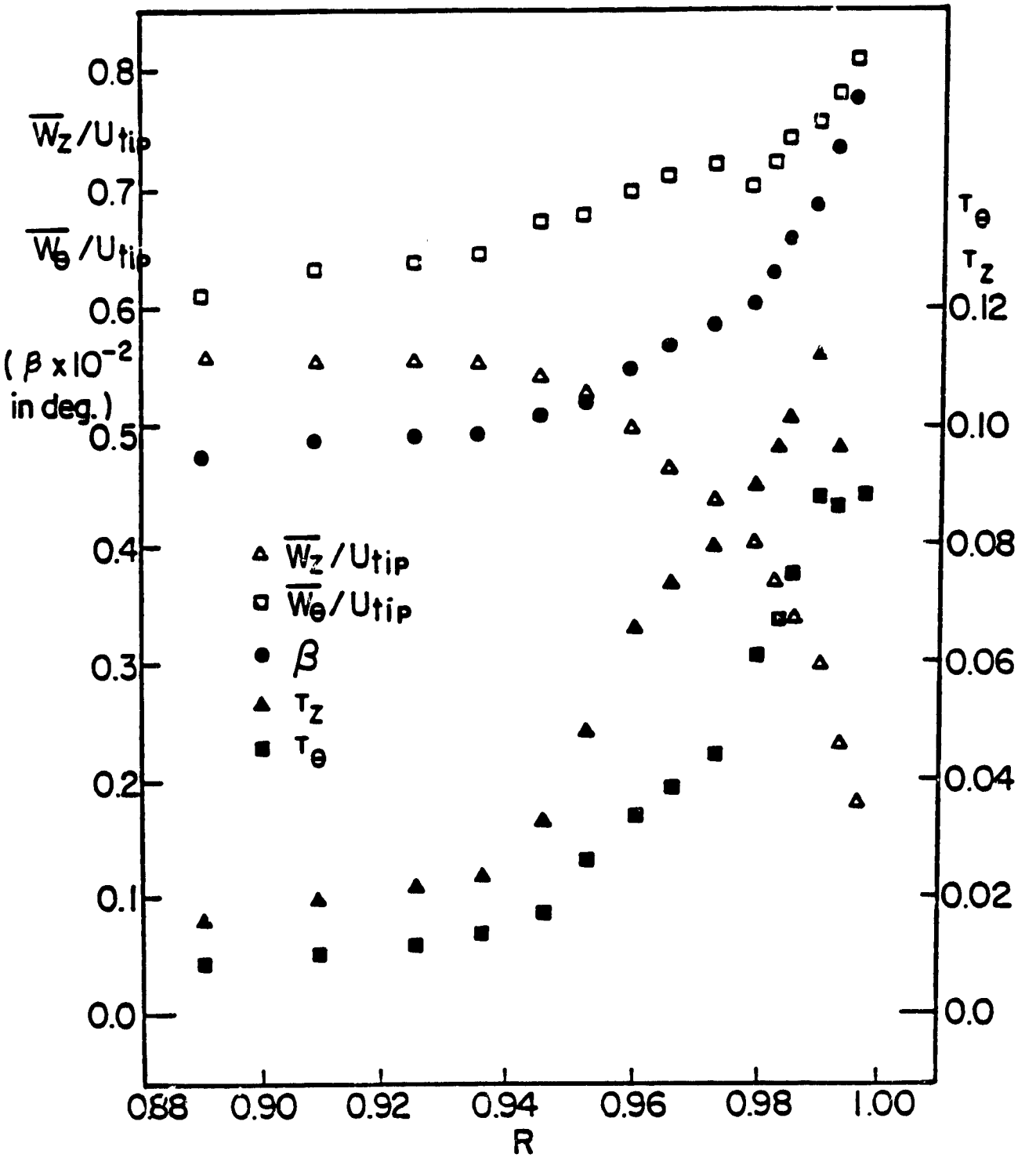

Figure 2.5 Inlet Velocity and Turbulence Profiles in the Tip Region Upstream of the Rotor (Z = -0.35)

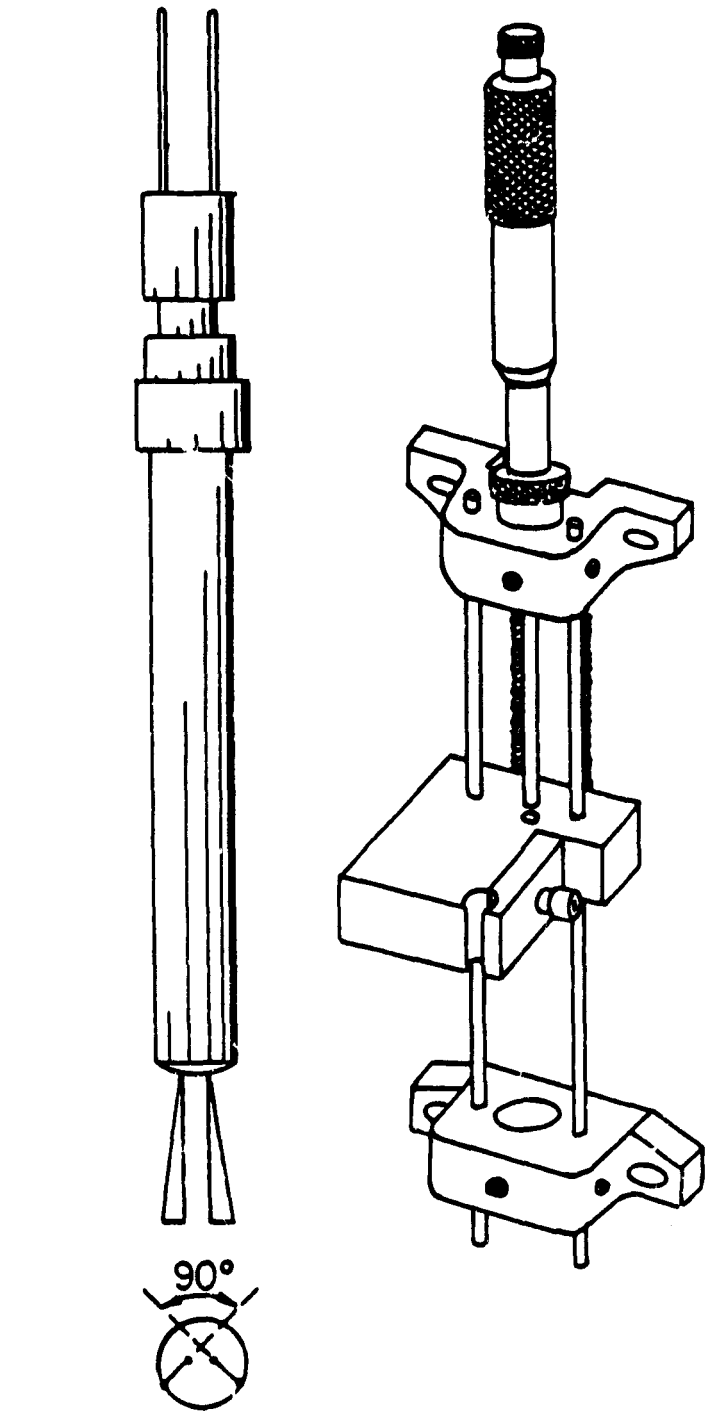

Figure 2.6 Two Sensor Hot Wire Probe and Probe Traverse Mechanism

on two metal bars attached to the frame of the traversing device. A micrometer is also attached to the frame. It holds one end of a 1/8 inch diameter metal rod, the other end of which touches the block which holds the probe. A downward movement of the micrometer pushes the probe downward by the same amount. Two springs which connect the probe holding block to the frame cause the upward movement of the probe when the micrometer is moved upwards.

2.3 Clearance Measurements

2.3.1 Instrumentation

Flowfield measurements in the clearance region using a hot-wire probe require very accurate measurement of the clearance (accuracy of the order of $\pm$ 1/1000 inch) so that the probe placed in the clearance is not damaged by the rotating blades. Besides accuracy, another important requirement of the clearance measuring instrument is a high frequency response. This requirement arises from the need to measure the clearance between the blade tip and the casing when the rotor is rotating at a very high speed (approximately 1100 r.p.m.).

A Fotonic sensor satisfies both these requirements. Besides having the required accuracy, it has a constant frequency response up to 45 kHz. The details of the fotonic sensor are included in Appendix B.

In static clearance measurements, the d.c. signal was measured by an HP model timer counter digital voltmeter with an accuracy of 1 millivolt. For dynamic measurements, a four channel Tektronix type RM561A oscilloscope displayed the instantaneous output from the fotonic sensor and tachometer pulse.

The traversing mechanism described in the previous section along with a proble holder was used to traverse the probe in the radial direction.

2.3.2 Procedure and Technique

The Fotonic sensor is very sensitive to the finish of the surface from which the distance is measured. Since it was not possible to polish the tips of all the 21 blades exactly to the same level, static and dynamic clearance measurements were carried out for one blade at a time, and for each blade, the calibration was carried out afresh.

The blade tip was polished so that 2 volts d.c. signal was obtained at the peak setting. The probe was made flush with the inner surface of the window. This was done by placing a piece of aluminum plate having the same curvature as the inner surface of the window under the hole and moving the sensor inside the hole till it touched the aluminum plate. After removing the plate, the probe was moved till it touched the blade tip. (This was indicated by zero output from the probe.) The difference between the two settings gave the static clearance.

For dynamic clearance measurement, the probe was positioned so that it was approximately in the middle of the linear sensing range. The output signal was observed on the oscilloscope when the compressor was running at the design conditions. The peak voltage was observed to remain constant which indicated that there was no appreciable difference between the static and the dynamic clearance. This process was repeated for four blades, and in all the four cases,

there was no difference between the static and the dynamic clearances. Hence, only static clearance was measured for the remaining blades.

2.4 Flowfield Measurements

Flowfield measurements inside the clearance region and the rotor exit flow measurements in the end-wall region were carried out using a stationary probe. The stationary probe technique adopted for the present investigation was originally developed by Poncet and Lakshminarayana [22] for the study of three-dimensional nature of rotor wakes. This section includes the discussion on the instrumentation and experimental procedure.

2.4.1 Two-Sensor Hot-Wire Probe

The choice of the probe suitable for the flowfield measurements in the clearance region was severely limited by the clearance height. Figure 2.6a shows the two-sensor hot-wire probe specially designed for these experiments. Unlike the conventional two-sensor hot-wire probe (x configuration) both the sensors are in the same plane in a "V" configuration. The probe sensors were made from copper coated tungsten wire. In order to reduce the probe interference effects on sensors, only the middle third of each wire was etched with nitric acid to expose the tungsten wire to the flow. The length to diameter ratio for the sensors was 300.

For all the measurements reported here, the probe was introduced in the flowfield through the holes made at several axial locations on the lucite window. Care was taken to avoid a sudden step (and thereby generation of eddies) at the location where the probe was introduced.

As shown in Figure 2.7, the probe with 6-inch-long holder was encased in a hollow tube, and the cavity between the prongs and the tube was filled with Silastic 732RTV adhesive/sealant which on drying provided a smooth surface flush with the inside wall of the casing. A small gap around the prongs allowed the movement of the probe inside the tube.

The distance of the sensors from the edge of the tube was adjusted to .05 inch very accurately under the microscope with the help of a calibrated eyepiece, and the setscrew on the tube was tightened.

The sensors were calibrated separately using a low turbulence open jet calibration tunnel.

2.4.2 Data Acquisition System

Figure 2.8 shows the schematic of the instrumentation for hot wire measurements.

The sensors were connected to two DISA 55M10 constant temperature anemometer units. The d.c. components of the anemometer signals were measured with an integral digital voltmeter. The fluctuating components of these signals were amplified and recorded with SAVRE IV FM signal recorder/reproducer at the tape speed of 15 i.p.s.

The r.p.m. of the rotor was monitored by a photocell circuit which used a 60 slot calibrated disk mounted on the rotor shaft. The output of the photocell circuit was displayed on a digital counter. The photocell circuit also provided one sharp pulse for each revolution of the rotor. This pulse was also recorded along with the a.c. signals to identify a specific blade passage.

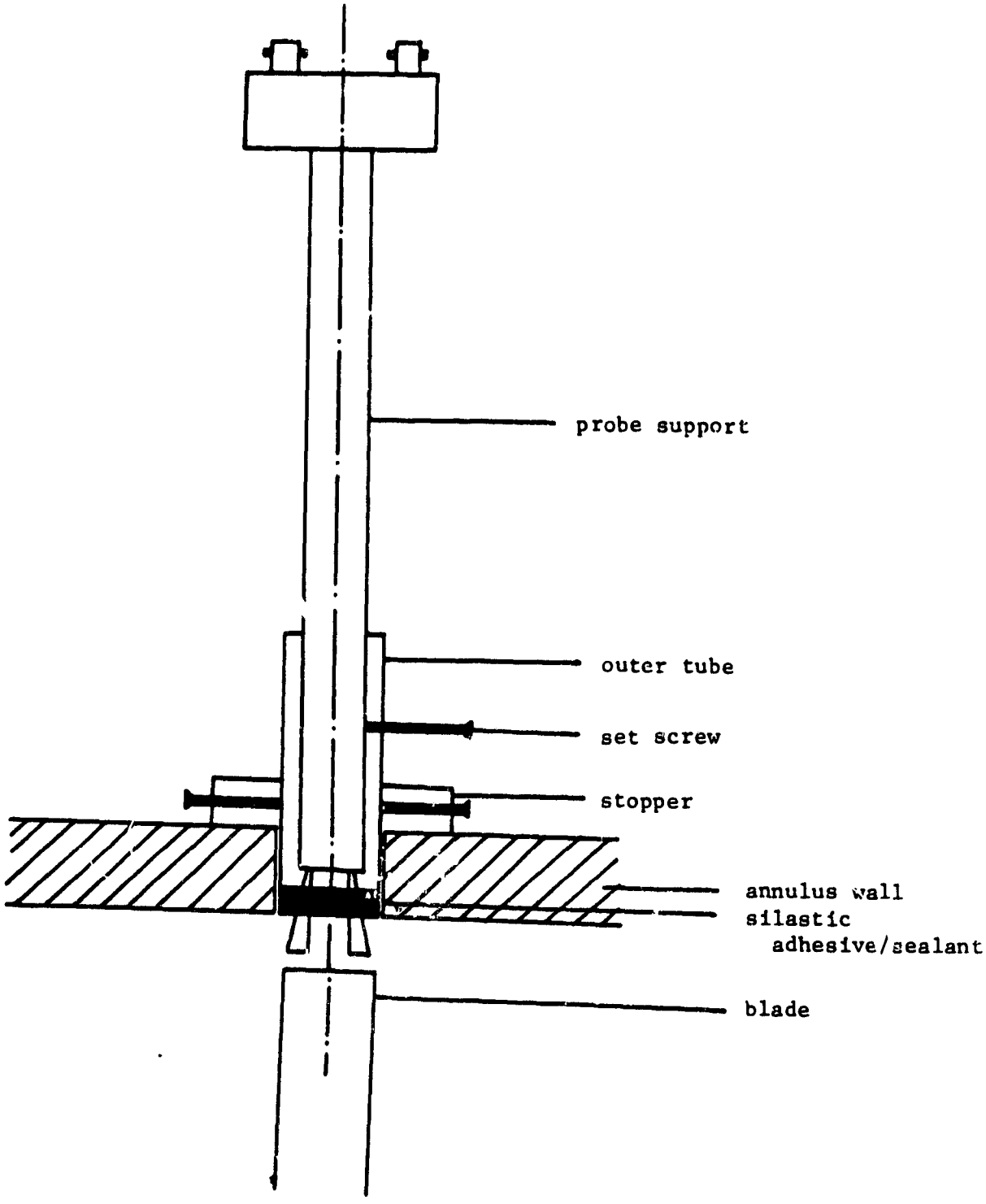

Figure 2.7 Schematic of the Flow Field Measurement Technique

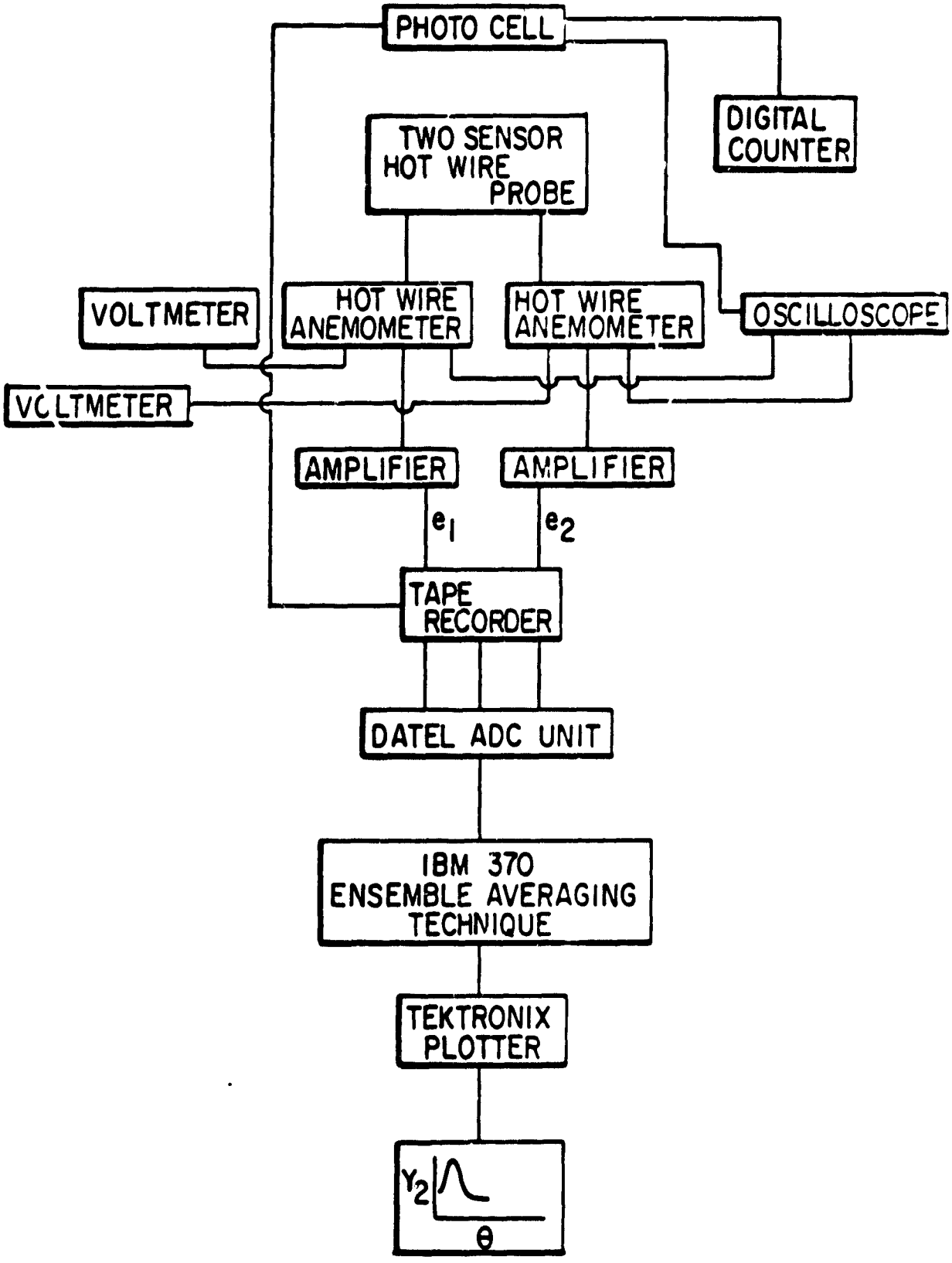

Figure 2.8 Schematic of the Instrumentation for Hot Wire Measurements

The instantaneous signals from the anemometer and the pulse were displayed on a Tektronix type '. 561A storage oscilloscope.

2.4.3 Procedure

Measurements were taken at five axial locations for tip leakage flow and four locations for rotor exit flow. Rotor inlet flow was measured at one location, 1/2 inch upstream of the leading edge. The axial and the radial locations at which the measurements were taken are listed in Table 2.2. Figure 2.9 also shows these locations.

During leakage flow measurements for a given axial location, the probe was traversed as near the blade as possible (0.020 inch away from the blade tip with minimum clearance) without damaging the probe. The probe was traversed at the interval of .005 inch away from the blade tip. The same procedure was repeated for the measurements at the off-design conditions.

For the rotor exit flow measurements, in the region away from the wall where measurements were taken by Davino [23], the probe was traversed at the interval of .025 inch. In the region very near the wall, the probe was traversed at the interval of .010 inch.

Table 2.3 lists the various parameters at two operating conditions at which the measurements were carried out.

2.5 Data Processing

The analog signals were digitized using an HP 2100 ADC unit for some axial stations. For the rest of the axial stations, a DATEL ADC unit at the Applied Research Laboratory was used. In order to get an adequate number of points inside the clearance region, the analog to digital conversion was carried out at tape reproduction speed 15/16 i.p.s.

Table 2.2

Axial and Radial Locations for Leakage Flowfield Measurements

	Z \ $\tau^{\#}$		10	15	20	25	30	35	40	45	50	60	75	100	125	150	175	180	80	Clearance, in inches
Rotor Inlet Flow	-0.012	ϕ=.55	*	-	*	*	*	*	-	*	*	-	*	*	*	*	-	-	-	-
		ϕ=.60	*	-	*	*	*	*	-	*	*	-	*	*	*	*	-	-	-	
Leakage Flow	0.003	ϕ=.55	*	*	*	*	*	*	*	*	*	-	-	-	-	-	-	-	-	0.081
		ϕ=.60	*	*	*	*	*	*	*	*	*	-	-	-	-	-	-	-	-	
	0.50	ϕ=.55	*	*	*	*	*	*	*	*	*	-	-	-	-	-	-	-	-	0.087
		ϕ=.60	*	*	*	*	*	*	*	*	*	-	-	-	-	-	-	-	-	
	0.75	ϕ=.55	*	*	-	*	*	*	*	-	-	-	-	-	-	-	-	-	-	0.060
		ϕ=.60	*	*	-	*	*	*	*	-	-	-	-	-	-	-	-	-	-	
	0.979	ϕ=.55	*	*	*	*	*	*	-	-	-	-	-	-	-	-	-	-	-	0.061
		ϕ=.60	*	*	*	*	*	*	-	-	-	-	-	-	-	-	-	-	-	
Rotor Exit Flow	1.055	ϕ=.55	*	*	*	*	-	*	*	*	*	-	-	-	-	-	-	-	-	-
		ϕ=.60	*	*	*	*	-	*	*	*	*	-	-	-	-	-	-	-	-	
	1.179	ϕ=.55	-	-	*	-	*	-	*	-	*	-	*	*	*	*	-	*	-	-
		ϕ=.60	-	-	*	-	*	-	*	-	*	-	*	*	*	*	-	*	-	
	1.440	ϕ=.55	-	-	*	-	*	-	*	-	-	*	-	*	*	*	-	*	*	-
		ϕ=.60	-	-	*	-	*	-	*	-	-	*	-	*	*	*	-	*	*	
	1.593	ϕ=.55	-	-	*	-	*	-	*	-	*	-	*	*	*	*	-	*	-	-
		ϕ=.60	-	-	*	-	*	-	*	-	*	-	*	*	*	*	-	*	-	
	1.731	ϕ=.55	*	-	*	-	*	*	*	-	*	-	*	*	*	-	-	-	-	-
		ϕ=.60	*	-	*	-	*	*	*	-	*	-	*	*	*	-	-	-	-	

$\tau^{\#}$ is the distance in thousands of an inch from the annulus-wall.

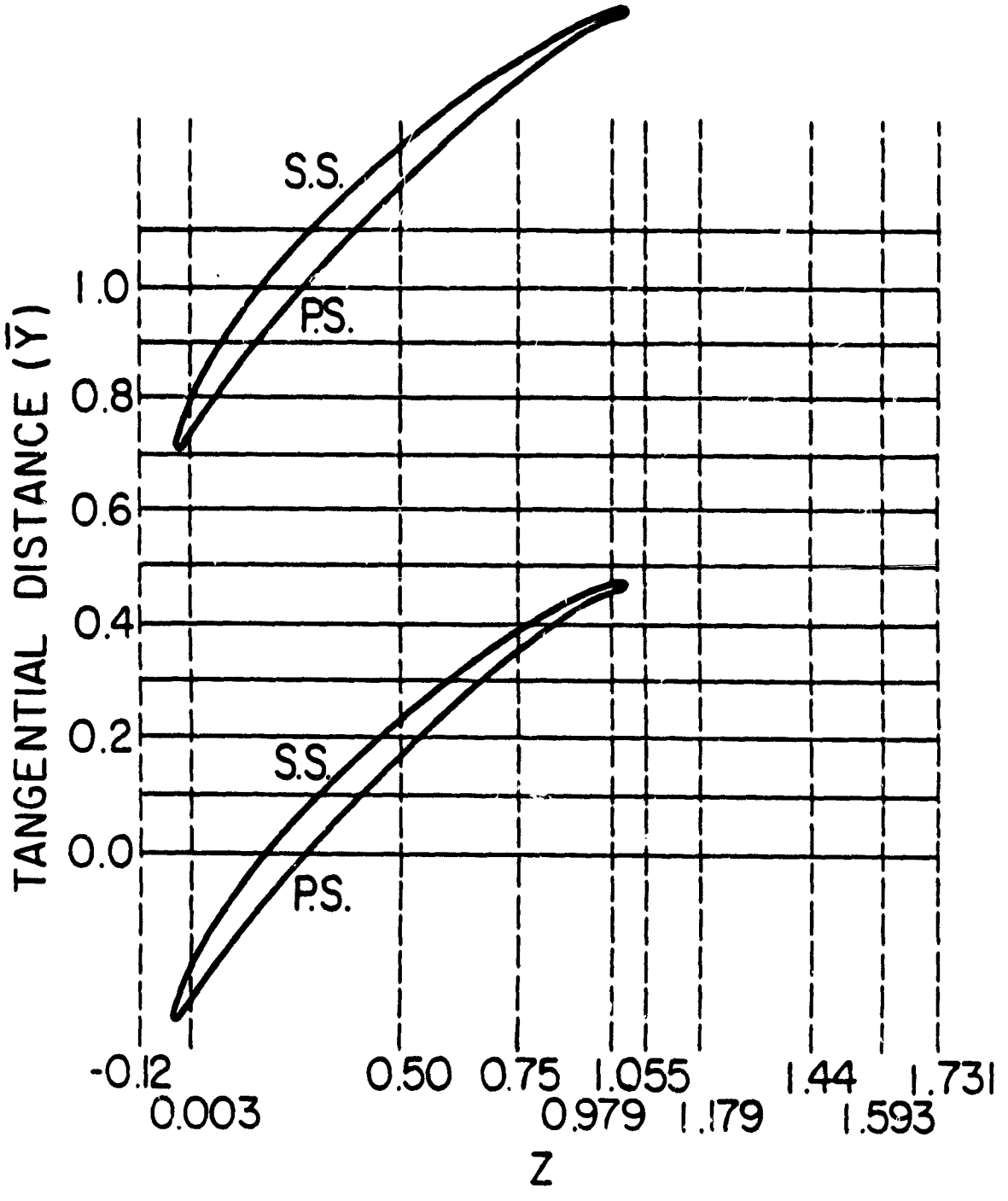

Figure 2.9 Axial Stations of Measurement and Definitions of $\bar{Y}$ at Design Conditions

Table 2.3

Compressor Parameters at Design and Off Design Conditions

	Design Condition	Off Design Condition
RPM	1100	930
Inlet static pressure	-5.08 cm of H_2O	-4.356 cm of H_2O
Inlet velocity	28.37 m/sec	26.28 m/sec
Flow coefficient ϕ	0.55	0.60
Average pressure rise coefficient ψ	0.51	0.375

A computer code which was originally developed by Reynolds and Lakshminarayana [24] to process three-sensor hot wire data was modified for two-sensor data. This code was used to:

1. Convert digitized hot-wire signal to instantaneous cooling velocity.

2. Obtain instantaneous flow velocities from cooling velocities using hot-wire equations.

3. Obtain various mean and turbulent flow characteristics from the instantaneous velocities.

A detailed discussion of data processing procedure is given by Reynolds and Lakshminarayana [24]. Various errors in hot-wire data and data processing are discussed in Appendix A. The data is corrected for some of these errors in the computer program discussed earlier.

CHAPTER III

INTERPRETATION AND DISCUSSION OF THE EXPERIMENTAL RESULTS AT DESIGN CONDITIONS

Although the measurements were made at all the locations listed in Table 2.2, the discussion in this chapter is limited to four representative radial locations for some selected axial stations at the design condition ($\phi = 0.55$). In addition, the blade static pressure near the tip of the blade, the inlet annulus-wall boundary layer profile, as well as the flow data below 4 percent of the span presented in reference [9], are extremely useful in the interpretation of these results.

3.1 Mean Properties of the Flowfield

3.1.1 Velocity Profiles and Angles Inside the Tip Clearance Region

The variations of the mean axial velocity W_z, and the mean tangential velocity in the stationary frame of reference V_θ, and the relative flow angle (β) for each of the axial stations at four different radial locations are shown in Figures 3.1-3.4 and 3.6(a,b,c). In these figures, the blade locations are marked by dotted lines on $\overline{Y}$ axis. Figure 2.9 also shows the blade locations on the $\overline{Y}$ axis for all the axial locations. The velocities W_z and V_θ are normalized by the local maximum axial velocity $(W_z)_{max}$. Variations of $(W_z)_{max}$ and $(V_\theta)_{max}$ with radial distance at each axial location is shown in Figures 3.1d, 3.2d, 3.3d, 3.4d, and 3.6d.

The decreasing trend in W_z and V_θ and the increasing absolute value of relative flow angle β near $\overline{Y} = 0.7$ in Figure 3.1 reflect

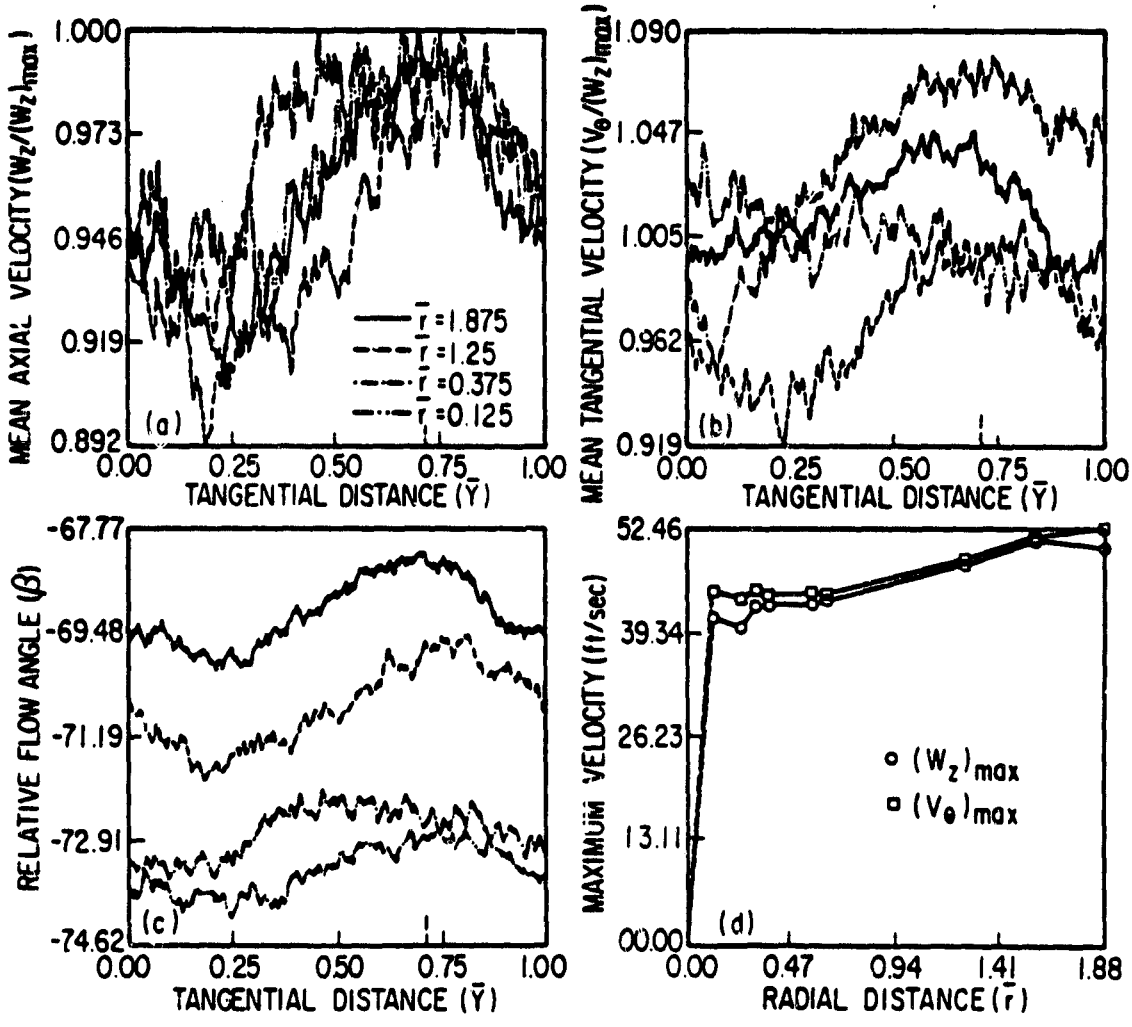

Figure 3.1 Variation of Mean Flow Properties at the Inlet of the Rotor (Z = -0.012)

the effect of the unsteady flowfield due to the rotor on the incoming flow upstream of the rotor. It is important, however, to note that these variations are rather small in magnitude and that the flow closer to the wall shows greater degree of uniformity compared to that in the vicinity of the blade tip. The variation in the relative flow angle is less than 7°. The variation of maximum velocity shows an unusual behavior, with a rapid increase in velocity from $\bar{r} = 0.15$, beyond which the increase is more gradual. $\bar{r} = 1.88$ is well within the annulus-wall boundary layer profile as indicated in Figure 2 of reference [9].

At $Z = 0.003$, near the blade leading edge, the pressure difference across the blade is not large enough to induce a strong leakage flow. But, a noticeable dragging effect of the blade on the flow can be observed as evidenced by a considerable increase in the tangential velocity. Variation of the mean axial velocity (Figure 3.2a) shows a peak near $\bar{Y} = 0.49$. As it can be seen from this figure, a large change in W_z takes place over a small distance approximately mid-way between the passage, indicating possible flow separation regions near the blade surfaces and the presence of scraping effect. Both of these effects tend to decrease the tangential velocity near the blade surfaces and increase it near the mid passage. The variation in the relative flow angle shows a trend similar to the incoming flow at $Z = -0.12$. A dramatic decrease in the tangential velocity from the blade tip to the annulus-wall region is evident from Figure 3.2b. The radial variation of the maximum tangential velocity and the axial velocity at this location indicate a dramatic change from those at

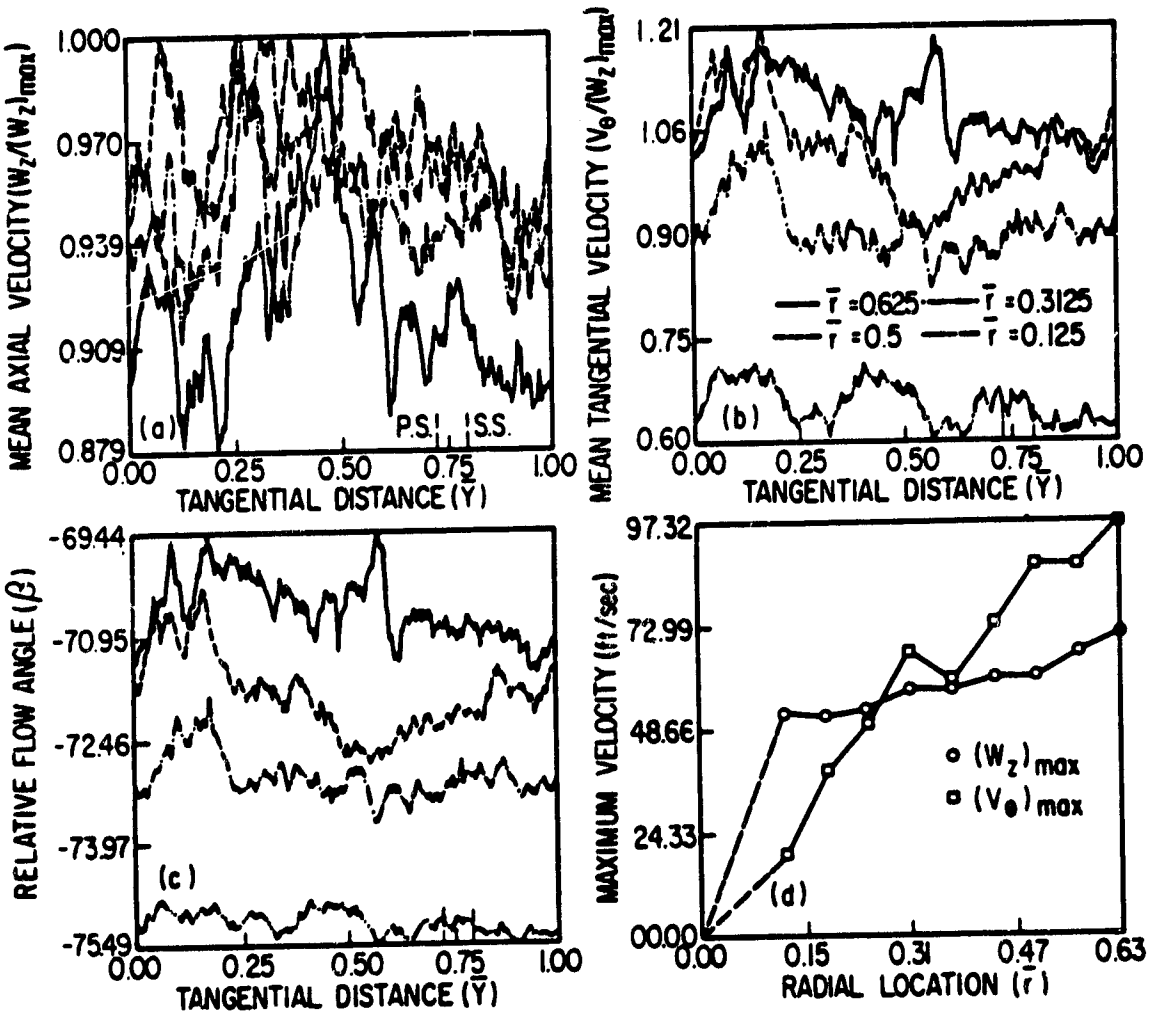

Figure 3.2 Variation of Mean Flow Properties at the Leading Edge (Z = 0.003)

$Z = -0.12$. The axial velocity profile at this location shows an increase in axial velocity, but the tangential velocity distribution shows a large gradient near the annulus-wall, decreasing drastically beyond $\bar{r} = 0.15$. The maximum values of tangential and axial velocities have increased slightly from their inlet values for $\bar{r} > 0.3$.

The flowfield at $Z = 0.5$, shown in Figure 3.3, is very complex. Such a behavior could result from the interaction of the leakage flow with other features present in this region. These features may include secondary flow, annulus-wall boundary layer, the rolling up of the leakage flow to form a vortex and the presence of a vortex generated by the scraping of the annulus-wall boundary layer by the blade. Because the pressure difference across the blade at this station is quite high, one might even expect a washing away of the boundary layer leading to the above complex flow behavior.

The axial velocity profile at $Z = 0.5$ (Figure 3.3) shows low velocities on either side of the blade near the annulus-wall, while the velocities in the clearance region are quite high. This again may have been caused by the leakage flow which has a "blowing" effect on the annulus-wall boundary layer in this region. The axial velocities near the blade tip are nearly uniform. The tangential velocity also shows a similar trend, with large values near the suction side of the blade near the annulus-wall. The blade motion augments the leakage flow and tends to move it farther away from the suction side. The low velocity region observed at $\bar{Y} = 0.85$ for two radial locations near the annulus wall ($\bar{r} = 0.29, 0.12$) may have been caused by the roll up of the leakage flow in this region. The tangential velocities in this

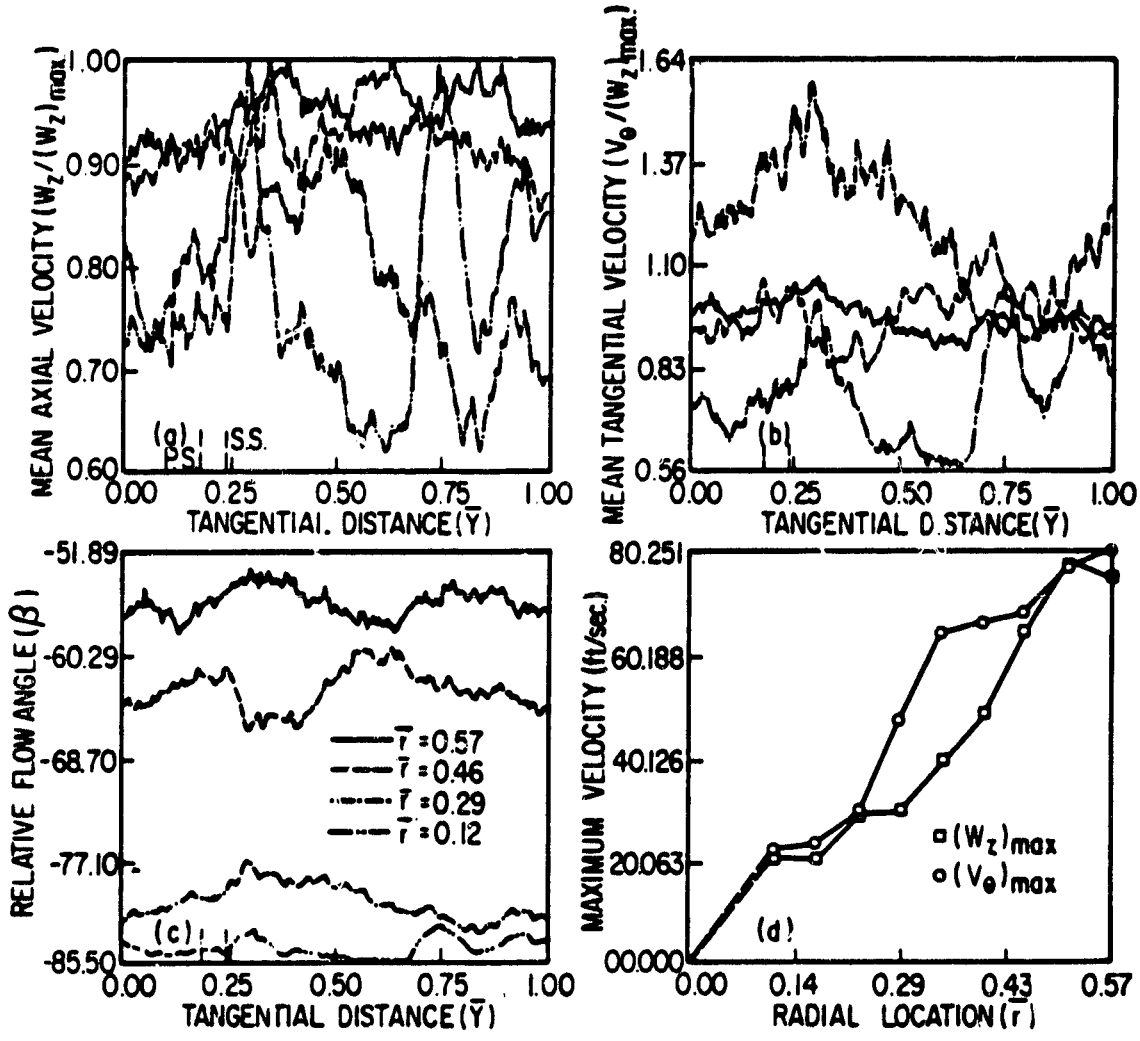

Figure 3.3 Variation of Mean Flow Properties at 1/2 Chord (Z = 0.50)

region are lower than those observed at Z = -0.003, an indication that the flow in this region proceeds through the blade row from Z = 0.003 to Z = 0.5 with a change in energy level or tangential momentum opposite that of the free stream. The relative flow angles show the usual trend with large angles near the annulus wall. The angle changes from Z = 0.003 to Z = 0.5 are small. The maximum axial and tangential velocities shown in Figure 3.3d at this location indicate very little change in radial variation of the maximum axial velocity from the previous axial location. The maximum tangential velocity is decreased at most radial locations, with the exception of the blade tip region. The radial variation of both velocities is found to be gradual.

At Z = 0.75, a clearly defined leakage flow can be seen from Figure 3.4. In Figure 3.4a, a sudden decrease in the mean axial velocity takes place just before the pressure side at $\overline{Y}$ = 0.20 over a very small distance. A similar trend in V_θ is also observed in Figure 3.4b. Figure 3.4c shows a sudden increase in the absolute value of the relative flow angle β in the same region. All the three facts together indicate a very clearly defined leakage flow in this region. The significance of these features is better explained in Figure 3.5, where a vector diagram of the flow velocities with and without the leakage flow is shown. As it can be seen from this figure, the leakage velocity which is defined as the component of the relative velocity normal to the blade surface, tends to turn the flow away from the blade. This causes an increase in the absolute value of β and a decrease in the axial and the absolute tangential velocities. This trend is clear from Figure 3.4.

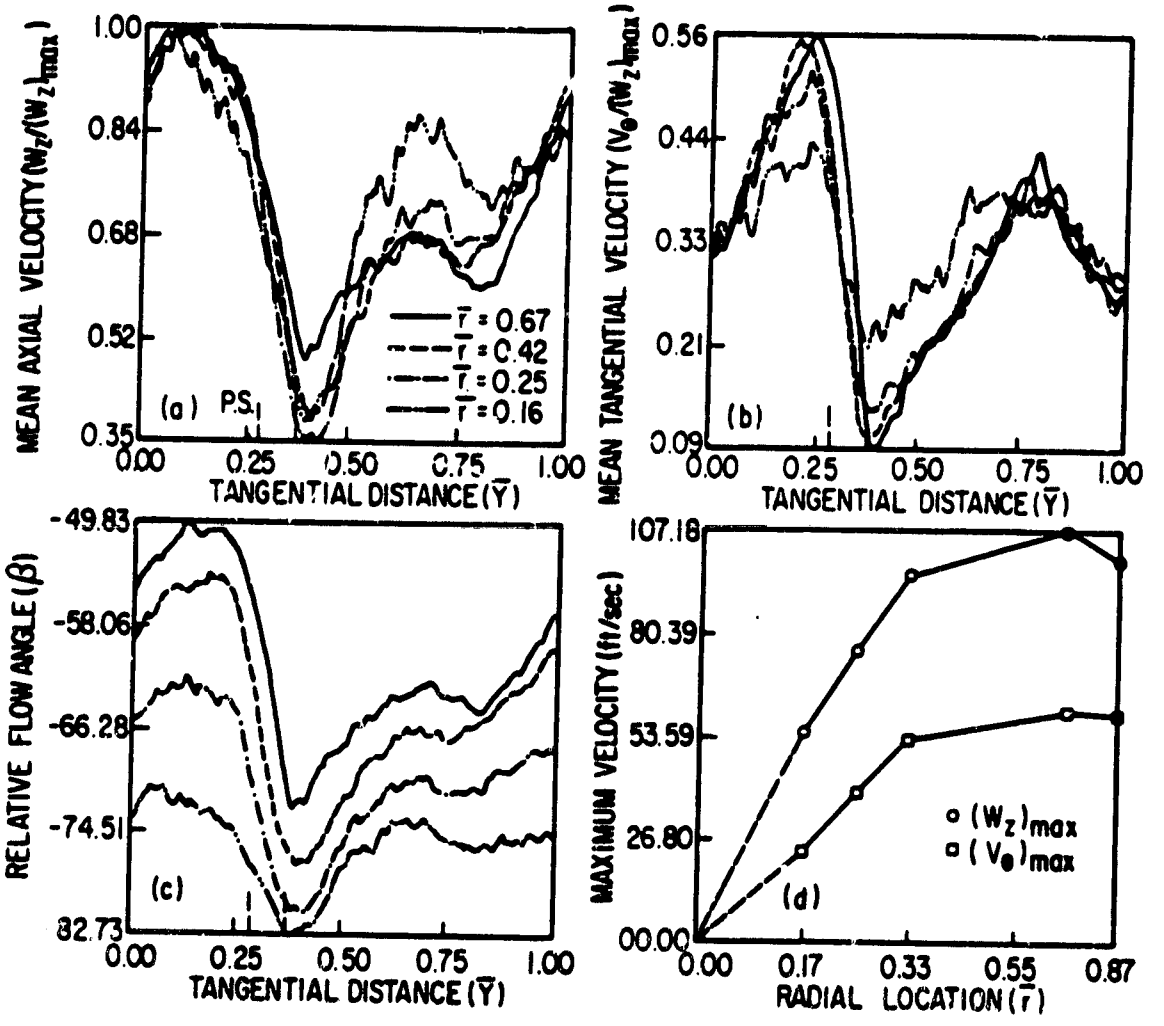

Figure 3.4 Variation of Mean Flow Properties at 3/4 Chord (Z = 0.75)

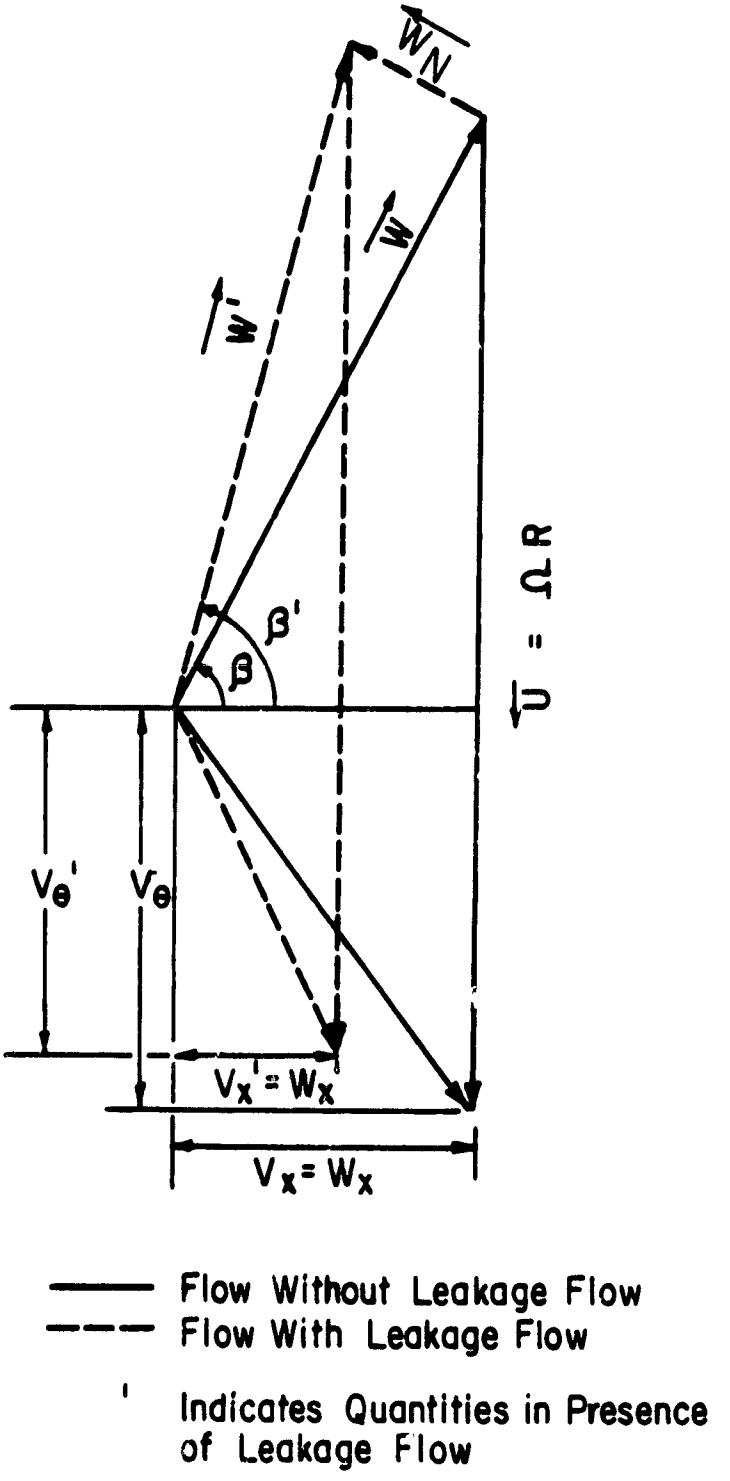

Figure 3.5 Velocity Triangles With and Without the Leakage Flow

In Figure 3.4a, another peak in W_z occurs at $\bar{Y} = 0.70$. A similar peak in V_θ occurs at $\bar{Y} = 0.75$ but a similar peak in β is not very clearly defined. This phenomenon clearly indicates the presence of the tip leakage vortex and scraping vortex. The most interesting feature of the flowfield at this axial location is that though the variations in W_z, V_θ and β are comparatively very large for a particular radial location, the variation from one radial location to another is very small. All the non-dimensionalized profiles nearly collapse into a single curve, indicating the similarity in the velocity profiles. It is thus clear that the leakage flow is the most predominant flow in the clearance region at this location.

Figure 3.4d showing the variation of $(W_z)_{max}$ and $(V_\theta)_{max}$, indicates a gradual increase in both the velocities away from the wall. A maximum occurs at approximately 57 percent of the clearance height from the wall.

The flowfield at the next axial station at $Z = 0.979$ (Figure 3.6) has features similar to the previous axial station but is less pronounced. This may be due to a rather small blade pressure difference and the fact that the thickness of the blade is quite small at this location and a clearly defined clearance region does not exist. The presence of a leakage vortex, characterized by low axial velocity and low tangential velocity is evident near the suction surface of the blade. The relative flow angles are also large in this region, indicating a large region of underturning. A defect in W_z is observed near $\bar{y} = 0.250$ at $\bar{r} = 0.167$ and may indicate the presence of a scraping vortex. The maximum axial and tangential velocities plotted in

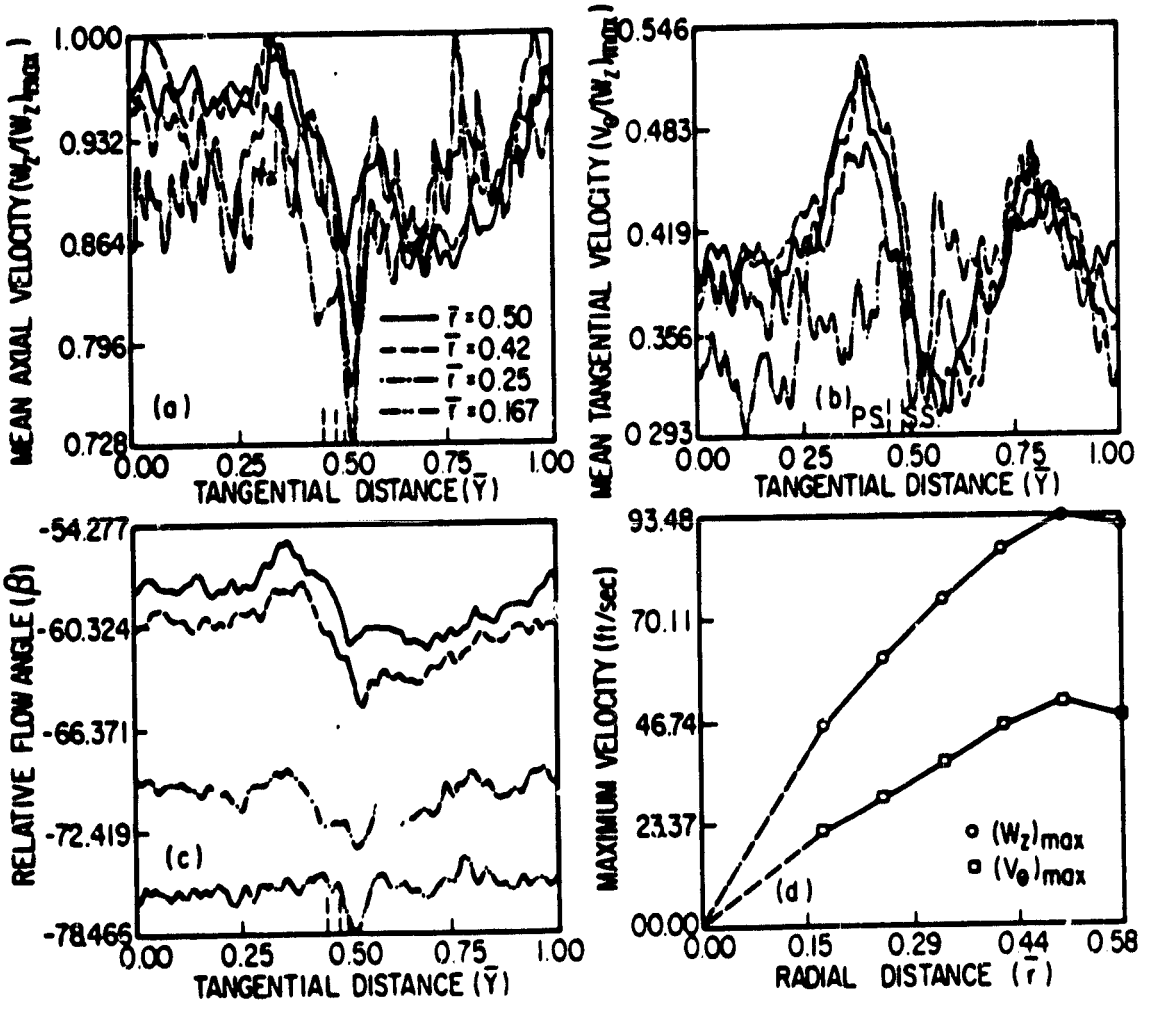

Figure 3.6 Variation of Mean Flow Properties at the Trailing Edge (Z = 0.979)

Figure 3.6 indicate that these are substantially the same as those at $Z = 0.75$. The axial velocity variation across the passage shows near uniform flow, except at the tip vortex region. This seems to indicate that the separated region observed near the suction side at $Z = 0.75$ has been reduced.

A comparison of Figures 3.3c, 3.4c and 3.6c shows that there is a considerable variation of the relative flow angle with the radius. This seems to indicate a large underturning of the flow near the annulus-wall.

3.1.2 Velocity Profiles and Angles at the Exit of the Rotor

Figures 3.7-3.9 provide information regarding the rotor exit flow. Figure 3.7 shows the variation of the mean properties at $Z = 1.055$. From Figure 3.7a, it can be observed that the mean axial velocity variation shows a trend similar to that of a wake at the radial station very near the blade tip ($\bar{r} = 0.83$). This wake profile is marked by a minimum in the velocity at $\bar{Y} = 0.60$. The wake width is large. The blade wake may have moved towards the wall at the trailing region due to the radial outward transport inside the blade boundary layer. The suction side again shows the presence of separated regions. At $\bar{r} = 0.67$ this wake seems to be spreading and instead of a sharp minimum as observed at $\bar{r} = 0.83$, the velocity shows a defect from $\bar{Y} = 0.2$ to 0.55. However, both the defects in velocities are small. This implies that there is a strong interaction between the exit flow and the annulus-wall boundary layer. The presence of the leakage vortex is not evident at these two radial locations, indicating radially downward movement or dissipation of the vortex. At the last two radial stations

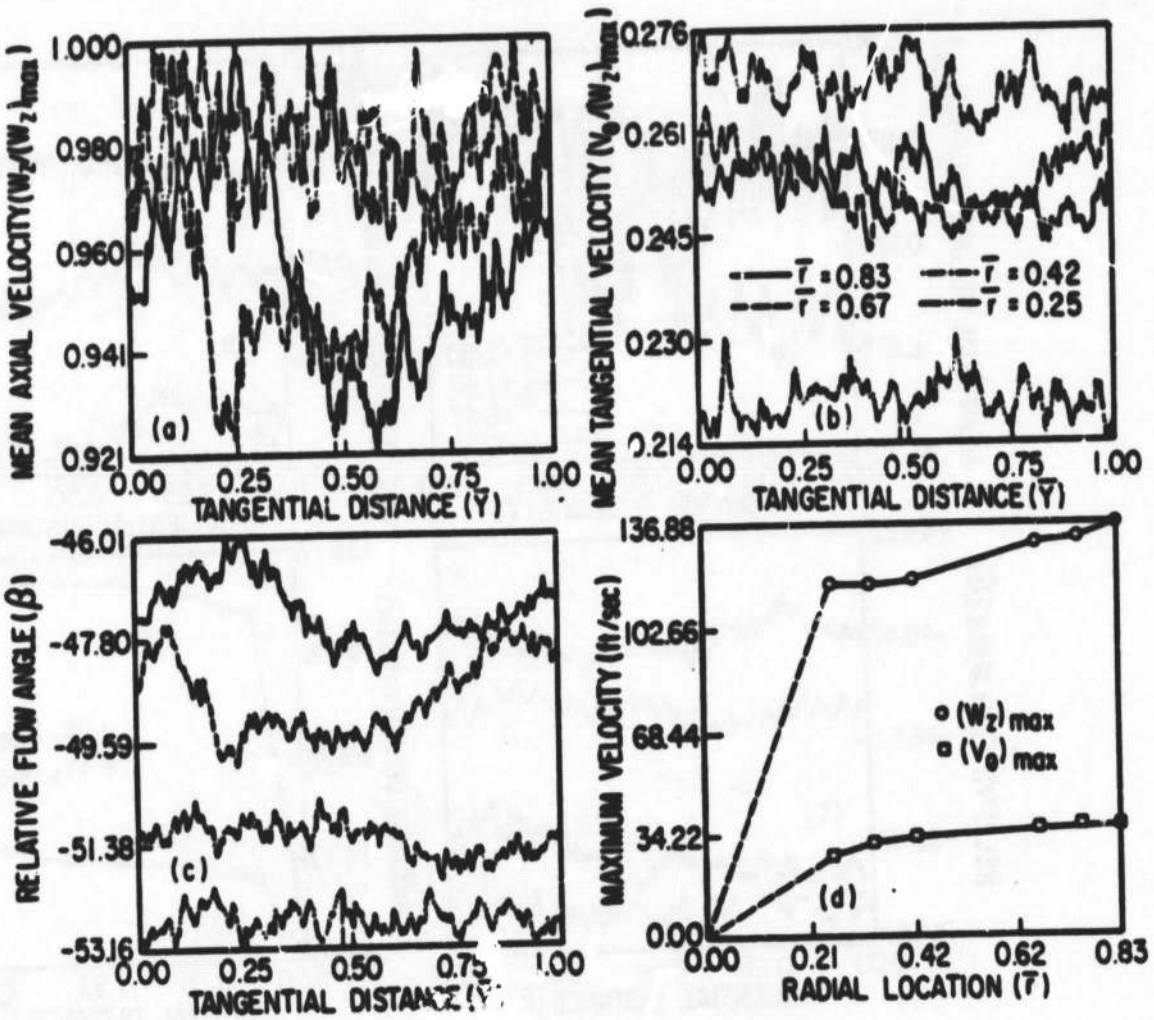

Figure 3.7 Variation of Mean Flow Properties at Z = 1.055

ORIGINAL PAGE IS
OF POOR QUALITY

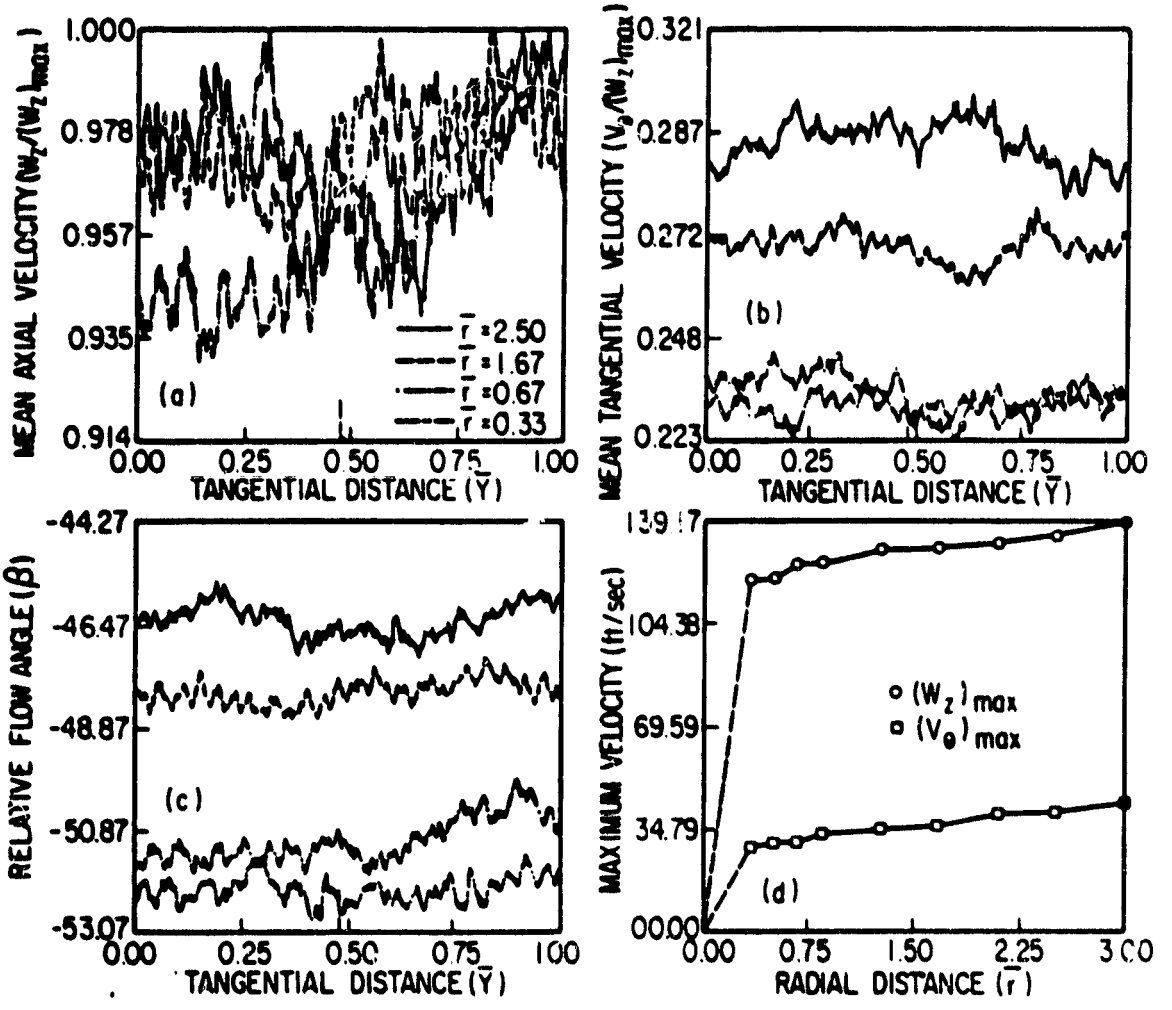

Figure 3.8 Variation of Mean Flow Properties at Z = 1.179

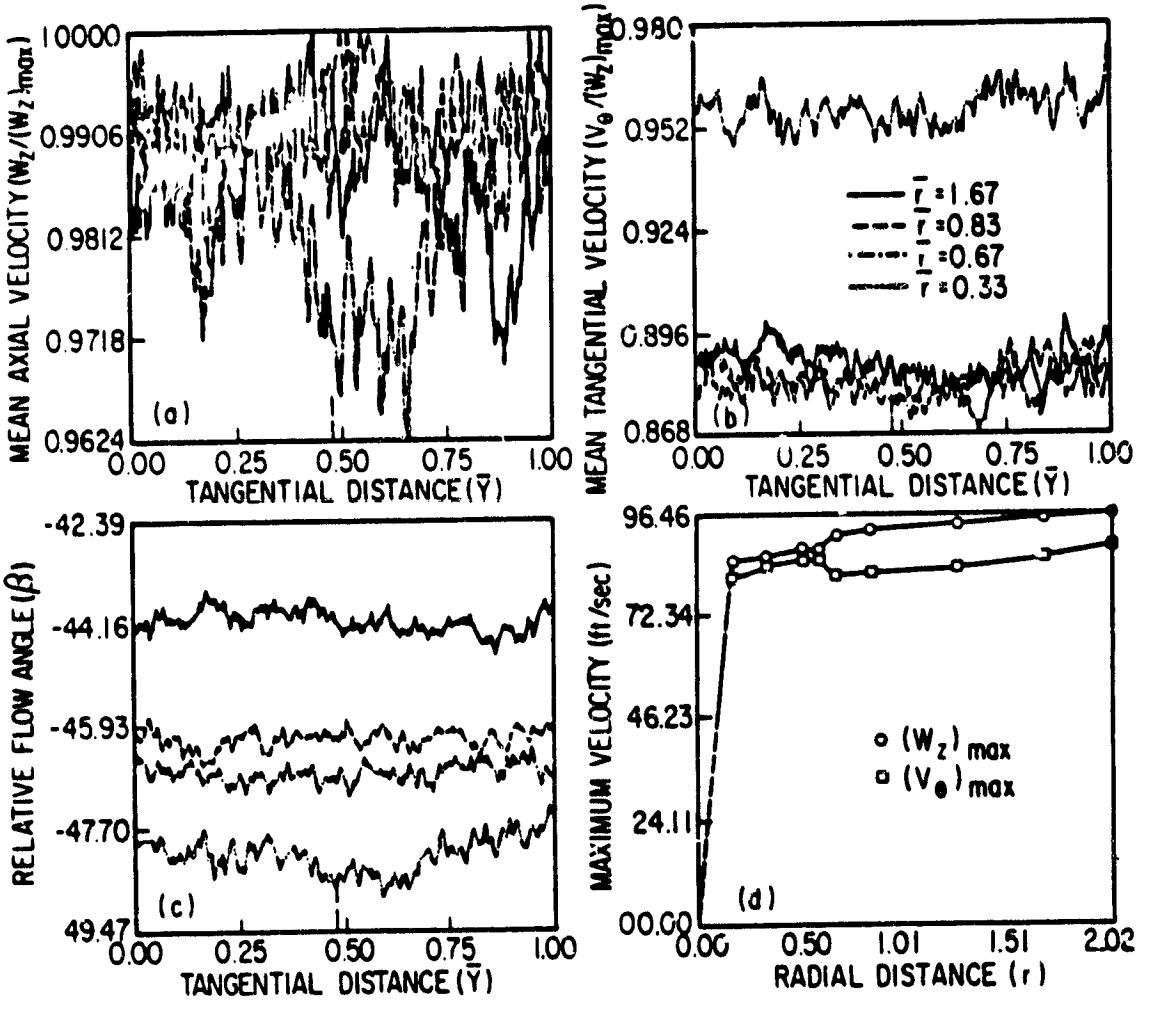

Figure 3.9 Variation of Mean Flow Properties at Z = 1.731

near the wall, ($\bar{r}$ = 0.47, 0.25) the mean axial velocity seems to be fairly uniform. Compared to the variations in the axial velocity at the trailing edge, W_z variations at this station are very small.

The variation of V_θ in Figure 3.7b shows a uniform distribution of velocity across the passage for all the radial locations. Variation of β also shows a similar behavior. The variations in β from one radial location to the other are not very large (7°), indicating a uniform turning of the flow at all the radial locations.

Figure 3.7d shows a very interesting feature. The maximum axial velocities are very high compared to the maximum tangential velocities at all the radial locations. There is a sudden jump in the axial velocity from those measured at the previous axial station (trailing edge). This may be attributed to the absence of the blockage effect of the blade present inside the passage.

The next axial location (Z = 1.179) was farther from the blade and it was possible to probe the flowfield within 4 percent of the blade span from the tip. Consequently, it was possible to capture the details of the wake near the blade. Figure 3.8a shows that at $\bar{r}$ = 2.5, the mean axial velocity has a defect between $\bar{Y}$ = 0.4 to $\bar{Y}$ = 0.7. A similar profile exists for $\bar{r}$ = 1.67. The actual variations in the velocity, however, are quite small indicating a rapid decay of the wake. At $\bar{r}$ = 0.67 the velocity remains uniform through most of the passage with a rapid increase at $\bar{Y}$ = 0.70. At $\bar{r}$ = 0.33, W_z is fairly uniform.

Tangential velocity variations shown in Figure 3.8b indicate a fairly uniform flow at all the radial locations. The variation of

V_θ in radial direction is not very large (6 percent). The same is true for β also. The maximum velocity variations shown in Figure 3.8b do not reveal any remarkable change in the behavior from the previous axial station except for the fact that the difference in the two velocity components is decreasing continuously.

The measurements at the two subsequent axial stations (Z = 1.44 and 1.593) are not reported here as they indicated that the flow-field was becoming more or less uniform and reached near-equilibrium conditions. However, the tangential velocities were considerably smaller than the axial velocities at these locations. Figure 3.9 shows that at Z = 1.731, both the components of the velocity and the relative flow angle are uniform in the tangential direction and the difference between the two components of the velocity is very small.

3.1.3 Leakage Velocity

In the absence of any clearance between the rotor blade and the annulus-wall, the flow should follow the blade contours near the blade surfaces and the velocity component in the direction normal to the blade should be zero. Any deviation of the flow from the blade contour in the tip clearance region will give rise to a component normal to the blade, which is termed as the leakage velocity in this report. A true representation of the leakage flow should take into account the normal component of the velocity at the inlet (W_{N_o}). The change in velocity triangle due to leakage flow is shown in Figure 3.5. W_N is the leakage velocity in the terminology adopted in this report.

Figure 3.10 shows the variation of the leakage velocity at the suction surface ($W_N - W_{N_o}$) in the radial direction for four axial

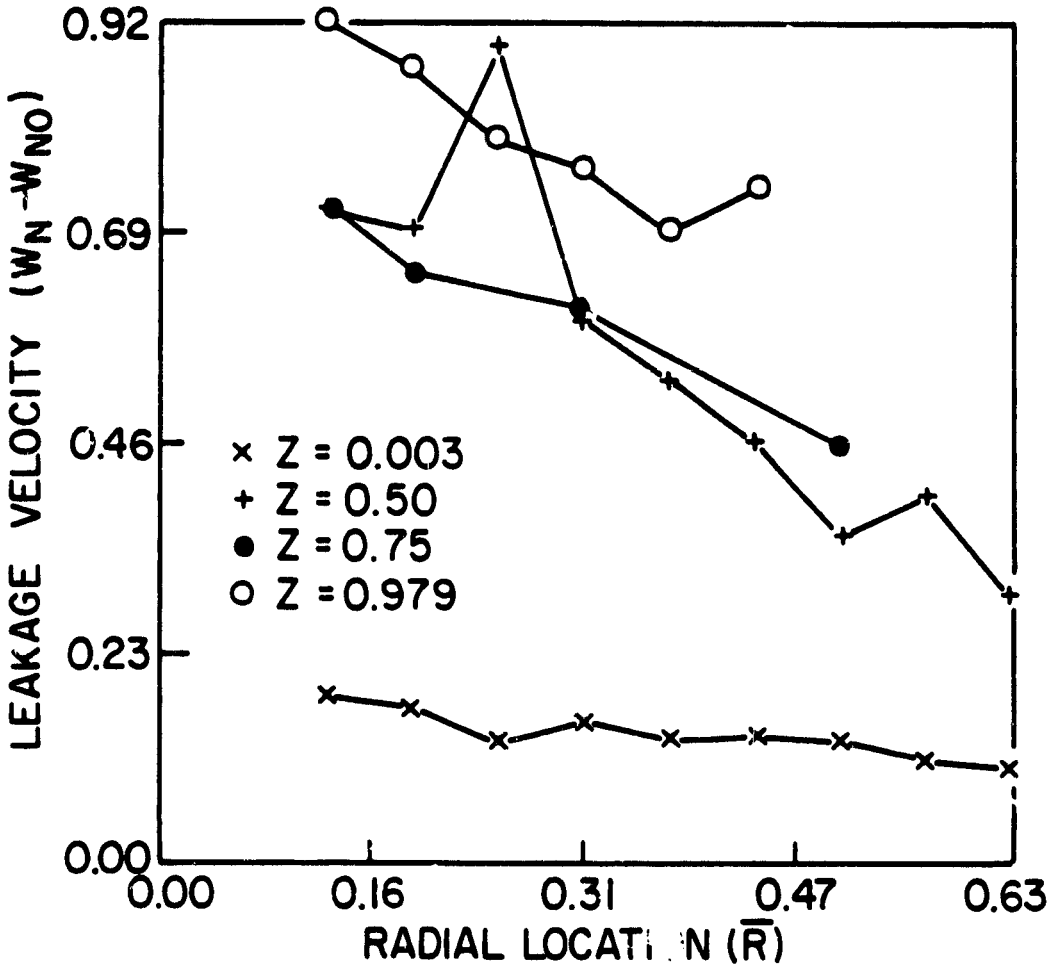

Figure 3.10 Variation of the Leakage Velocity at the Suction Surface

locations inside the passage. The velocities are normalized by the blade tip speed and the inlet component is also subtracted from the leakage velocity. At the leading edge the leakage velocity is very small which is in accordance with the fact that the pressure gradient across the blade is very small in this region. A considerable jump in the leakage velocity at Z = 0.50 is due to the existence of a large pressure gradient across the blade. There is no appreciable change in $(W_N - W_{N_O})$ from Z = 0.50 to Z = 0.75. The leakage velocity at the trailing edge is larger than that at Z = 0.50 which does not seem to follow from the argument based on pressure gradient alone. This may result from the formation of the leakage vortex, and the consequent entrainment by the vortex. It is also evident that the leakage velocities are maximum away from the annulus-wall and the blade tip. A plot of these velocities (Figure 3.11) near the pressure surface shows a similar trend.

3.1.4 Velocity Vector Plots

Figures 3.12 and 3.13 show the relative velocity vectors in the z-θ plane at two different radii. At $\bar{R}$ = 0.3125, as indicated in Figure 3.12, the flow follows the blade contour at the leading edge, implying the absence of any leakage flow. This agrees well with the expected trend. At Z = 0.5, the flow has turned towards the tangential direction giving rise to a substantial leakage velocity as shown in Figure 3.10. An abrupt change in the flow angle approximately at the middle of the passage can be attributed to the rolling of the leakage flow as discussed earlier and in reference [9]. At Z = 0.75, a large change in the flow angle from the pressure surface to the suction

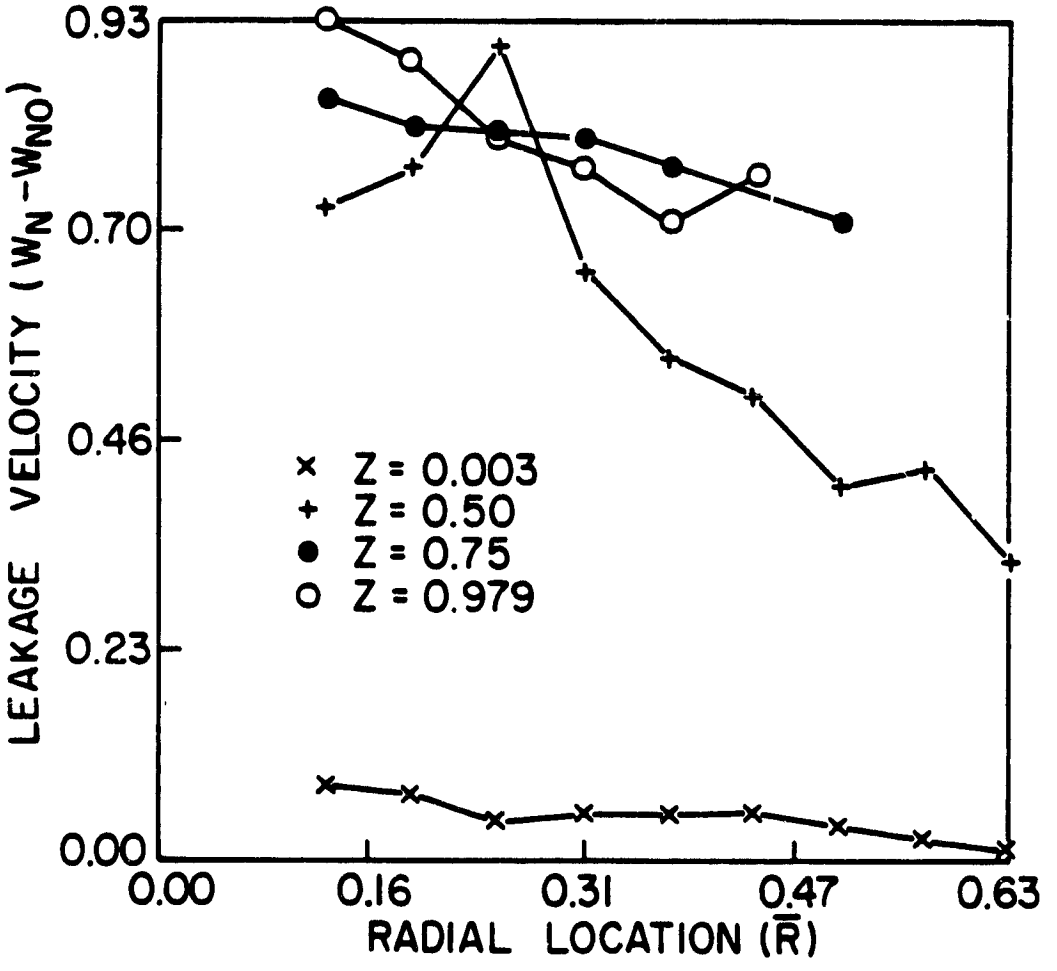

Figure 3.11 Variation of the Leakage Velocity at the Pressure Surface

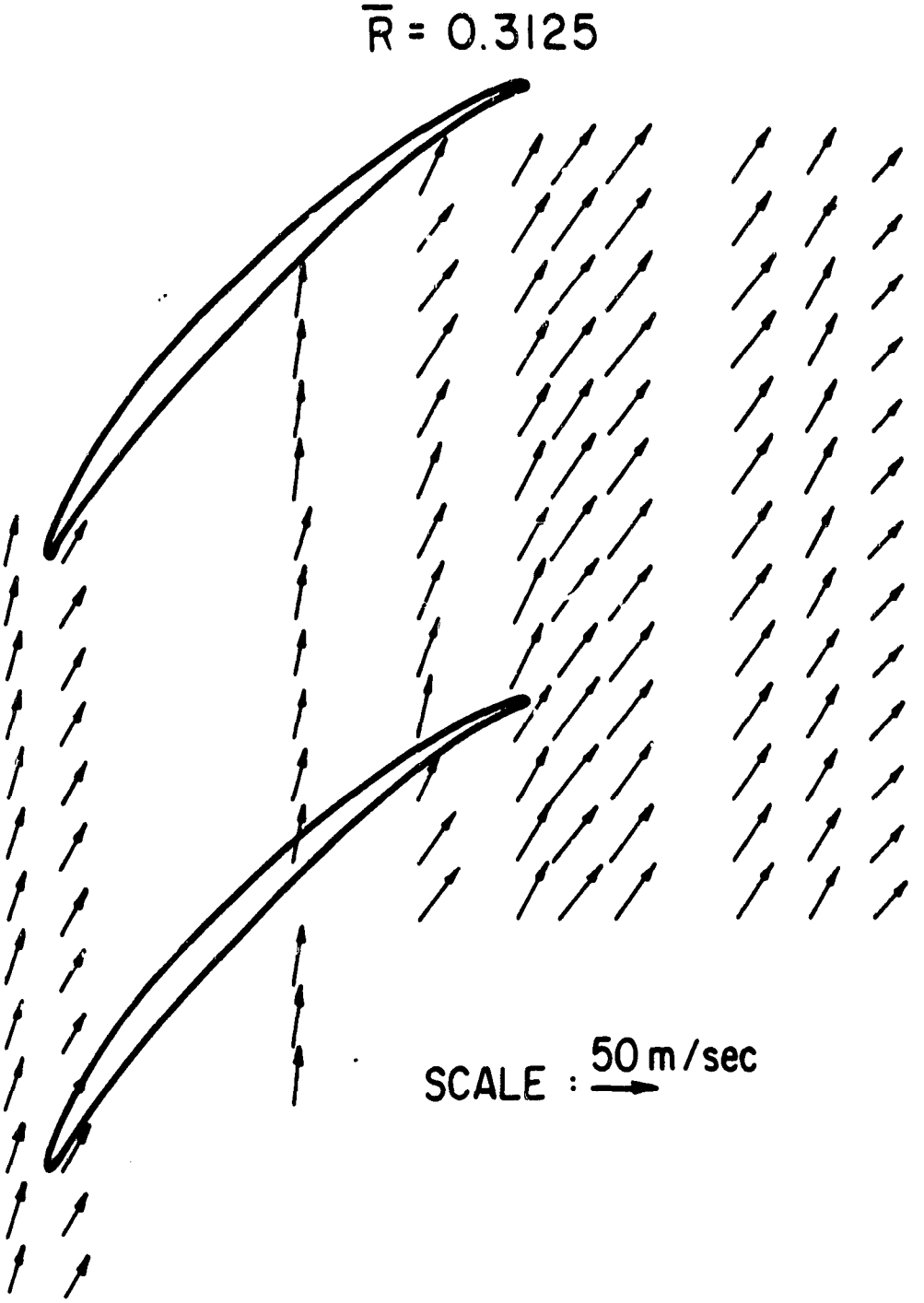

Figure 3.12 Relative Velocity Vectors Inside the Clearance Region at $\bar{R}$ = .3125

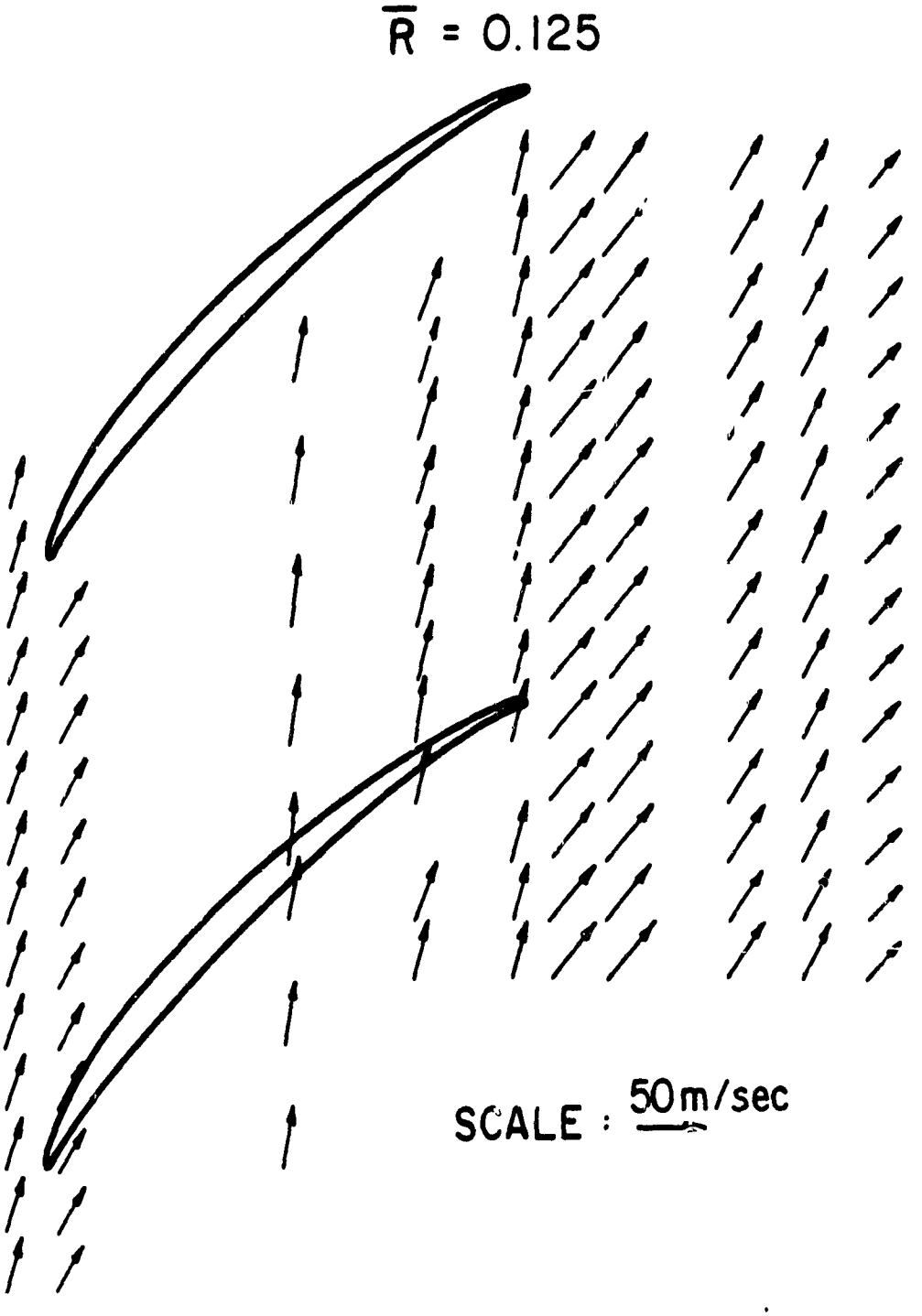

Figure 3.13 Relative Velocity Vectors Inside the Clearance Region at $\bar{R}$ = .125

surface observed experimentally shows the effect of a predominant leakage flow in this region. A similar change is evident at Z = 0.979. A similar vector diagram at $\bar{R}$ = 0.125 (Figure 3.13) shows all the features mentioned above but the main difference is in the relative flow angle which is more inclined towards tangential direction at the radial location nearer to the annulus-wall. In both the cases, the flow near the wall is nearly axisymmetric at the exit, indicating that the leakage flow and the vortex may have moved downward.

3.1.5 Annulus-Wall Boundary Layer Profile

The radial variation of the axial and absolute tangential velocities averaged over the passage at various axial locations is plotted in Figure 3.14. These velocities are normalized by the blade tip speed. The annulus-wall boundary layer profile within the passage, from 4 percent span to 22 percent span is given in reference [9]. Figure 3.14 gives an overall picture of the boundary layer growth as the flow proceeds from the inlet to the rotor and then downstream, where the flow has become nearly uniform across the passage.

At Z = -0.012, the radial gradient in velocity is very sharp near the wall. This indicates that the shear stresses in this region should be large. The tangential and axial velocities are of the same order of magnitude, even though the axial velocity is found to be nearly twice as much as the tangential velocity [9] in the free stream. As the flow approaches the leading edge (Z = 0.003), these large velocity gradients are reduced, both axial and tangential velocities increase away from the wall. The axial velocity undergoes a dramatic change from Z = 0.003 to Z = 0.5, with considerable reduction in its

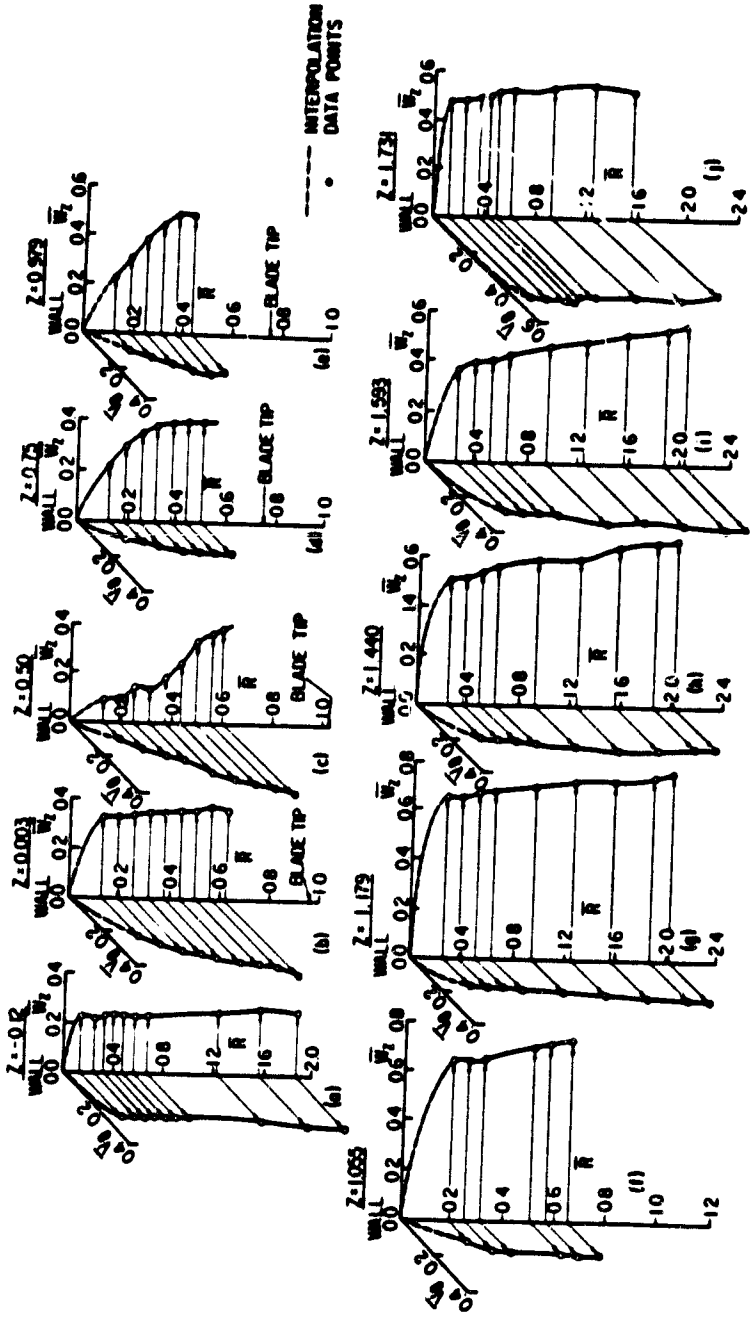

Figure 3.14 Measured Development of the Annulus Wall Boundary Layer

magnitude at most radial locations. The tangential velocity profile undergoes a very small change from Z = 0.003 to Z = 0.5, indicating little or no energy transfer from blade to blade flow. The effect of the leakage flow and its interaction with the annulus-wall boundary layer can be clearly seen at Z = 0.5. As indicated earlier, the boundary layer may be getting washed off by a strong leakage jet resulting in such an unconventional boundary layer. The annulus-wall boundary layer profiles in the clearance region from Z = 0.75 to 0.979 (Figure 3.14d,e) indicate that the leakage flow has either reached an equilibrium stage or has moved downward along the radius, providing rather smooth profiles with very little variation from Z = 0.75 to 0.979, even though there is a slight increase in the axial velocity towards the trailing edge.

A dramatic change occurs as the flow leaves the blade trailing edge. The axial velocity increases by almost 50 percent and tangential velocities decrease only slightly. The change in profile from trailing edge to Z = 1.731 indicates that the flow redistribution occurs continuously downstream, even though the flow is nearly uniform from blade to blade.

3.2 Turbulence Properties of the Flowfield

3.2.1 Turbulence Intensity Profiles

Blade to blade distributions of the axial and the tangential turbulence intensities at various radial and axial locations are shown in Figures 3.15-3.22. As with the mean velocity data, the blade locations are marked by dotted lines on $\overline{Y}$ axis. Both the turbulence

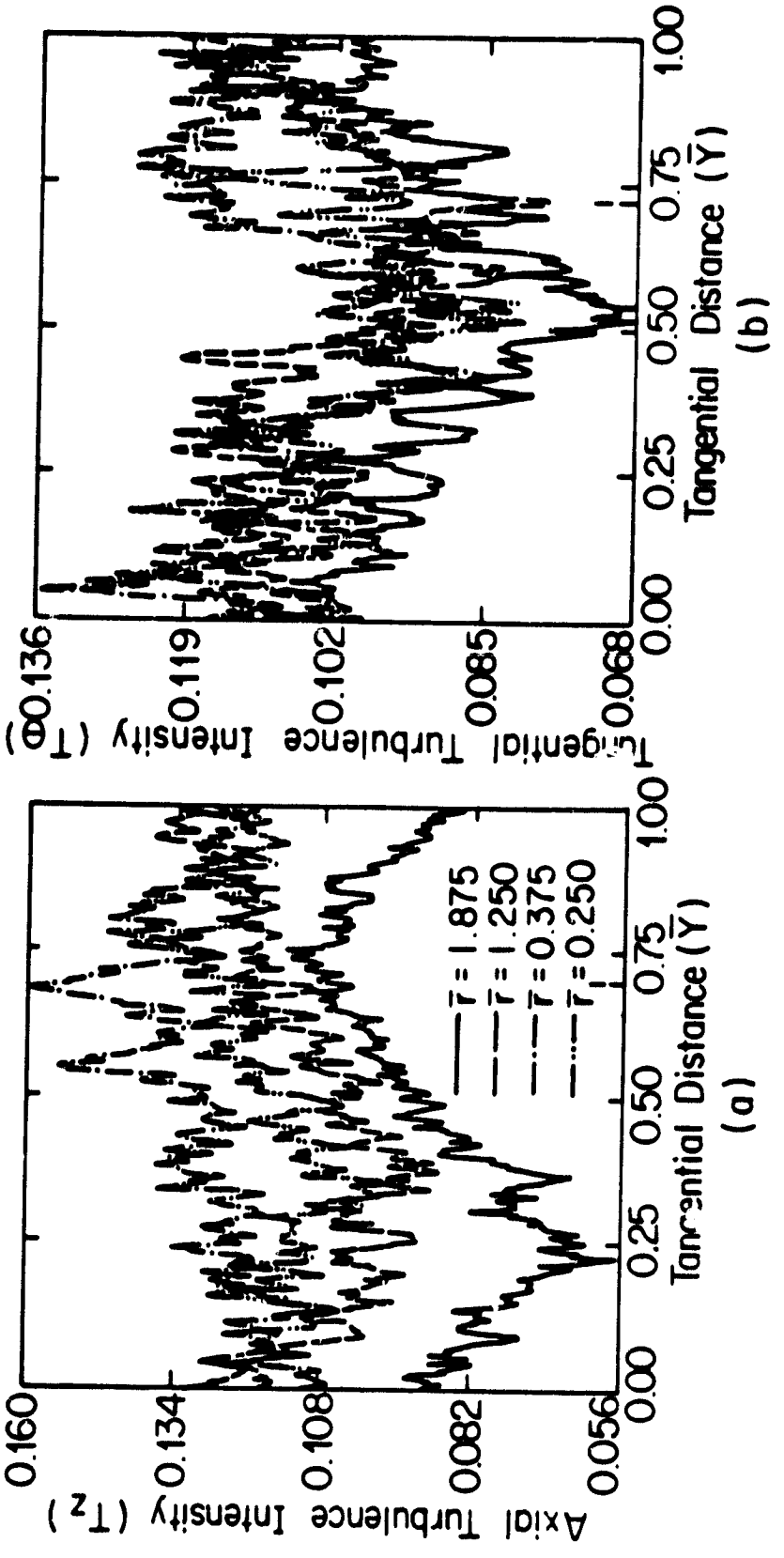

Figure 3.15 Variation of Turbulence Intensities at the Inlet of the Rotor (Z = -0.012)

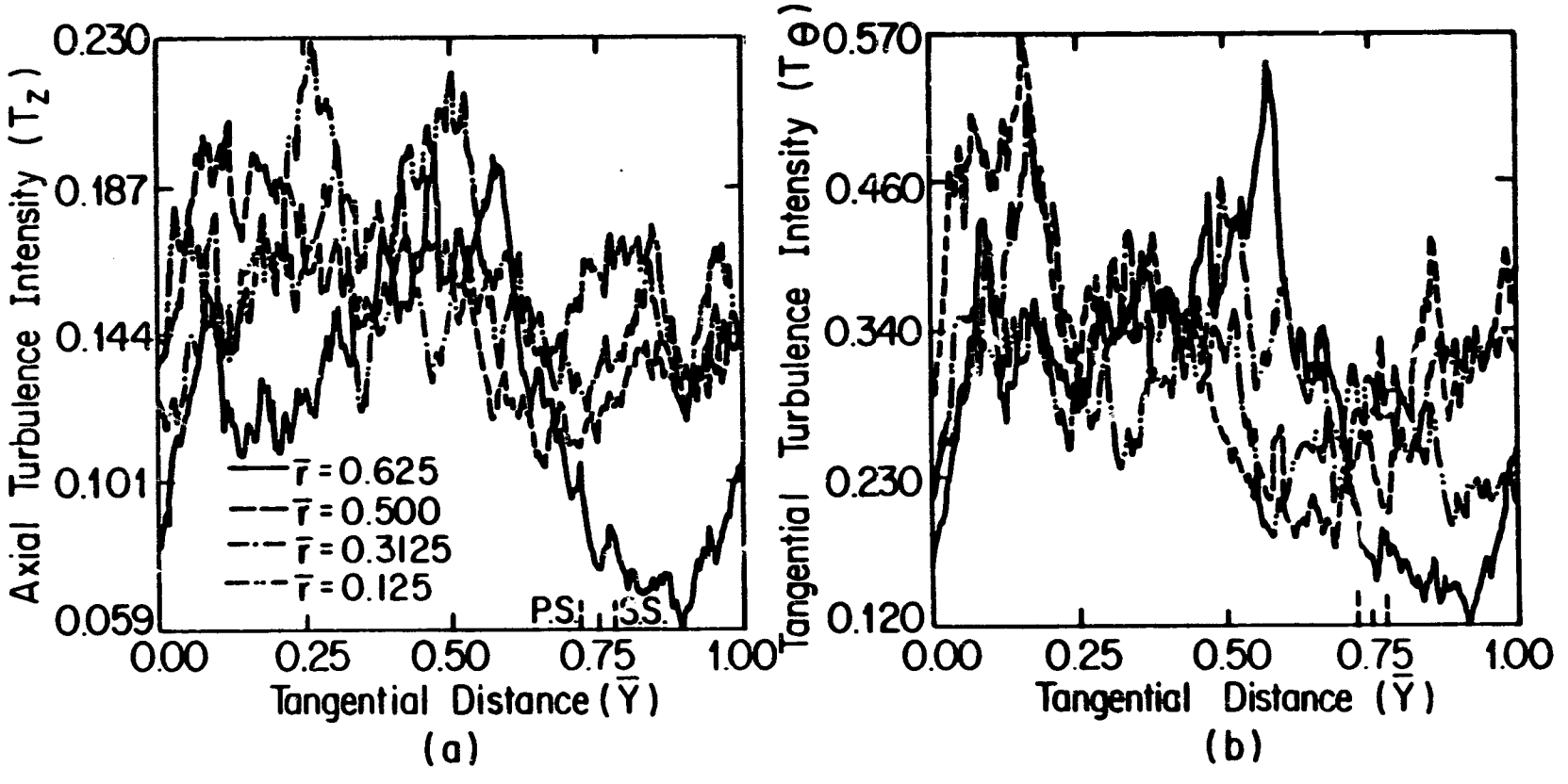

Figure 3.16 Variation of Turbulence Intensities at the Leading Edge (Z = 0.003)

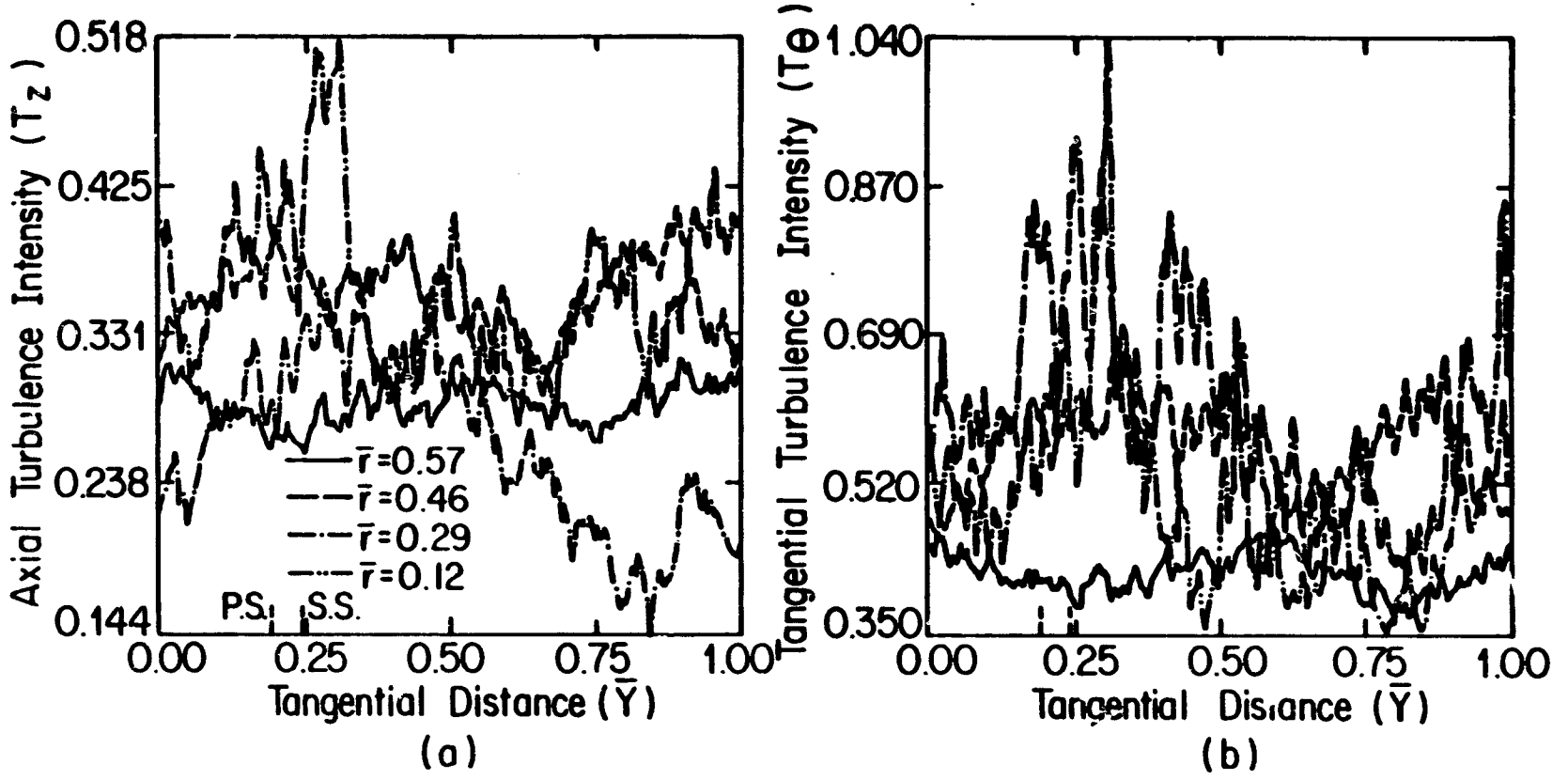

Figure 3.17 Variation of Turbulence Intensities at 1/2 Chord (Z = 0.50)

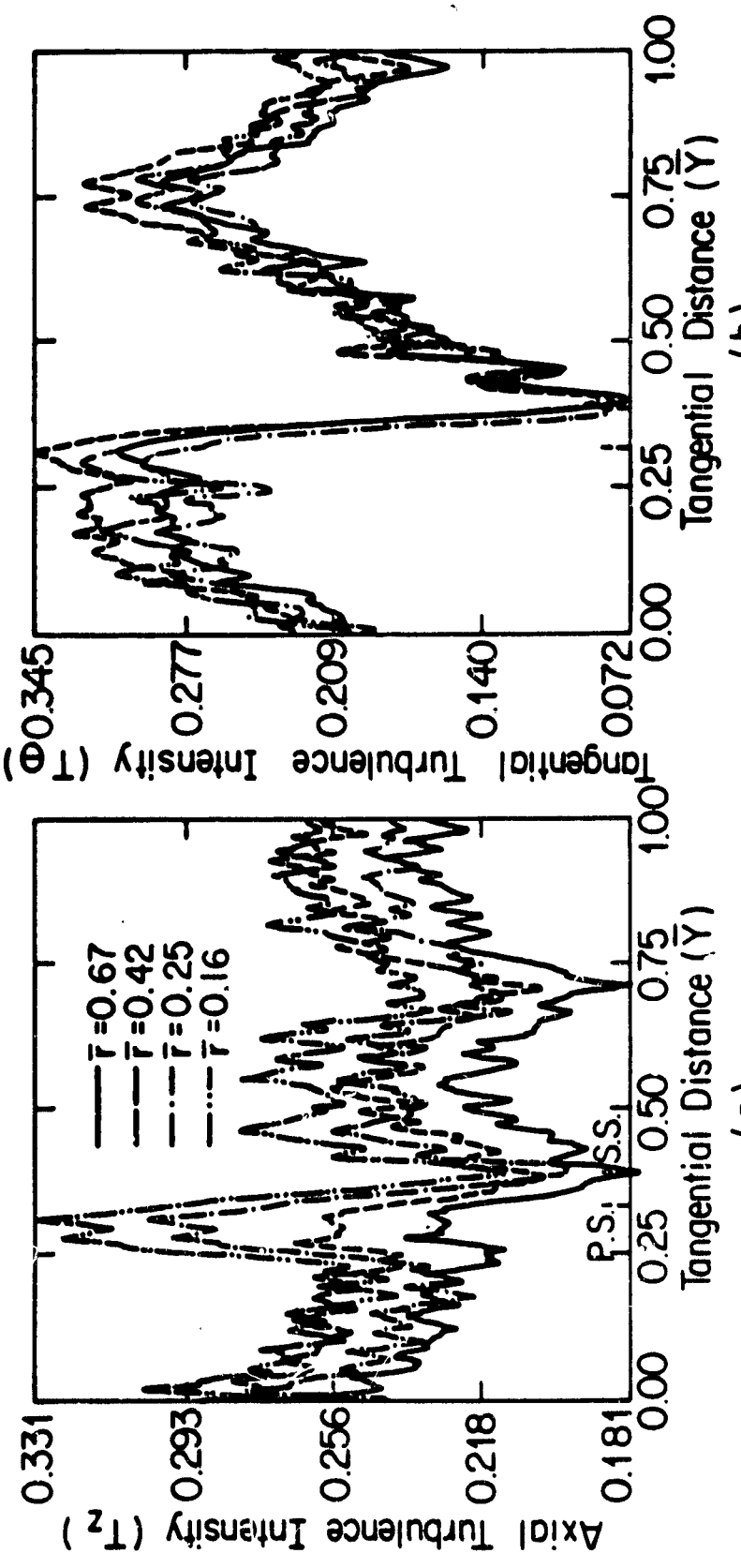

Figure 3.18 Variation of Turbulence Intensities at 3/4 Chord (Z = 0.75)

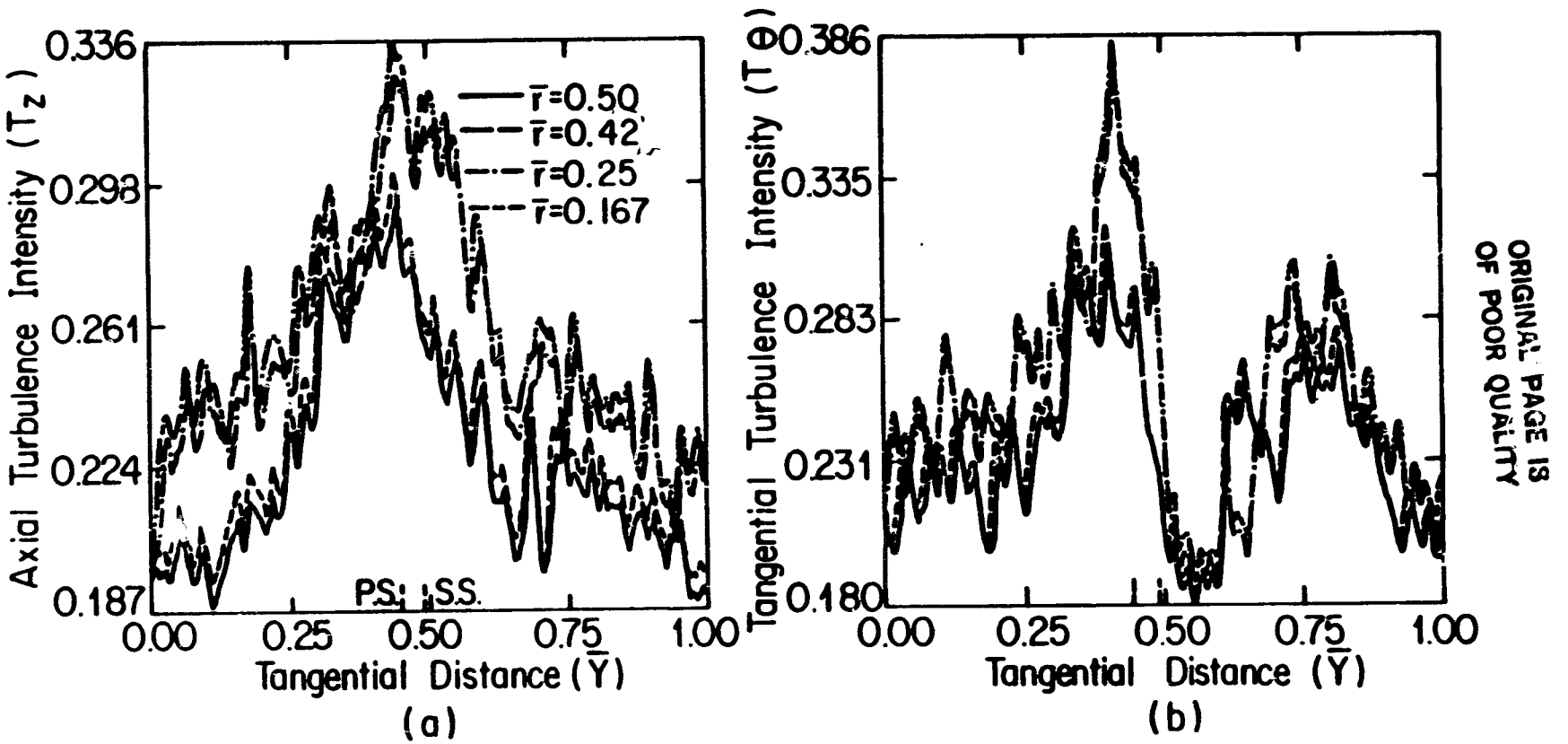

Figure 3.19 Variation of Turbulence Intensities at the Trailing Edge (Z = 0.979)

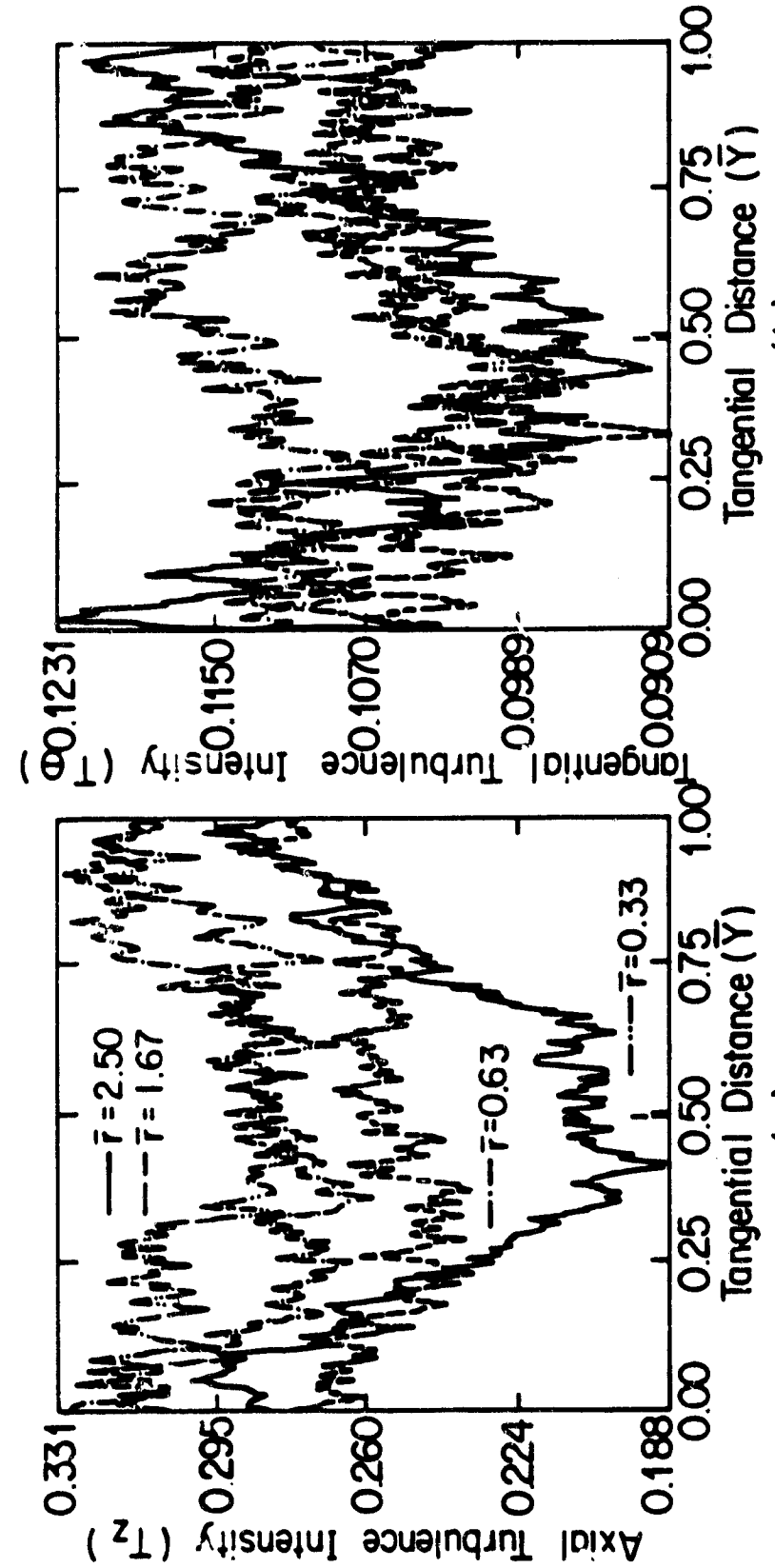

Figure 3.20 Variation of Turbulence Intensities at Z = 1.055

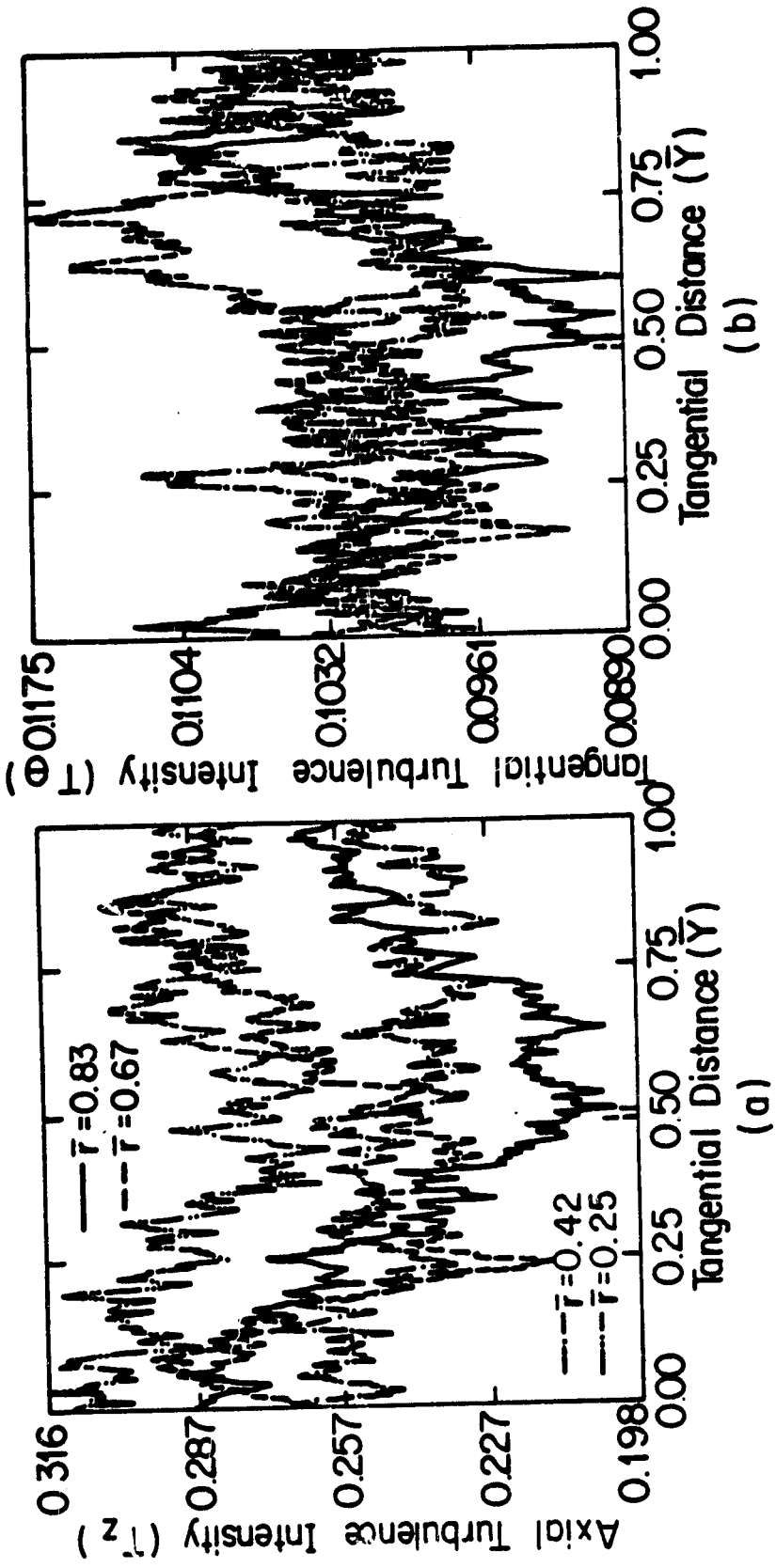

Figure 3.21 Variation of Turbulence Intensities at Z = 1.179

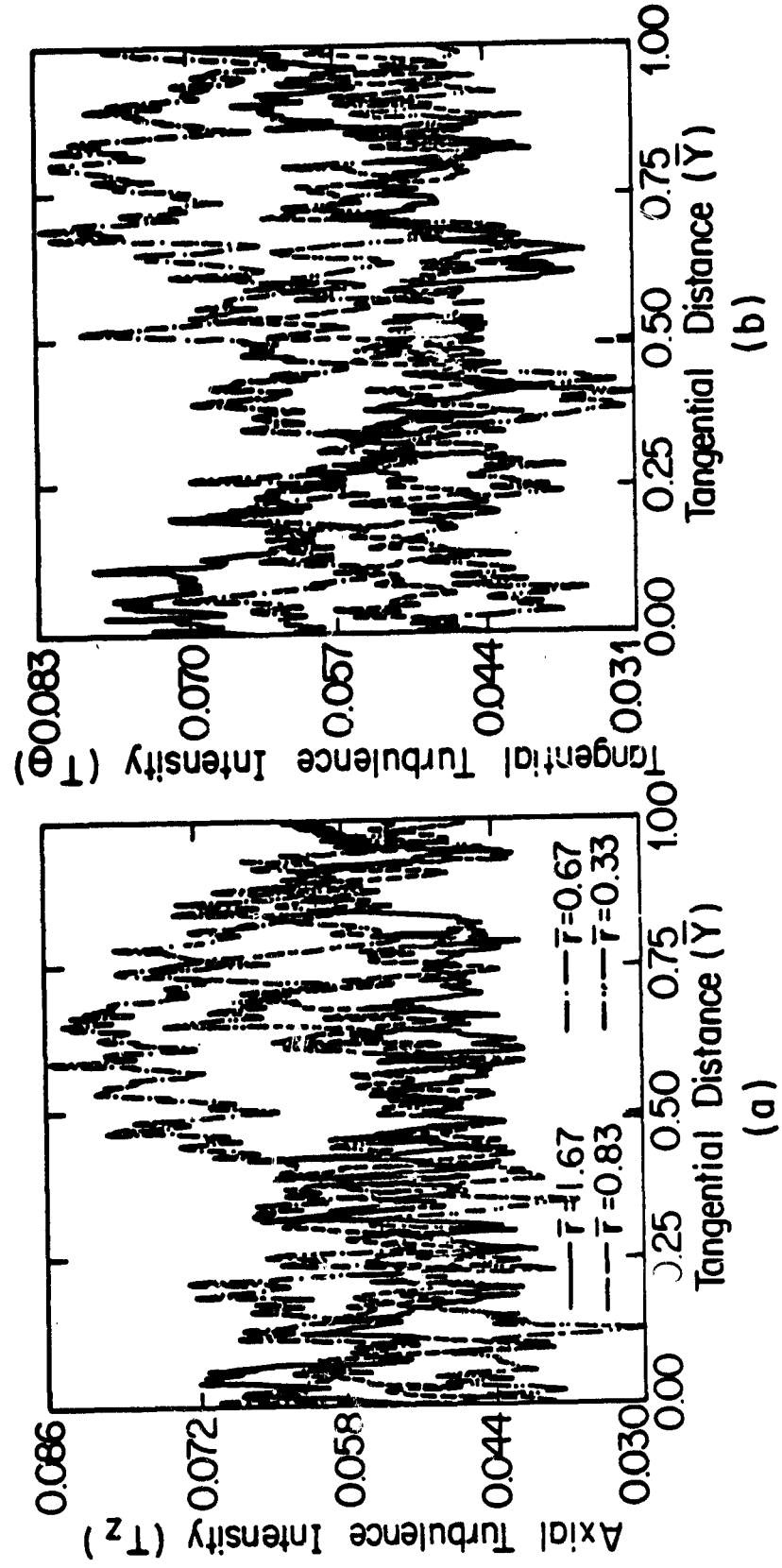

Figure 3.22 Variation of Turbulence Intensities at Z = 1.731

Table 3.1

Maximum Total Velocities* at Radial and Axial Stations of Measurement at ϕ=0.55

R \ Z	-0.012	0.003	0.50	0.75	0.979	1.055	1.179	1.440	1.593	1.731
1.875	0.409	-	-	-	-	-	0.772	0.714	0.660	-
1.5625	0.390	-	-	-	-	-	0.765	0.693	0.638	0.697
1.25	0.377	-	-	-	-	-	0.750	0.650	0.597	0.723
1.0	-	-	-	-	-	-	-	0.629	-	-
0.9375	-	-	-	-	-	-	0.718	-	0.546	0.703
0.75	-	-	-	-	-	-	-	0.615	-	-
0.625	0.337	0.613	0.604	-	-	0.800	0.709	-	0.517	0.693
0.5625	0.348	-	-	-	-	0.740	-	-	-	-
0.5	-	0.493	0.436	0.551	-	0.716	0.687	0.575	0.496	0.683
0.4375	-	-	-	-	0.516	-	-	-	-	0.698
0.375	0.342	-	-	-	0.530	0.687	0.662	0.553	0.489	0.682
0.3125	0.345	0.460	0.300	0.539	0.484	-	-	-	-	-
0.25	0.322	-	-	-	0.420	0.674	0.667	0.538	0.462	0.667
0.1875	-	-	-	0.426	0.343	0.660	-	-	-	-
0.125	0.340	0.386	0.160	0.305	0.256	-	-	-	-	-

*All the velocities are normalized by the blade tip speed (176.50 ft/sec).

intensity components are normalized by local maximum total velocity since the turbulence is dependent upon the local flow conditions. The normalizing velocities are listed in Table 3.1.

Figure 3.15(a,b) shows the axial and the tangential turbulence intensity profiles at the inlet of the rotor. It is evident from this figure that both the intensities increase as the annulus-wall is approached. The intensities have peaks at $\bar{r} = 0.375$ and decrease by about 2 percent at $\bar{r} = 0.125$ (0.01 inch away from the annulus-wall). The velocity gradients are high near the wall because of the annulus-wall boundary layer which implies greater mixing. Hence higher turbulence intensities near the annulus wall are expected. But as the viscous sublayer approaches, the turbulence intensities decrease considerably. This explains the slight decrease in the intensities at $\bar{r} = 0.125$. Blade to blade variation of the axial and the tangential turbulence intensities show some effect of the unsteady flowfield downstream, though the variation for a given radius is less than 5 percent.

Figure 3.16(a,b) shows the variation of T_z and T_θ at the leading edge. As suggested in the previous section, a noticeable dragging effect of the blade on the flow can be evidenced by a considerable increase in the tangential velocity. The drastic increase in the tangential turbulence intensities supports the above conclusion. Also, the decrease in T_θ near the blade surface and its increasing trend towards the middle of the passage supports the conclusions drawn from mean velocity profiles that the flow separates near the blade surface and the presence of the scraping effect. An increase in T_z is

also observed at this station but this increase is quite small compared to the increase in T_θ. It is interesting to note that the blade to blade distributions of both T_z and T_θ show a large variation at the radial locations close to the blade tip. But the radial stations close to the annulus-wall show more uniform distribution of T_z and T_θ though the level of intensities is higher at these stations compared to the stations near the blade tip. This implies that the effect of flow separation and dragging diminishes near the annulus-wall and the effect of the shear gradient due to the annulus-wall boundary layer is predominant in this region.

Figure 3.17(a,b) shows blade to blade variation of T_θ and T_z for four radial locations at Z = 0.50. As discussed in the case of mean velocity profiles, the flow at this axial station is quite complicated. A very high level of interaction of the leakage flow with the annulus-wall boundary layer, secondary flow, and the vortex generated by the scraping of the annulus-wall boundary layer is indicated by a very high level of turbulence intensities in the tangential direction. In contrast to the flow behavior at the leading edge, the blade to blade distribution of T_z and T_θ at radial locations close to the tip of the blade is nearly uniform, while the two stations ($\bar{r}$ = 0.29 and 0.12) near the annulus-wall show large variations. The variation in T_θ at $\bar{r}$ = 0.12 is nearly 65 percent while at $\bar{r}$ = 0.29 it is approximately 55 percent. The T_z variation in both the cases is about 20 percent. This trend in the flow behavior indicates the presence of a strong leakage jet which washes away the annulus-wall boundary layer causing a very high level of mixing in the region close to the annulus-wall.

This is in agreement with the similar inference derived from the mean velocity data in the previous section.

For $\bar{r}$ = 0.29 and 0.12, Figure 3.17b indicates a low turbulence region near $\bar{r}$ = 0.80, and on either side of this low turbulence region, T_θ increases. The vortex generated due to the rolling up of the leakage flow is indicated in this region. The vortex formation is closer to the pressure surface of the blade. The pressure difference across the blade pressure side and suction side is very high at Z = 0.05, hence the leakage flow velocity is expected to be high. A high leakage velocity is further augmented by the blade rotation. Hence, as pointed out above, the leakage flow should travel further away from the suction surface before rolling up. However, it should be noted here that only the axial and tangential components of the mean velocity and the turbulence intensities are insufficient to predict the exact nature of the interaction among the various flows present in the end-wall region and the exact nature of mixing. Additional information on the variations of the radial component of the mean velocity, the radial turbulence intensity and the correlation of the turbulence intensities is needed for interpreting the above data in further detail.

Variations of T_z and T_θ at Z = 0.75 are shown in Figure 3.18(a,b). A well defined behavior of the flow inside the tip clearance is evident from this figure. As it can be seen from this figure, there is a sudden decrease in both T_z and T_θ inside the tip clearance region. The narrow passage formed between the blade tip and the annulus wall tends to channelize the leakage flow which results in reduced turbulence intensities.

The blade to blade distribution of T_θ as shown in Figure 3.18b is very similar to that of $V_\theta/(W_z)_{max}$ shown in Figure 3.4b. It shows a peak at $\bar{y} = 0.75$ for all the radial locations after which T_θ starts decreasing. This clearly indicates the presence of a vortex due to rolling up of the leakage flow or scraping of the boundary layer. The variation of mean axial velocity $W_z/(W_x)_{max}$ is also in agreement with the T_θ variation. The local minima in $W_z/(W_z)_{max}$ at $\bar{Y} = 0.75$ corresponds to the maxima in T_θ at that location for all the radial stations.

Figure 3.18a shows a local minima near $\bar{r} = 0.70$ for all the four radial locations. This, accompanied with the radial velocity distribution, should indicate the presence of rolling vortex. However, the radial velocity measurements are not available in this region, making it difficult to interpret the data completely.

Comparing the T_θ and T_z distributions at this location of interesting feature of the flowfield can be observed. In the case of T_θ distribution the four curves at different radial stations nearly overlap each other, while the T_z distribution for different radial locations shows four distinct curves though the profiles are similar. It can be inferred from this behavior that in the tangential direction the leakage flow is very prominent and the effect of the annulus-wall boundary layer on the turbulence intensities is very weak. But in the axial direction the effect of the annulus-wall boundary layer is noticeable in the form of increasing intensity towards the annulus wall.

The axial turbulence intensity shows a decrease of about 20 percent from the previous axial station at $Z = 0.5$. The decrease in

the tangential turbulence intensity is very large indicating a stabilized leakage flow.

T_θ distribution at Z = 0.979 as shown in Figure 3.19b is very similar to that at Z = 0.75. One noticeable difference is in the location and magnitude of the local maxima which is smaller and has shifted slightly towards the suction surface. Since the pressure drop across the blade is very small, the leakage flow starts rolling up closer to the suction surface as indicated by the position of the local maxima in T_θ. T_z distribution, as illustrated in Figure 3.19a, shows a peak near the pressure side of the blade and then decreases continuously till the middle of the passage and then increases again. There is no appreciable difference in the level of T_θ and T_z from that at Z = 0.75.

The flow at the exit of the rotor in close proximity of the annulus-wall is characterized by low turbulence in the tangential direction. Figure 3.20(a,b) shows T_θ and T_z distribution at Z = 1.055. The tangential turbulence intensity distribution in Figure 3.20b is almost uniform for all the radial locations. Also, the T_θ values are very much lower than those at the last station inside the rotor passage. The leakage flow effects vanish very rapidly outside the passage. Figure 3.20a shows that T_z decreases near the blade surface and increases towards the middle of the passage for two radial locations near the blade tip while the stations closer to the wall show more or less uniform mixing. The turbulence characteristics of the flow at Z = 1.179 as shown in Figure 3.21(a,b) are very similar to those at Z = 1.055.

At Z = 1.440 and Z = 1.593, the blade to blade variations of T_θ and T_z are almost uniform at all the radial locations. But the T_z component is nearly twice as large as the T_θ component at Z = 1.440. The trend towards achieving isotropic flow condition is reflected in the slowly decreasing axial turbulence intensity level. At Z = 1.73 (Figure 3.22) both the components of the turbulence intensities are of the same order and the blade to blade variation of these components is nearly uniform at all the radial locations. The turbulence intensities vary from 3 percent to 8.5 percent.

3.2.2 Iso-Turbulence Intensity Contours in the Z-θ Plane

The contours of equal intensities in the clearance region at $\bar{R}$ = 0.3125 and $\bar{R}$ = 0.125 are shown in Figures 3.23-3.26. Figures 3.23 and 3.24 show the iso-contours for axial turbulence intensity. The overall level of turbulence is slightly higher at $\bar{R}$ = 0.125 than that at $\bar{R}$ = 0.3125. In both cases peak intensities occur slightly away from the suction surface at Z = 0.50. Figures 3.25 and 3.26 show the iso-contours for tangential turbulence intensity for the same radial locations mentioned above. It can be observed from these figures that maximum flow interaction takes place in the tangential direction. Over a small axial distance from Z = -0.012 to Z = 0.003, a rapid change in the tangential turbulence intensity level is observed at $\bar{R}$ = 0.3125 as shown in Figure 3.26. Two pockets of high intensity are observed at approximately 1/3 and 2/3 of the passage near the leading edge. At $\bar{R}$ = 0.125 a similar rapid increase from Z = -0.012 to Z = 0.003 is observed but two small regions of high intensity are absent. At Z = 0.5 an overall increase in the level of turbulence intensities is observed.

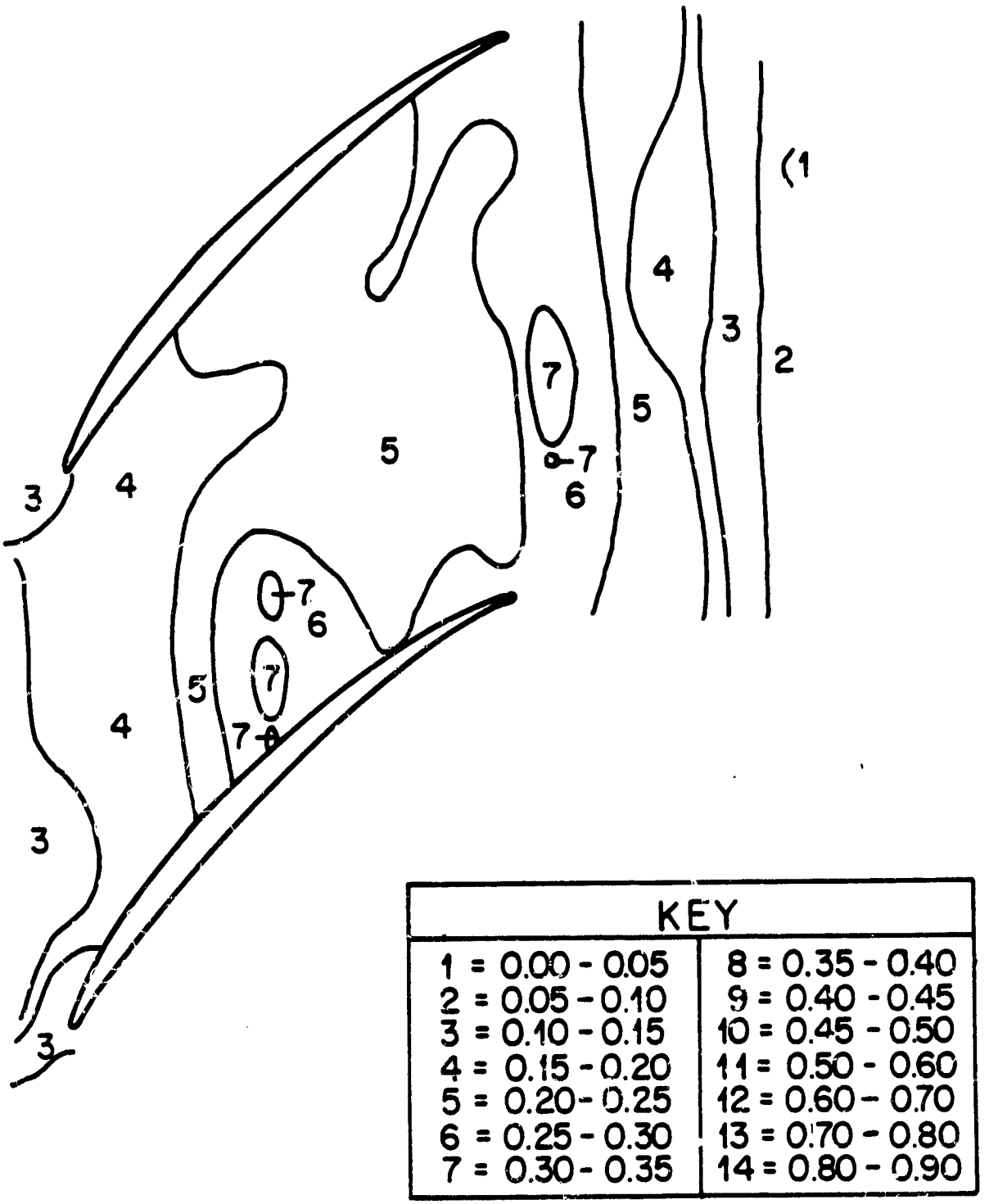

Figure 3.23 Iso-Contours for Axial Turbulence Intensity at $\bar{R}$ = 0.3125

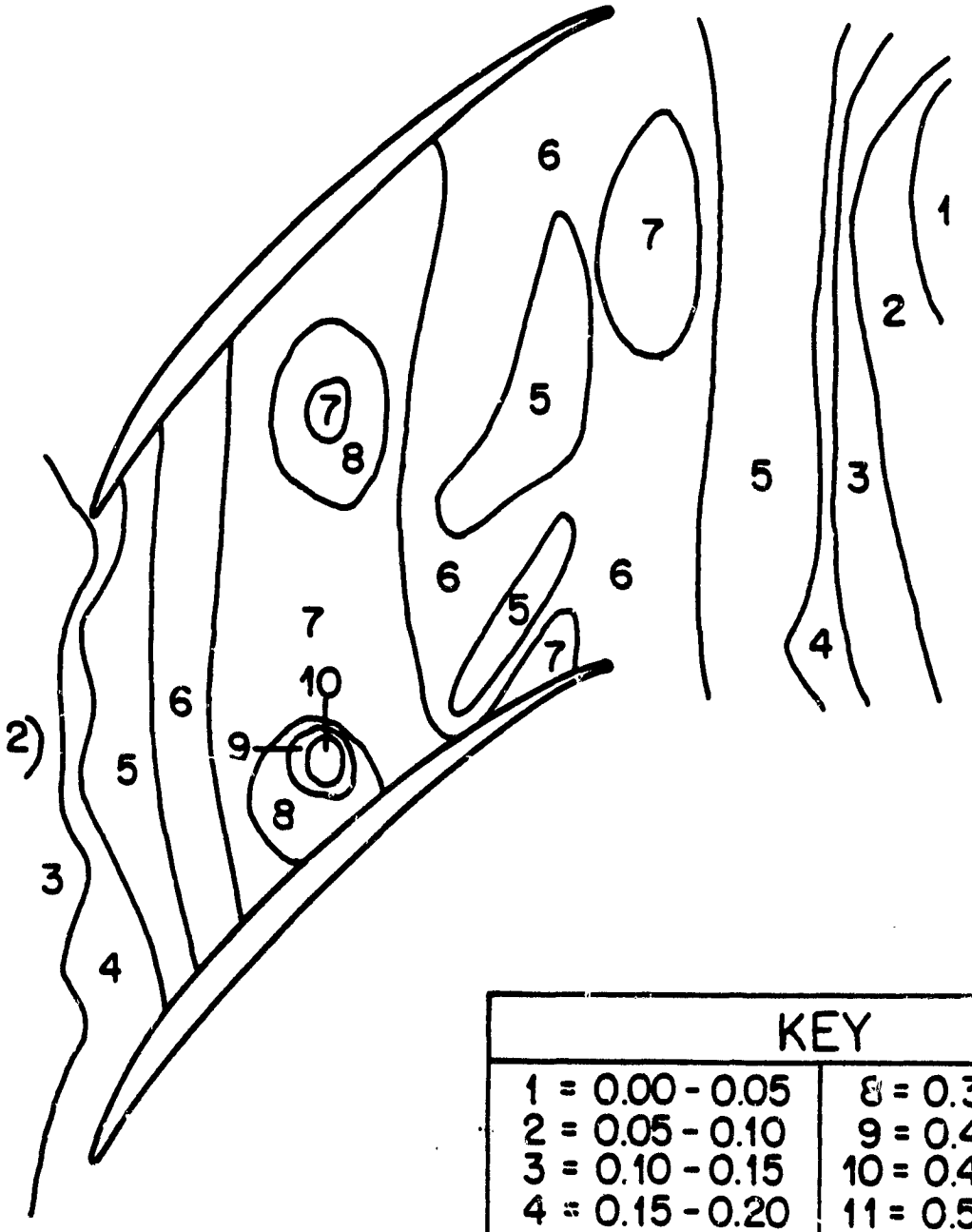

KEY	
1 = 0.00 - 0.05	8 = 0.35 - 0.40
2 = 0.05 - 0.10	9 = 0.40 - 0.45
3 = 0.10 - 0.15	10 = 0.45 - 0.50
4 = 0.15 - 0.20	11 = 0.50 - 0.60
5 = 0.20 - 0.25	12 = 0.60 - 0.70
6 = 0.25 - 0.30	13 = 0.70 - 0.80
7 = 0.30 - 0.35	14 = 0.80 - 0.90

Figure 3.24 Iso-Contours for Axial Turbulence Intensity at $\bar{R}$ = 0.125

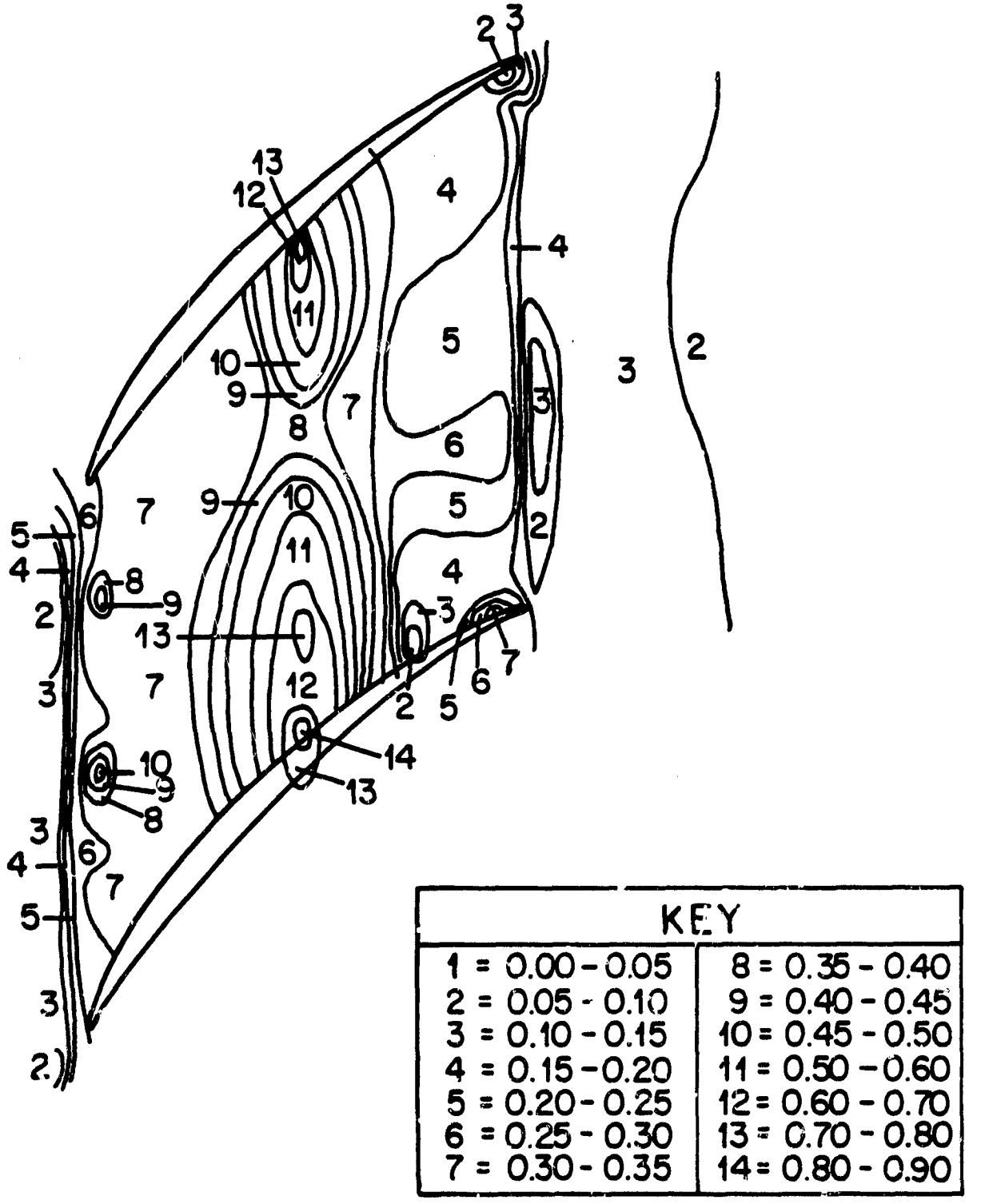

Figure 3.25 Iso-Contours for Tangential Turbulence Intensity at $\bar{R} = 0.3125$

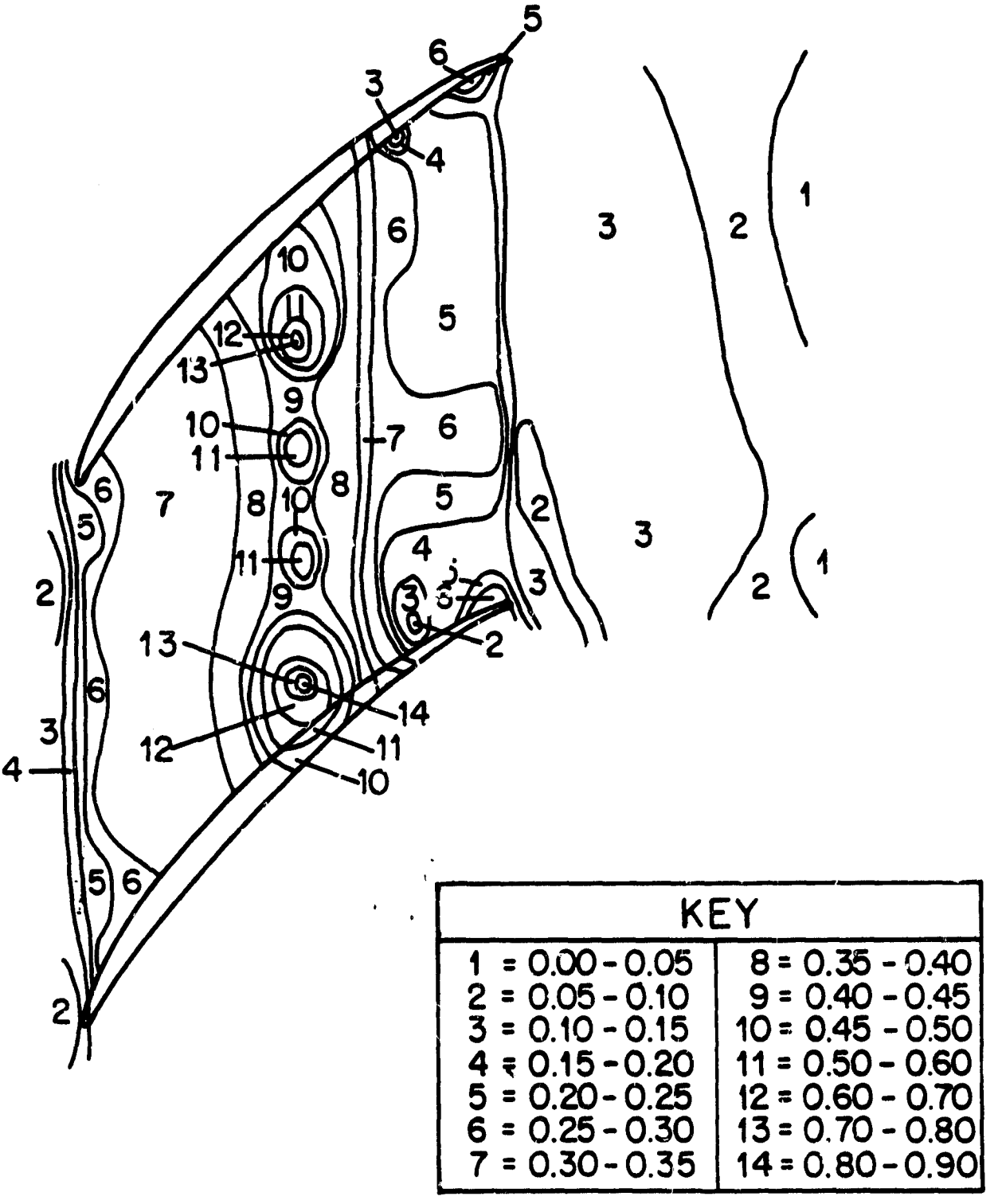

Figure 3.26 Iso-Contours for Tangential Turbulence Intensity at $\bar{R} = 0.125$

As explained earlier in this chapter, maximum leakage velocities and high level of mixing occur at Z = 0.5. At $\overline{R}$ = 0.125, peak intensities occur slightly away from the suction surface while at $\overline{R}$ = 0.3125 peak intensity level is observed inside the clearance region. At Z = 0.75, the low level of intensities inside the clearance region are in accordance with the earlier conclusion of the flow becoming almost laminar inside the clearance region.

The level of turbulence decreases as soon as the flow leaves the rotor passage.

CHAPTER IV

INTERPRETATION AND DISCUSSION OF THE EXPERIMENTAL RESULTS AT OFF-DESIGN CONDITION

Rotational motion of the compressor rotor is one of the factors that affect the leakage flow and the flow structure in the vicinity of the annulus-wall. The leakage flow is augmented by the rotation in the case of a compressor rotor. The rotation also induces centrifugal and coriollis forces which generate a spanwise flow in the blade boundary layer. This spanwise flow affects the leakage flow and its interaction with other flows in the annulus-wall region. Therefore, all the measurements reported in Chapter III were repeated at reduced r.p.m. in order to gain an understanding of the effect of rotation on the leakage flow development and its interaction with other flow structures. However, changing the r.p.m. changes the loading on the blade. Blade loading is another important parameter which affects the leakage flow. With the data presented here, it is not possible to isolate the effect of one parameter from that of the other. But the blade loading effect is anticipated to be a major reason for the changes observed. The blade loading was decreased in this case from $\overline{\psi} = 0.51$ to $\overline{\psi} = 0.375$.

4.1 Mean Flow Properties

Flowfield measurements were carried out at all the stations listed in Table 2.2 but the results at only those stations where the flowfield behavior differs significantly from the behavior at the design condition are presented and discussed in this section.

4.1.1 Velocity Profiles and Angles Inside the Tip Clearance Region

Figures 4.1, 4.2 and 4.3 show the variations of the mean flow properties at the inlet of the rotor, at half chord and at 3/4 chord, respectively. The notations and the conventions followed are the same as those followed in Chapter III for the flow properties at design condition. The static pressure distributions on the blade surface at $\phi = 0.55$ and $\phi = 0.60$ (measurements were carried out by N. Sitaram) shown in Figures 2.3 and 2.4 are also very useful in interpreting the results presented here.

It is clear from Figure 4.1(a,b,c) that the flow entering the compressor rotor is almost uniform. The axial velocity distribution shown in Figure 4.1a shows a slight nonuniformity for $\bar{r} = 0.375$ and 0.125. However, the actual magnitude of these fluctuations is only 7 percent and for all practical purposes the rotor inlet flow can be considered uniform. As shown in Figure 3.1, at design condition, the flow entering the rotor is distinctly affected by the unsteady flowfield downstream, though the perturbations are not very large. The absence of the effects of the unsteady flowfield propagating upstream at a higher flow coefficient and reduced r.p.m. may be attributed to the reduced loading on the rotor.

The major deviation in the flow properties at off-design condition can be observed in the relative magnitudes of the tangential velocities in stationary frame of reference. Comparing Figures 4.1b and 3.1b, it is evident that V_θ is considerably higher than W_z at the off-design condition, while at design condition V_θ and W_z are approximately the same order of magnitude. A similar trend in the radial

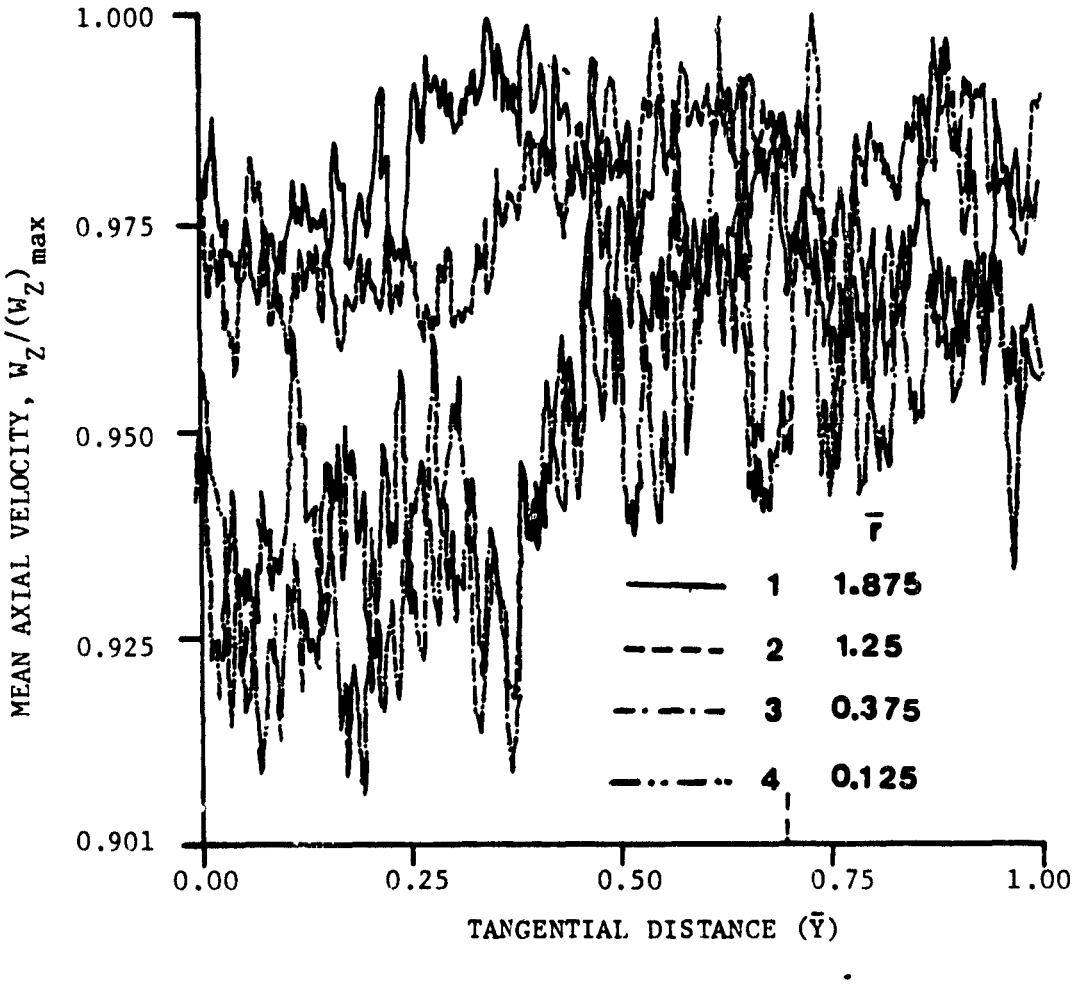

Figure 4.1a Variation of Mean Axial Velocity (Z = -0.012) at Off-Design Condition

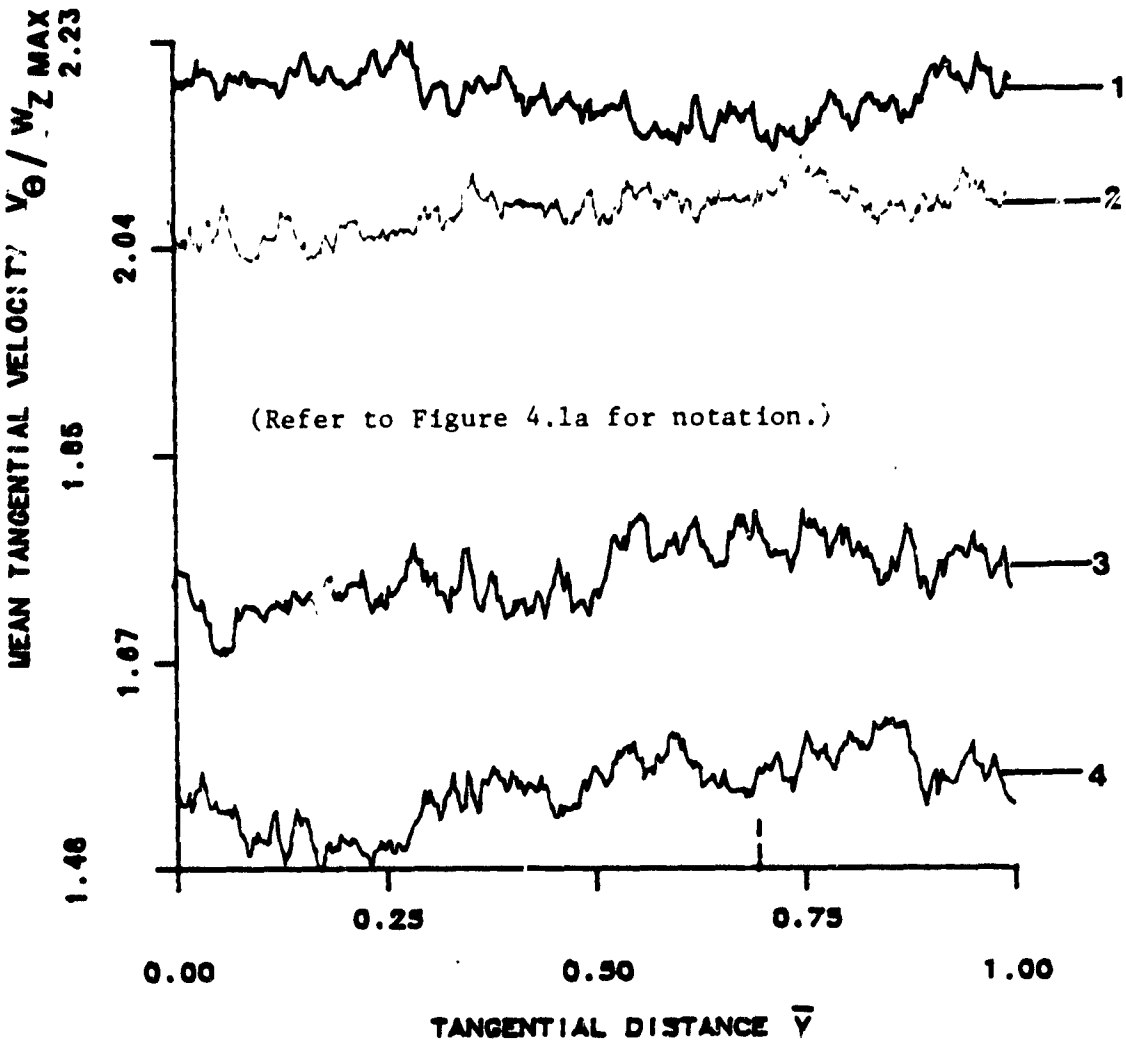

Figure 4.1b Variation of Mean Tangential Velocity (Z = -0.012) at Off-Design Condition

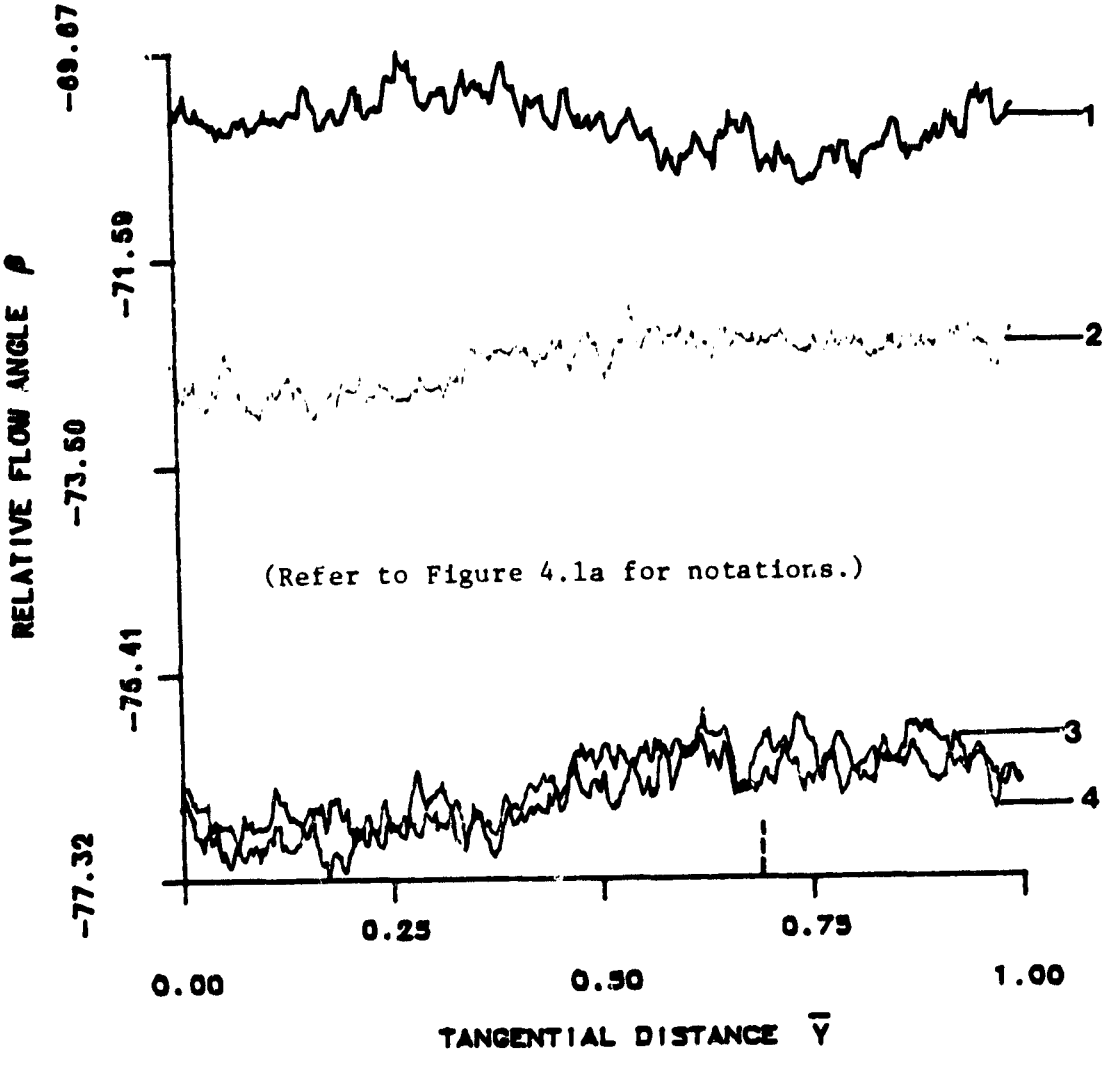

Figure 4.1c Variation of Relative Flow Angle (Z = -0.012) at Off-Design Condition

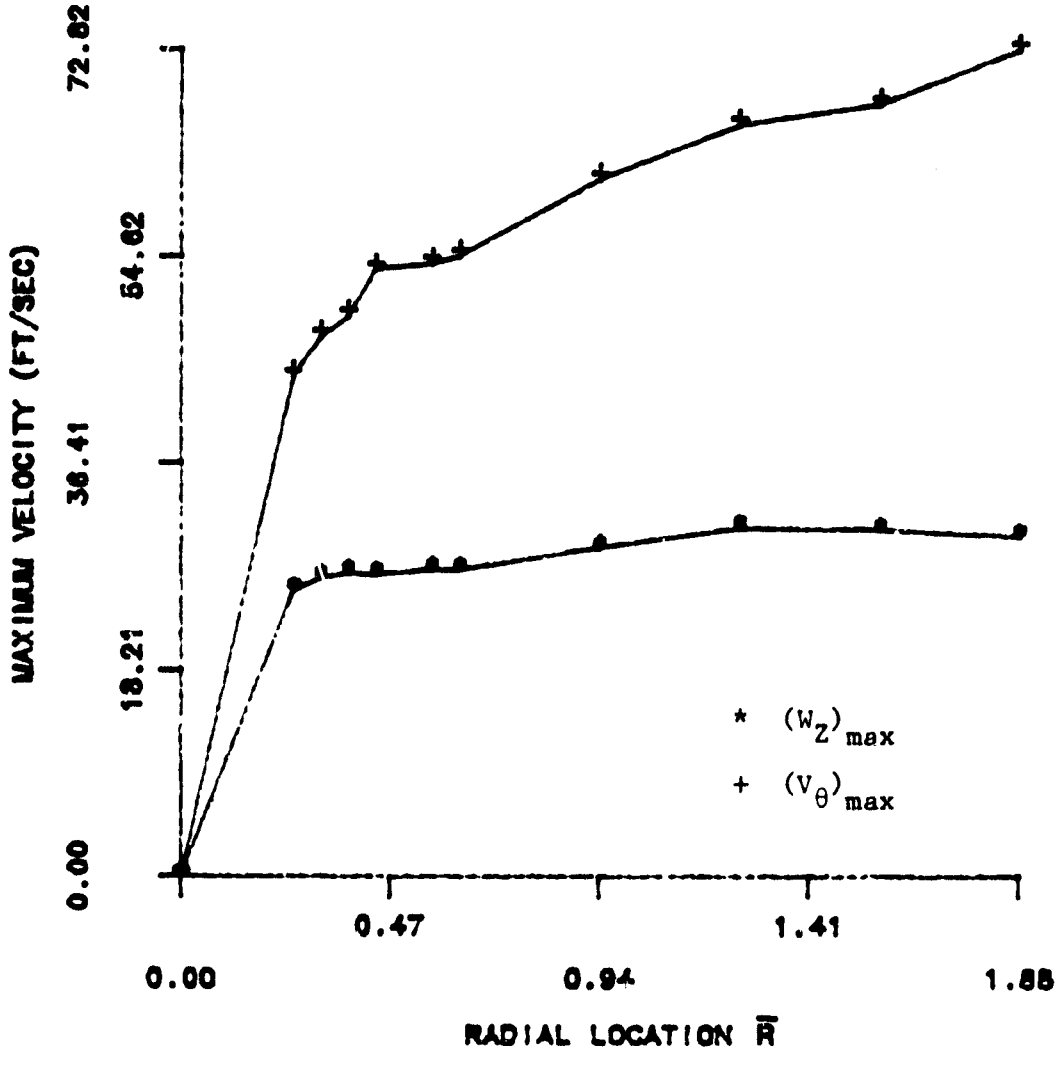

Figure 4.1d Variation of Maximum Axial and Tangential Velocities (Z = -0.012) at Off-Design Condition

variations of $(W_z)_{max}$ and $(V_\theta)_{max}$ (Figure 4.1d) is also observed. The magnitude of the relative flow angle β is slightly higher than that observed at the design condition for all the radial locations.

The variations in W_z, V_θ and β near the leading edge are very similar to those exhibited at the design condition. The only difference is in the relative magnitude of the tangential velocity which is considerably higher than the axial velocity. Since the incoming flow is highly skewed, such a behavior is expected.

Figure 4.2 shows the mean flow properties at Z = 0.50. From Figure 4.2a it is obvious that the flow is more stabilized than the flow observed from Figure 3.3a. At $\bar{r}$ = 0.625, the radial station closest to the blade tip, a well behaved leakage flow is indicated by a decrease in the axial velocity. This effect is absent at the radial stations away from the blade tip. As explained in Chapter III, the low velocity regions and a sudden variation in the velocity at the design condition is probably due to the flow separation. In the present case, the velocities and the blade loading are lower than the corresponding values at the design condition and hence the flow separation manifested by erratic changes in the axial velocity is absent. Variations in V_θ as shown in Figure 4.2b also indicate a decrease in the tangential velocity inside the clearance region at $\bar{r}$ = 0.625. Figure 4.2c shows that blade to blade variation of β at $\bar{r}$ = 0.125, 0.3125 and 0.5 is uniform. Comparing Figure 4.2c with Figure 3.3c it is obvious that the flow underturning is much higher at the off-design condition. Such a large underturning can be attributed to the highly skewed incoming flow. The magnitudes of $(W_z)_{max}$ and

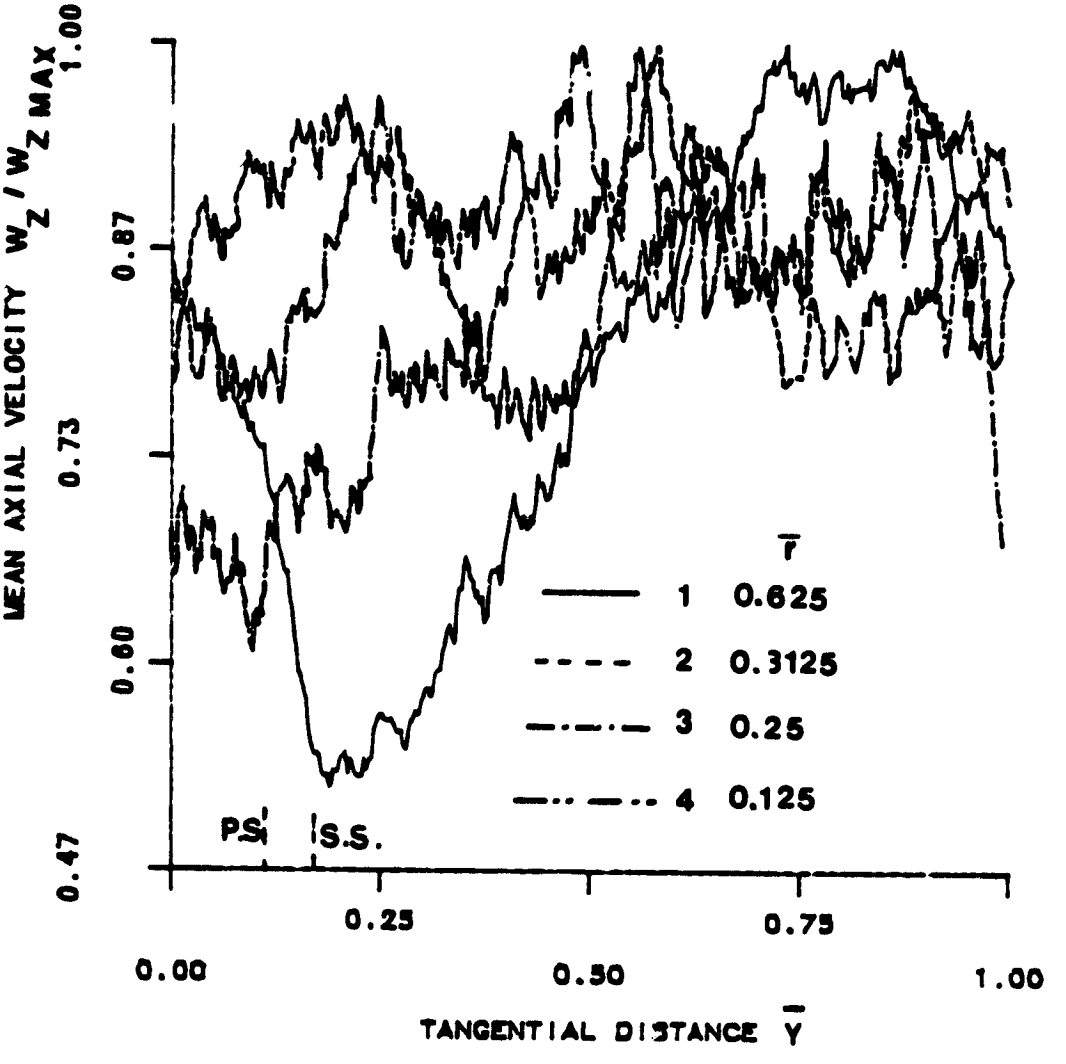

Figure 4.2a Variation of Mean Axial Velocity (Z = 0.50) at Off-Design Condition

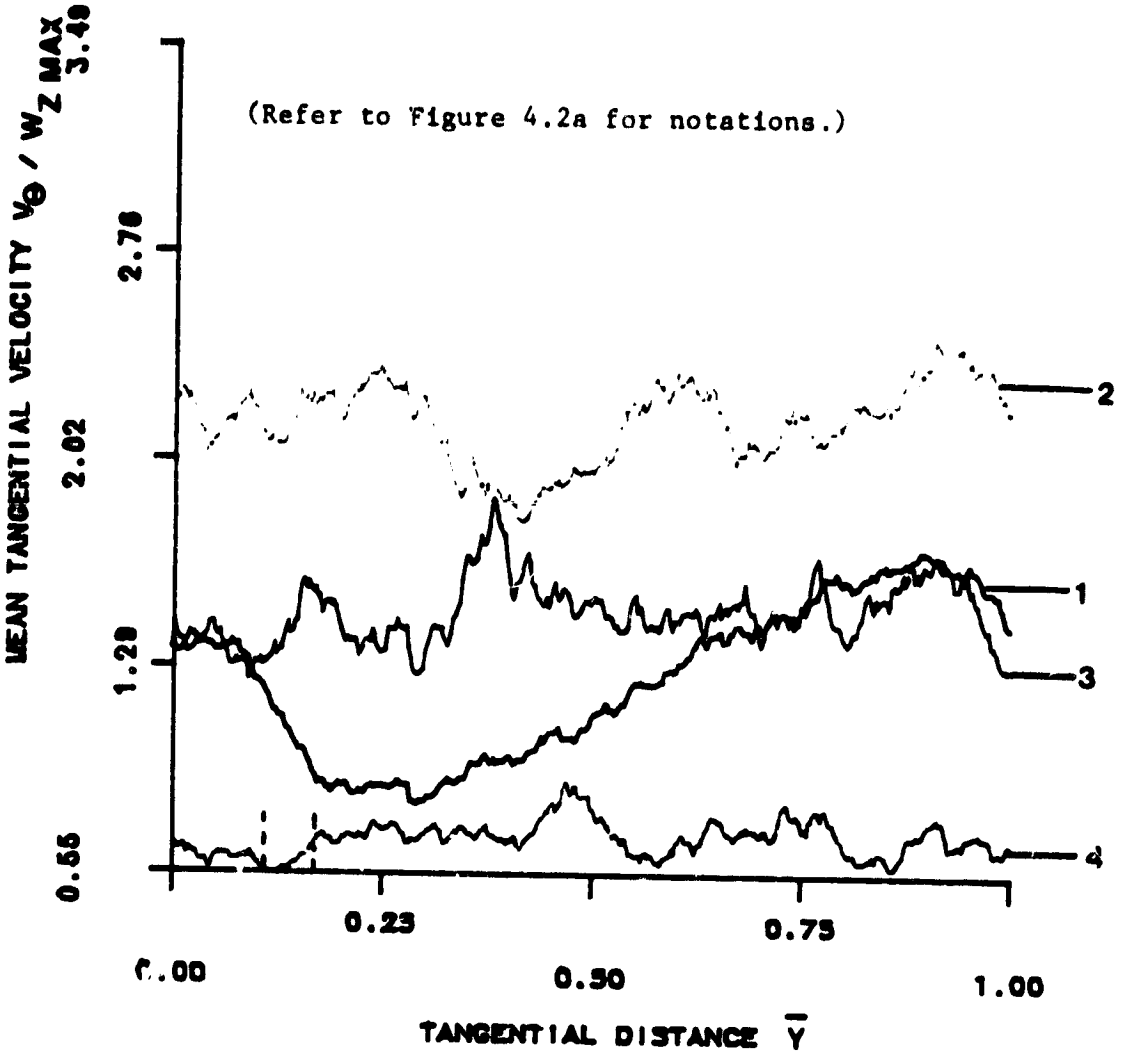

Figure 4.2b Variation of Mean Tangential Velocity (Z = 0.50) at Off-Design Condition

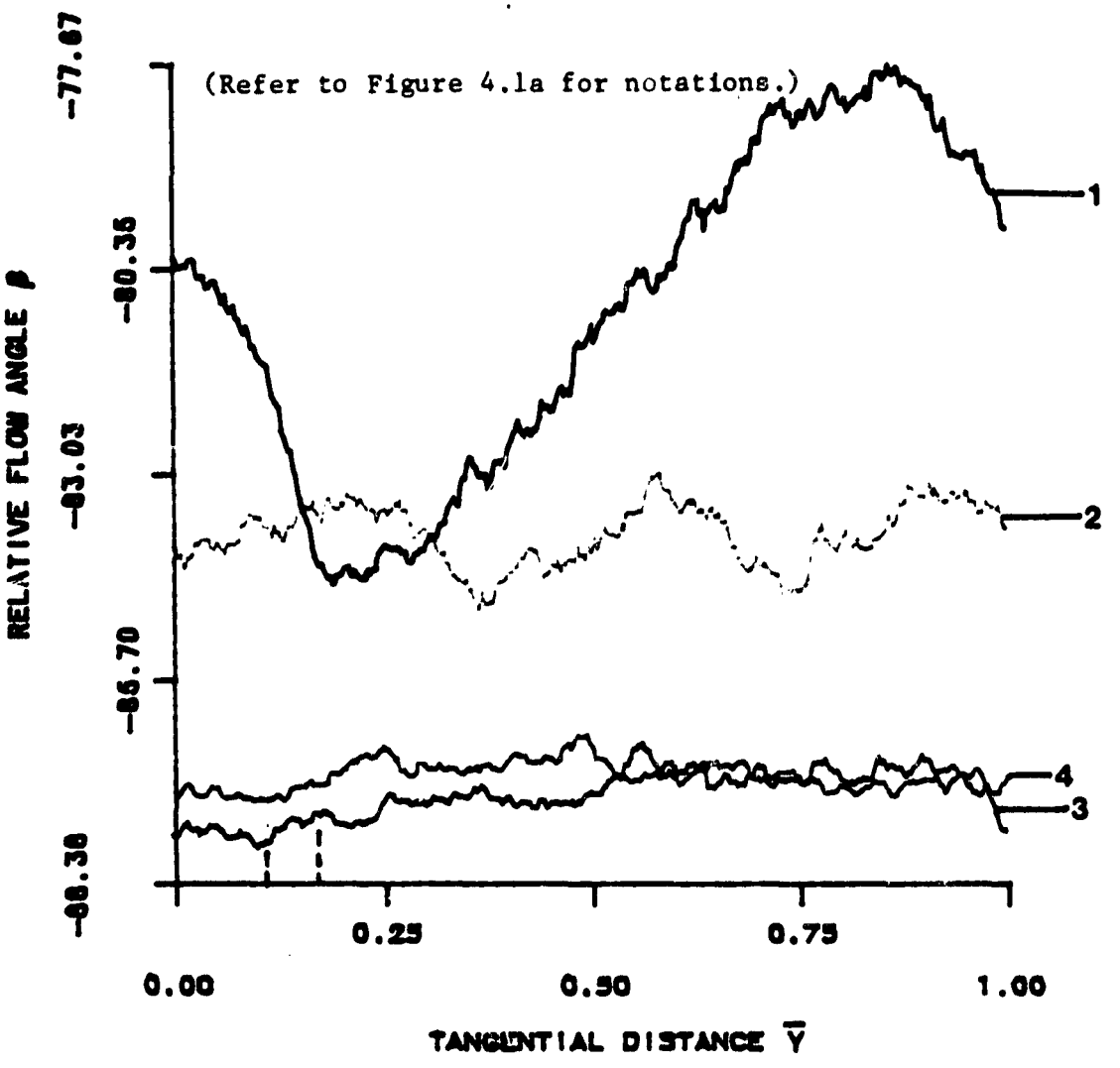

Figure 4.2c Variation of Relative Flow Angle (Z = 0.50) at Off-Design Condition

C - 2

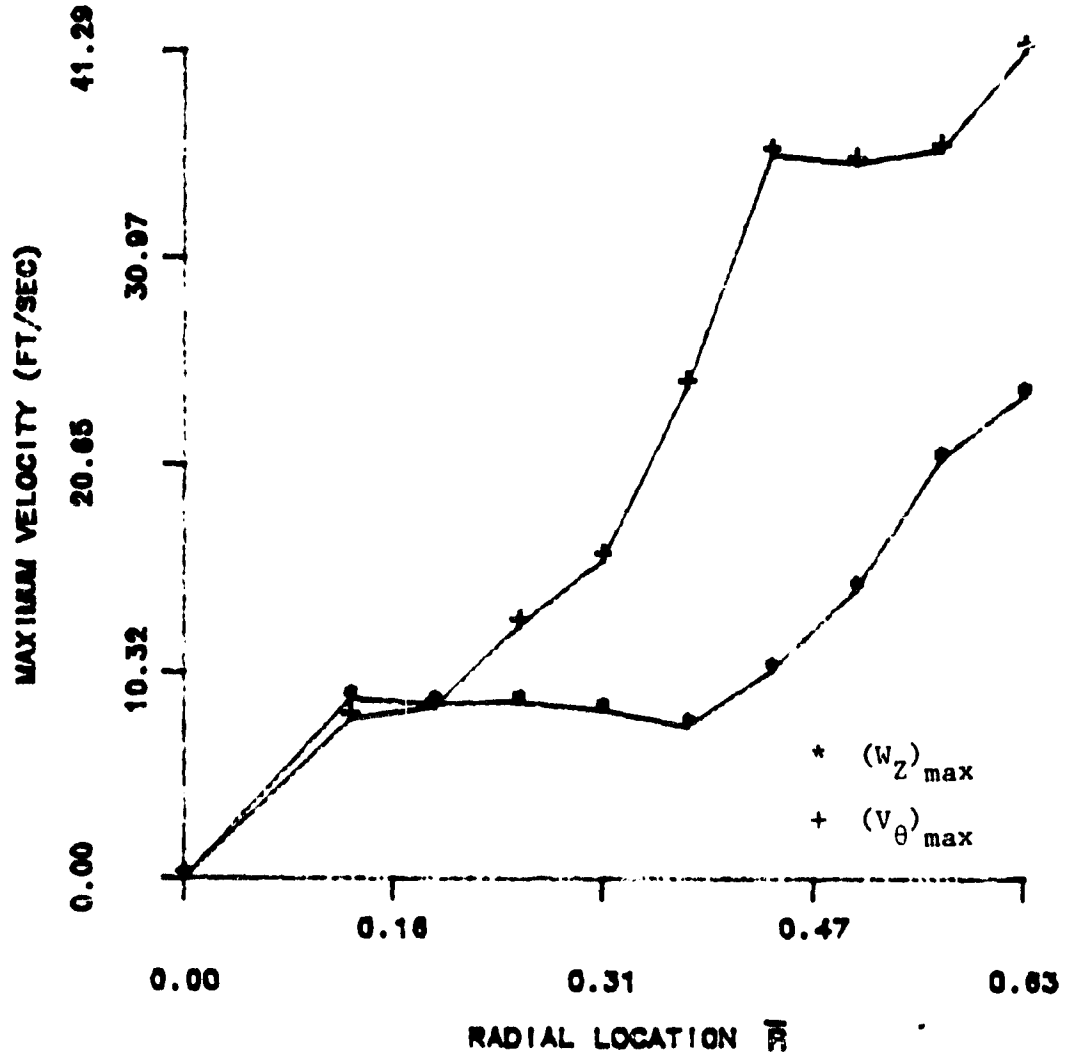

Figure 4.2d Variation of Maximum Axial and Tangential Velocities ($\bar{Z}$ = 0.50) at Off-Design Condition

$(V_\theta)_{max}$ shown in Figure 4.2d are considerably lower than those shown in Figure 3.3d.

The regular behavior of the flow at this station in comparison with the flow behavior at the design condition can also be explained in terms of the pressure distribution. Figure 2.3 and 2.4 show pressure distribution on the blade surface at various radial locations for $\phi = 0.55$ and $\phi = 0.60$, respectively. Considering the region between Z = 0.4 and Z = 0.5 in both these figures, it can be observed that at the radial locations far away from the blade tip, the loading at $\phi = 0.55$ is higher than that at $\phi = 0.60$. But near the blade tip the loading at $\phi = 0.55$ is lower than that at $\phi = 0.60$. High leakage velocities produce vortex due to rolling up of the leakage flow and intense interaction with annulus-wall boundary layer. Because of this the flow behavior is highly irregular at design condition. In the case of off-design condition, though the loading is reduced, the retained loading at the tip is higher than that at design condition. Hence, low leakage velocities are indicated which explain the regular flow behavior observed in Figure 4.2.

The flow behavior at Z = 0.75 and Z = 0.979 are very similar at both the flow coefficients. Figure 4.3 shows the variation of mean properties at Z = 0.75. One interesting feature of the flow can be observed in Figure 4.3b. Unlike the V_θ variation at design condition, where a clearly defined minimum in the velocity is observed at 2/3 of the passage width away from the suction surface (Figure 3.6b), no such clearly defined peaks and dips in the velocity are observed except in the tip clearance. This indicates the absence of rolling vortex. Low

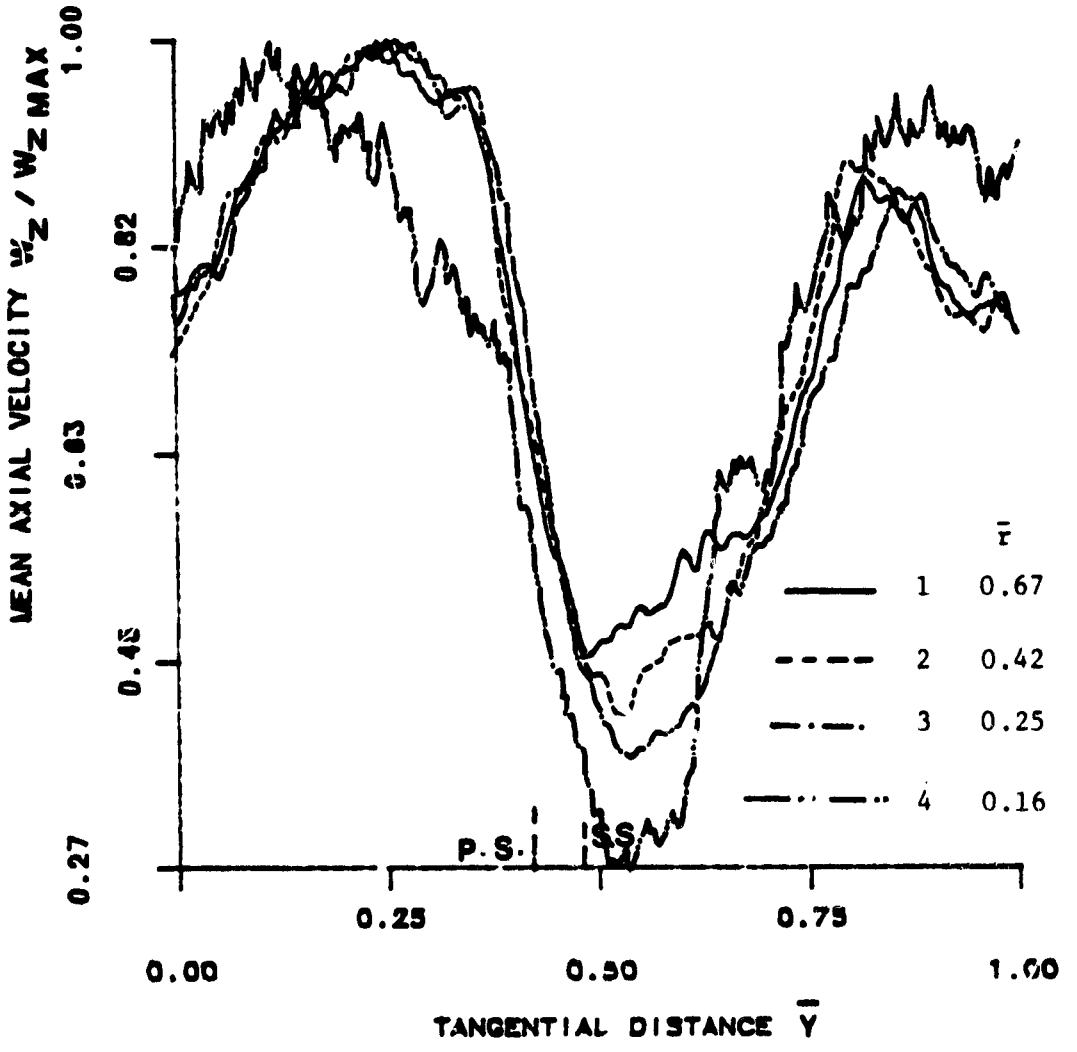

Figure 4.3a Variation of Mean Axial Velocity (Z = 0.75) at Off-Design Condition

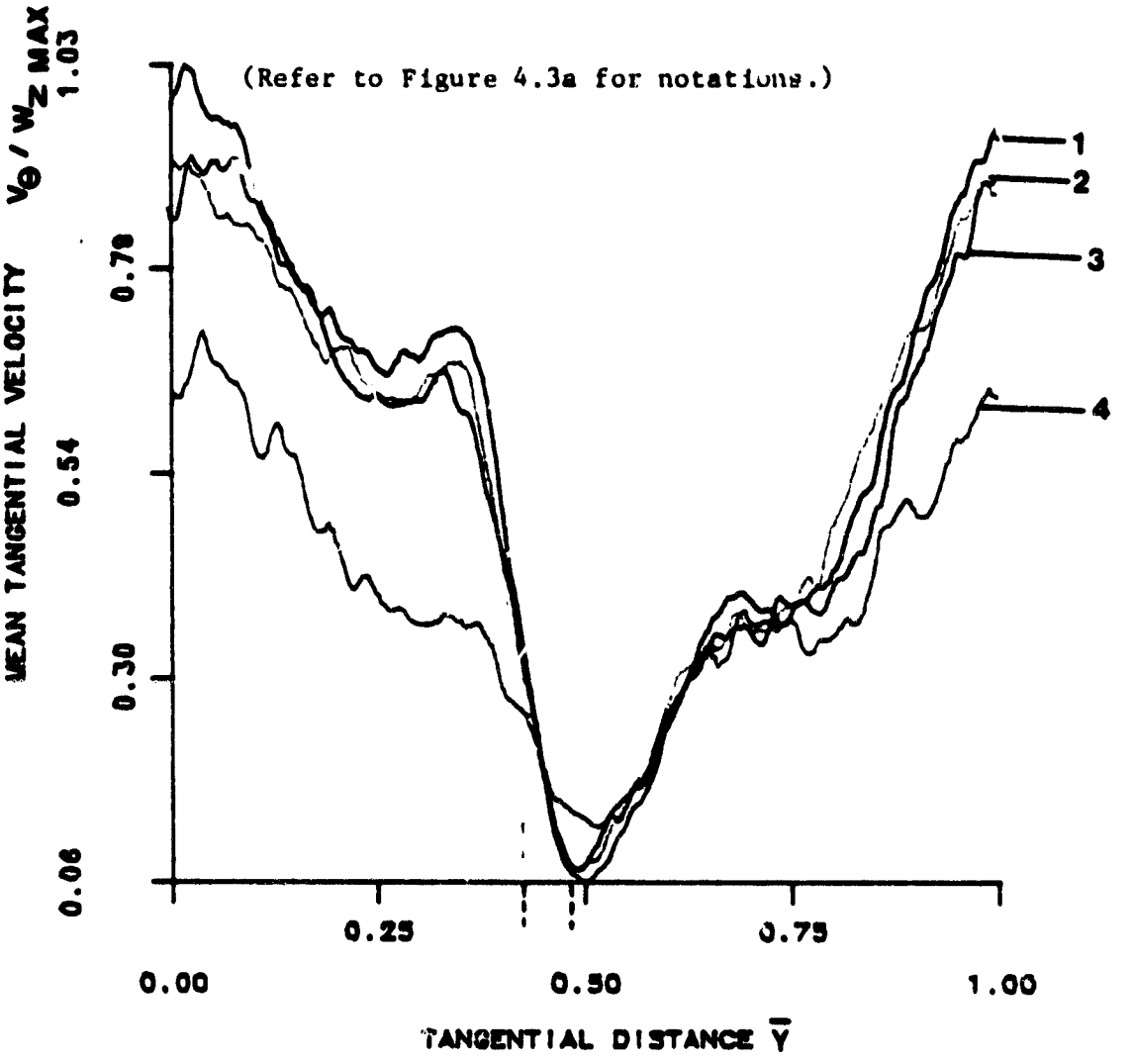

Figure 4.3b Variation of Mean Tangential Velocity (Z = 0.75) at Off-Design Condition

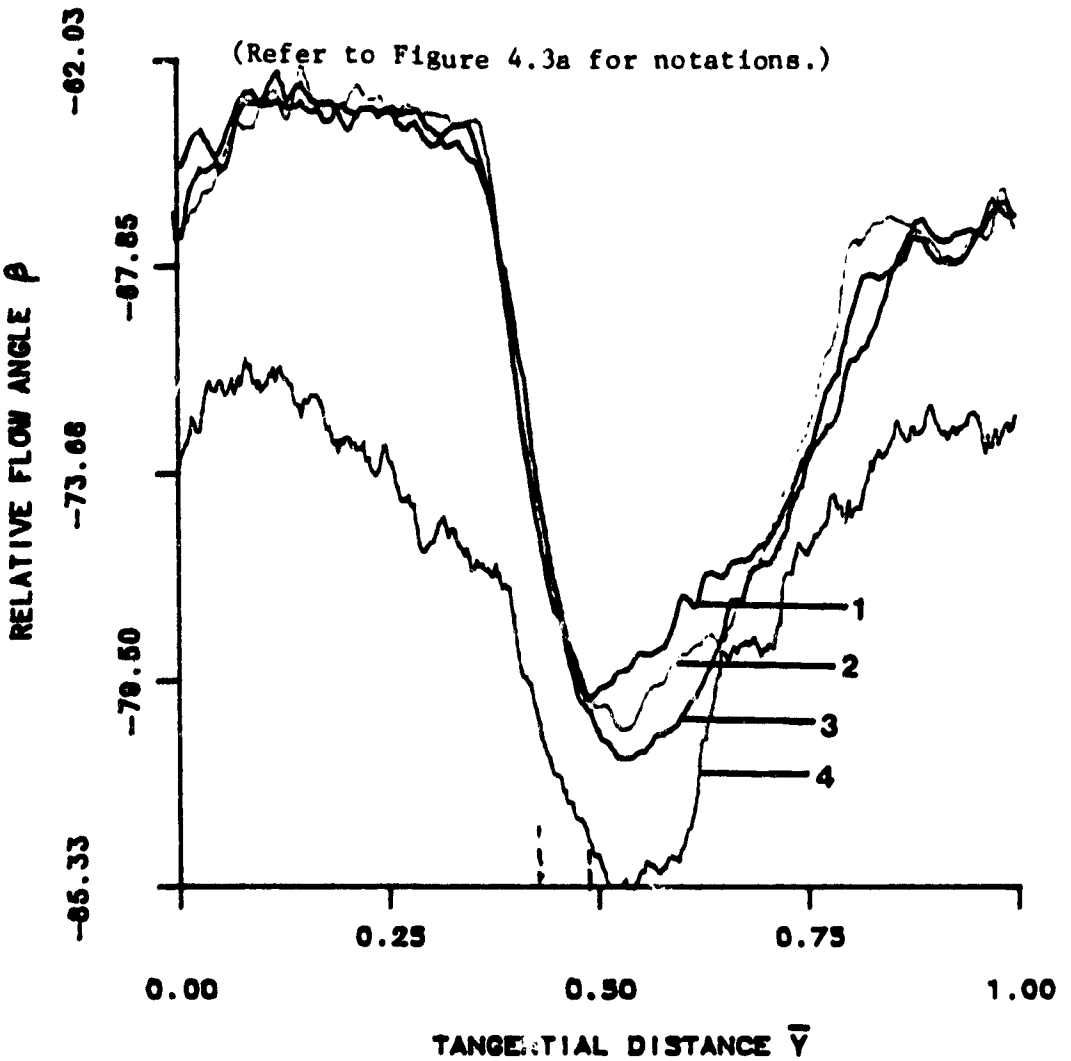

Figure 4.3c Variation of Relative Flow Angle (Z = 0.75) at Off-Design Condition

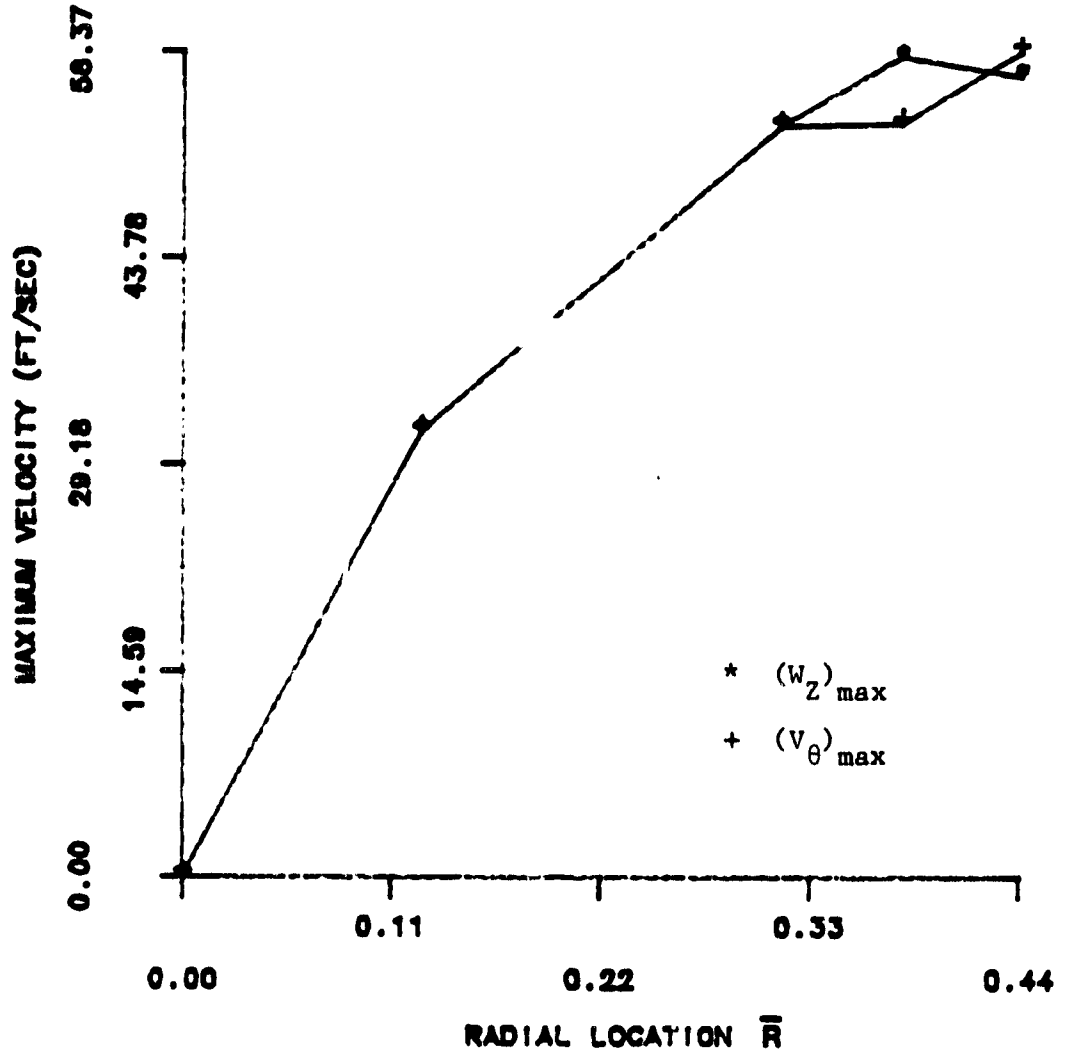

Figure 4.3d Variation of Maximum Axial and Tangential Velocities (Z = 0.75) at Off-Design Condition

leakage velocities due to reduced loading and lower r.p.m. do not permit the leakage flow to travel far away from the suction surface. Instead, it merely diffuses in the mainstream. The number of samples used for ensemble averaging was much smaller in the case of data at $\bar{r}$ = 0.16. Hence, the curves for $\bar{r}$ = 0.16 do not overlap the curves for other three radii.

4.1.2 Velocity Profiles and Angles at the Exit of the Rotor

The rotor exit flow at the off-design condition shows a considerable deviation from the flow at design condition. Figure 4.4 shows the variations in V_z, V_θ and β at Z = 1.055. The interesting features of the flow are observed in Figure 4.4a showing W_z variation. At $\bar{r}$ = 0.83 and 0.42 the variation in W_z is only 4 percent. At $\bar{r}$ = 0.67 the variation in W_z is about 8.1, and it shows a dip in the velocity near the blade. However, the variation is very small and the flow can be considered almost uriform for $\bar{r}$ = 0.83, 0.67 and 0.42. But at $\bar{r}$ = 0.25 a distinct wake-like profile is observed. It can be inferred that the leakage flow interaction is very high in the region near the blade tip. Hence, the wake structure is completely destroyed. At $\bar{r}$ = 0.25 the leakage flow influence is not felt, since the flow has a tendency to move radially downward and a wake-like profile (the flow has not moved over a solid surface) is observed. In the case of design condition data at this station, the radial locations closer to the blade tip showed a wake-like profile while the stations close to the annulus-wall indicated a region of intense interaction among the leakage flow and annulus-wall boundary layer and the wake. Since the leakage velocities are considerably higher, due to higher loading, further

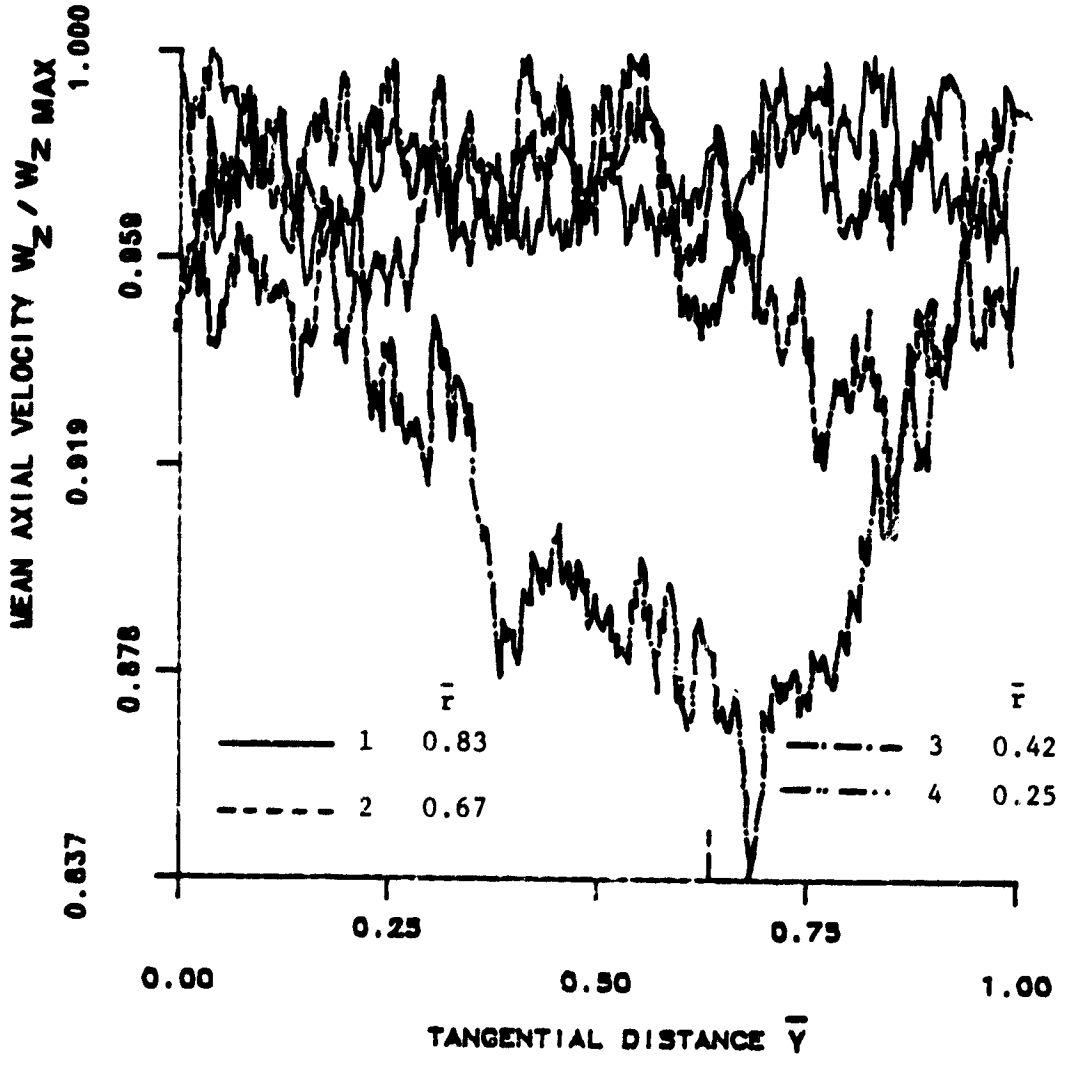

Figure 4.4a Variation of Mean Axial Velocity (Z = 1.055) at Off-Design Condition

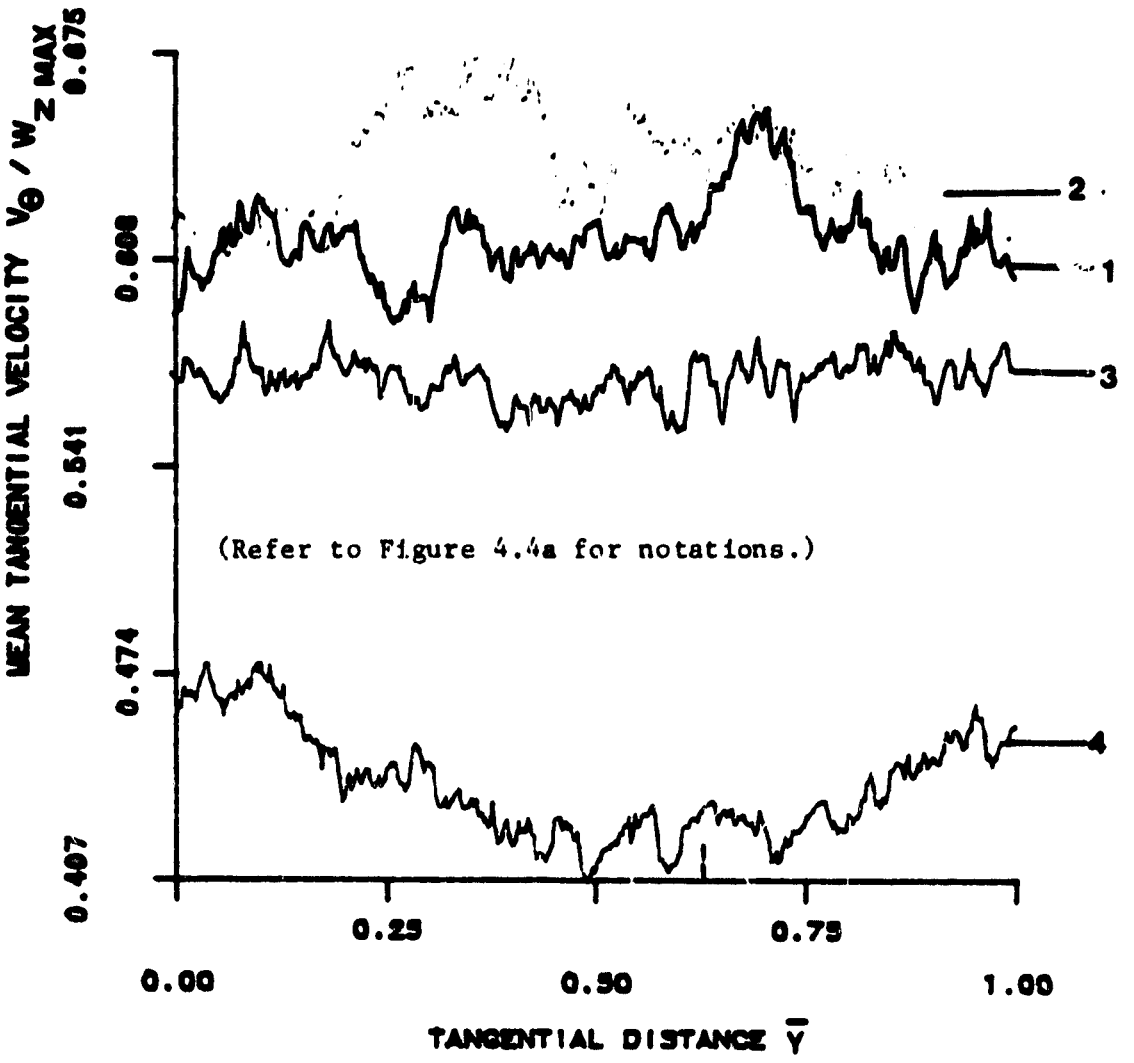

Figure 4.4b Variation of Mean Tangential Velocity (Z = 1.055) at Off-Design Condition

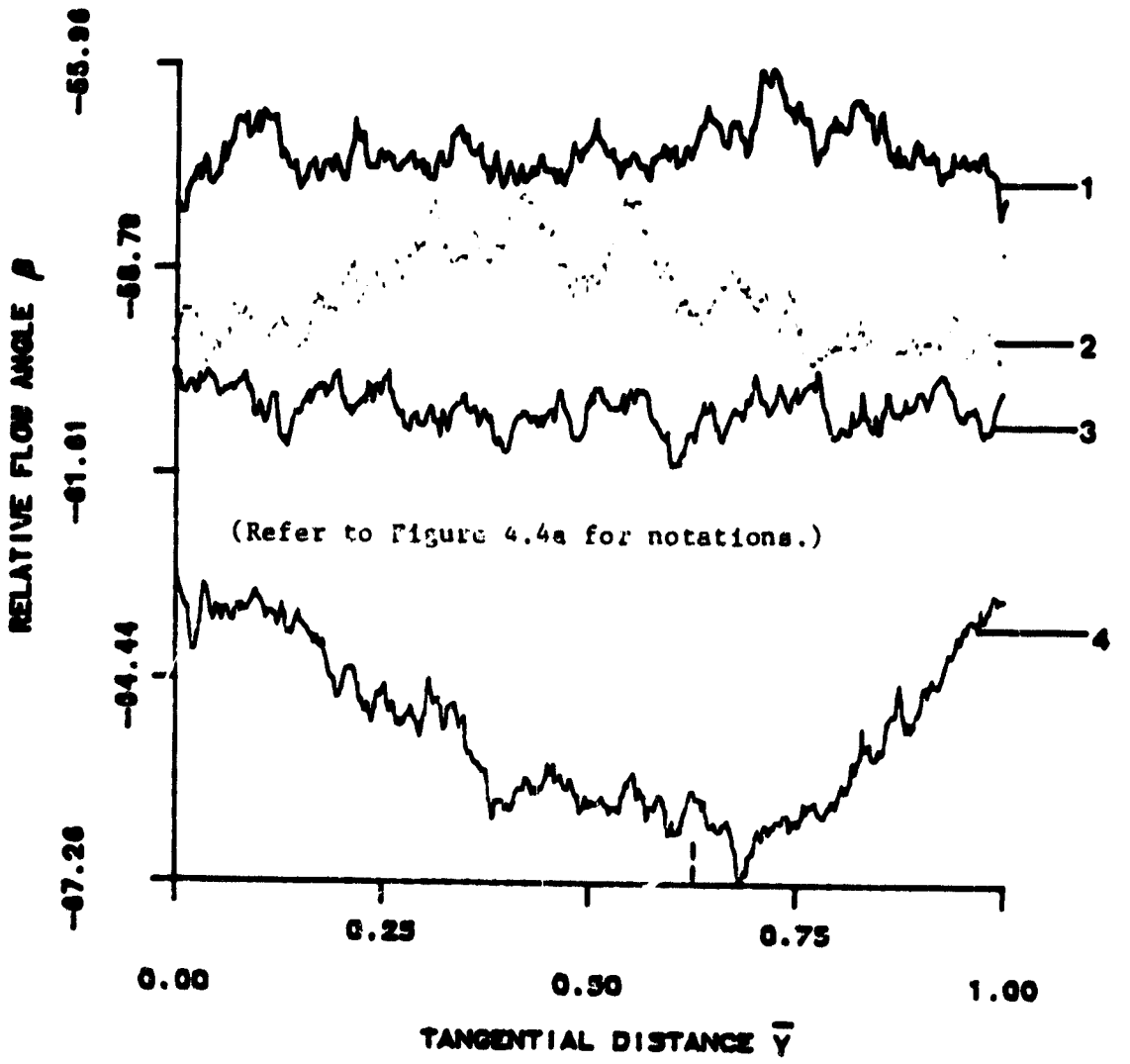

Figure 4.4c Variation of Relative Flow Angle (Z = 1.055) at Off-Design Condition

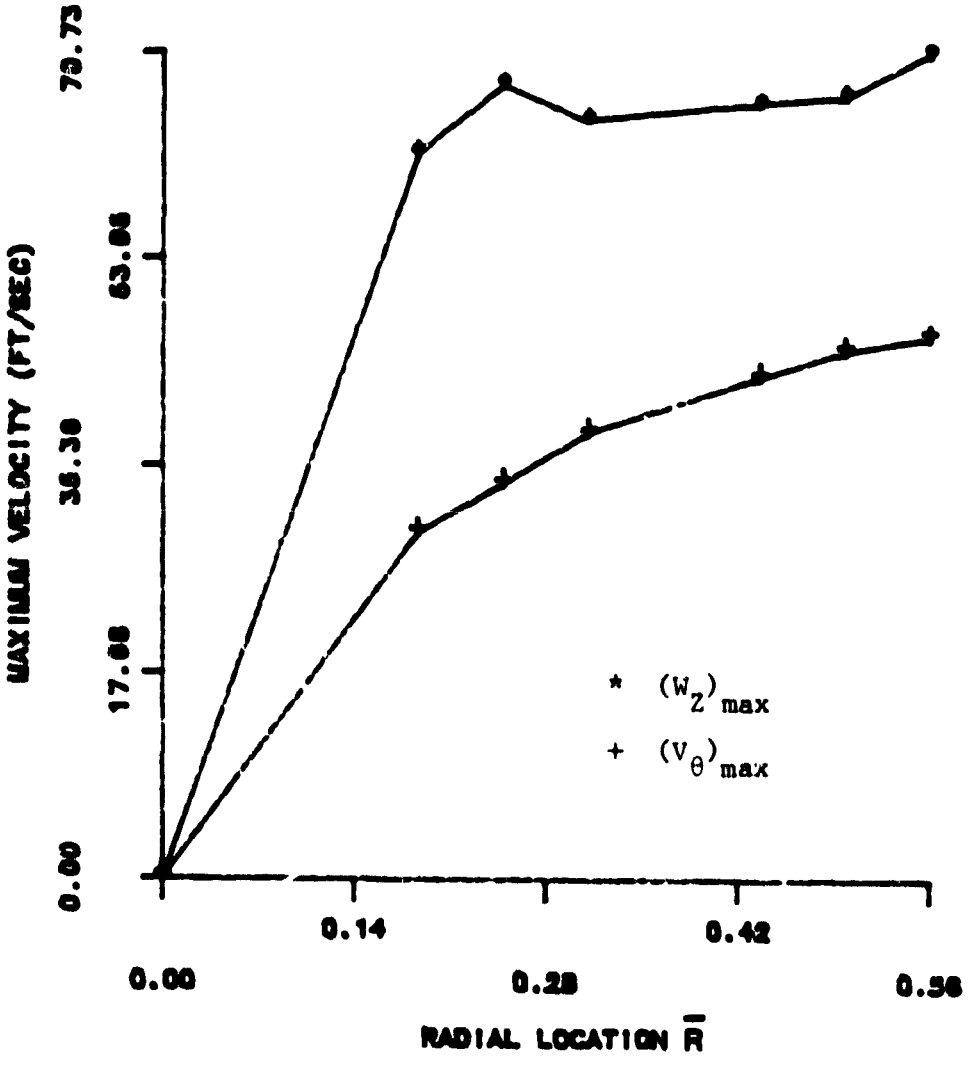

Figure 4.4d Variation of Maximum Axial and Tangential Velocities (Z = 1.055) at Off-Design Condition

augmented by higher r.p.m., the leakage flow moves farther away from the blade at the same radial location before rolling downwards. Hence, the wake is completely destroyed in the region very close to the wall. At off-design conditions, the leakage flow is weak and starts rolling up and moving downwards as soon as it leaves the rotor passage. Hence, the velocity profiles at the radial locations near the blade tip indicate the region of intense flow interaction.

At Z = 1.179, 1.440 and 1.593, the variations of W_z show characteristic wake profiles (Figures 4.5, 4.6, 4.7) for all the radial locations with the wake spreading as the radial locations get closer to the annulus-wall. At the design condition, the flow was found to be uniform at all these stations. A strong leakage flow at the design condition completely destroys the wake structure. At reduced loading (ϕ = 0.60) the leakage flow is comparatively weak which simply diffuses in the main stream, and the characteristics of the rotor wake are preserved as indicated in Figures 4.5, 4.6 and 4.7.

The flow at Z = 1.731 is almost uniform with the maximum variation of 7 percent in W_z. However, there is a considerable difference in the two components of the velocities.

4.1.3 Leakage Velocity Profiles

Figure 4.8 shows the variation of the leakage velocity at the suction surface ($W_N - W_{N_o}$) for four axial stations inside the rotor passage. As expected, the leakage velocities are smaller than the leakage velocities at design conditions. There is a sudden increase in the leakage velocities from Z = 0.003 to Z = 0.5, after which the velocities show a decreasing trend towards the trailing edge

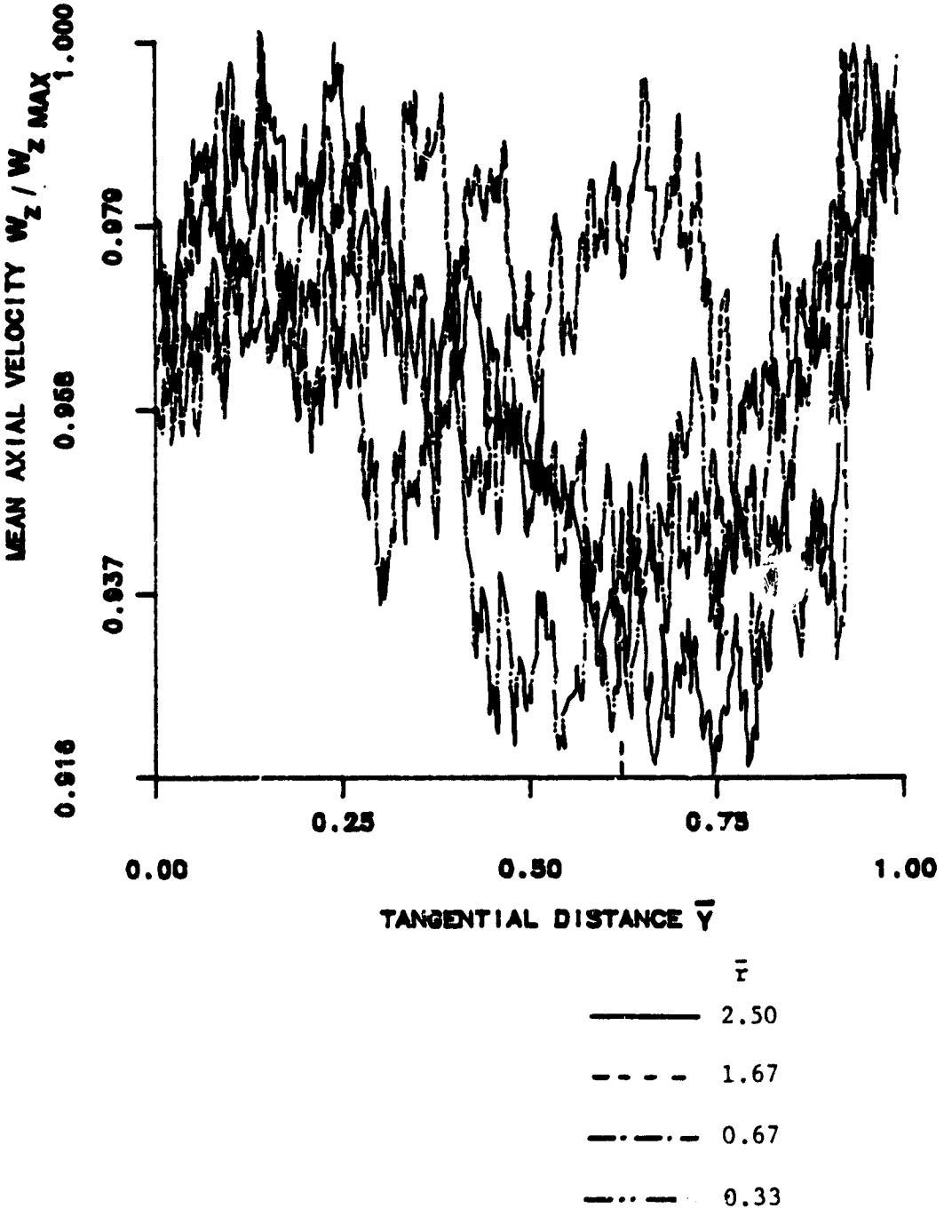

Figure 4.5 Variation of Mean Axial Velocity ($\bar{Z}$ = 1.179) at Off-Design Condition

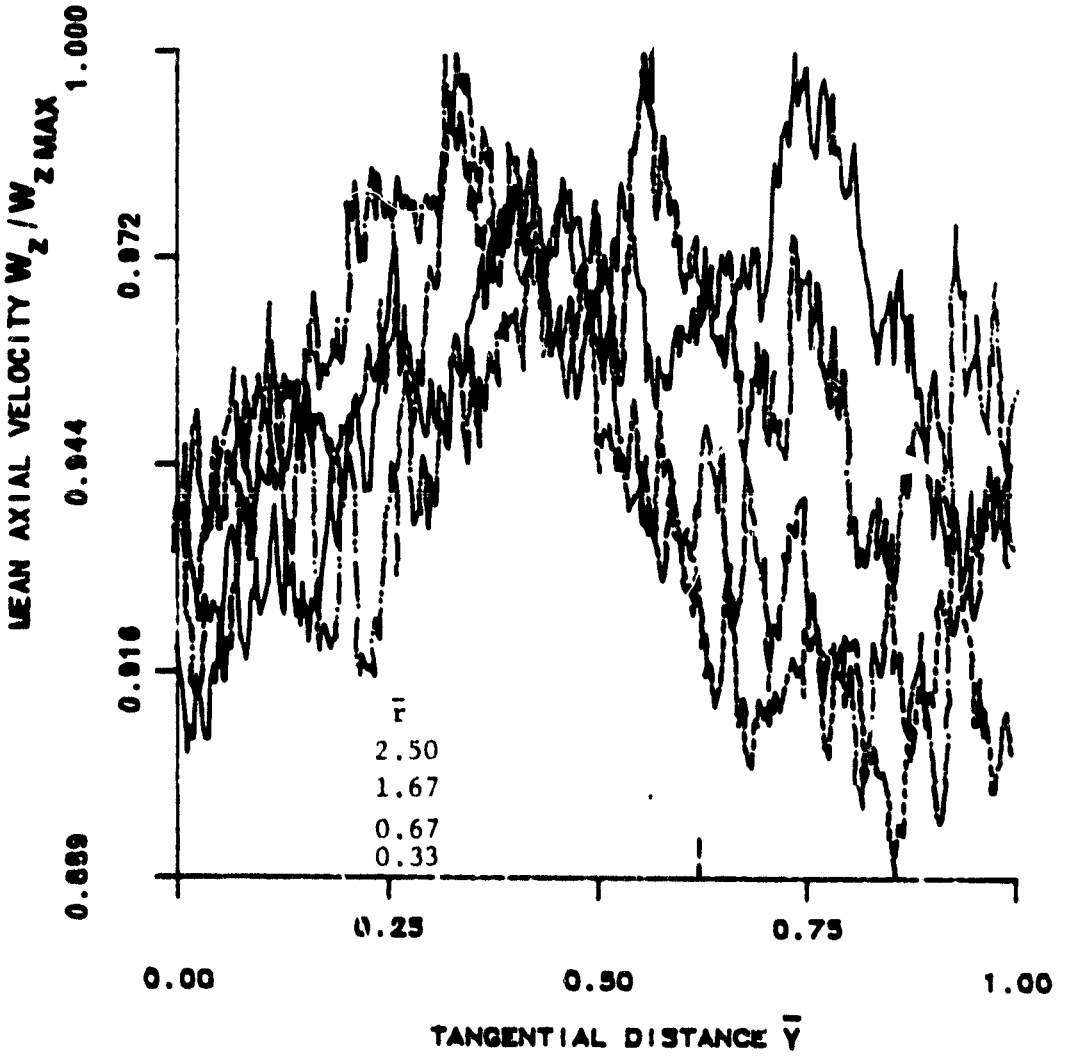

Figure 4.6 Variation of Mean Axial Velocity (Z = 1.440) at Off-Design Condition

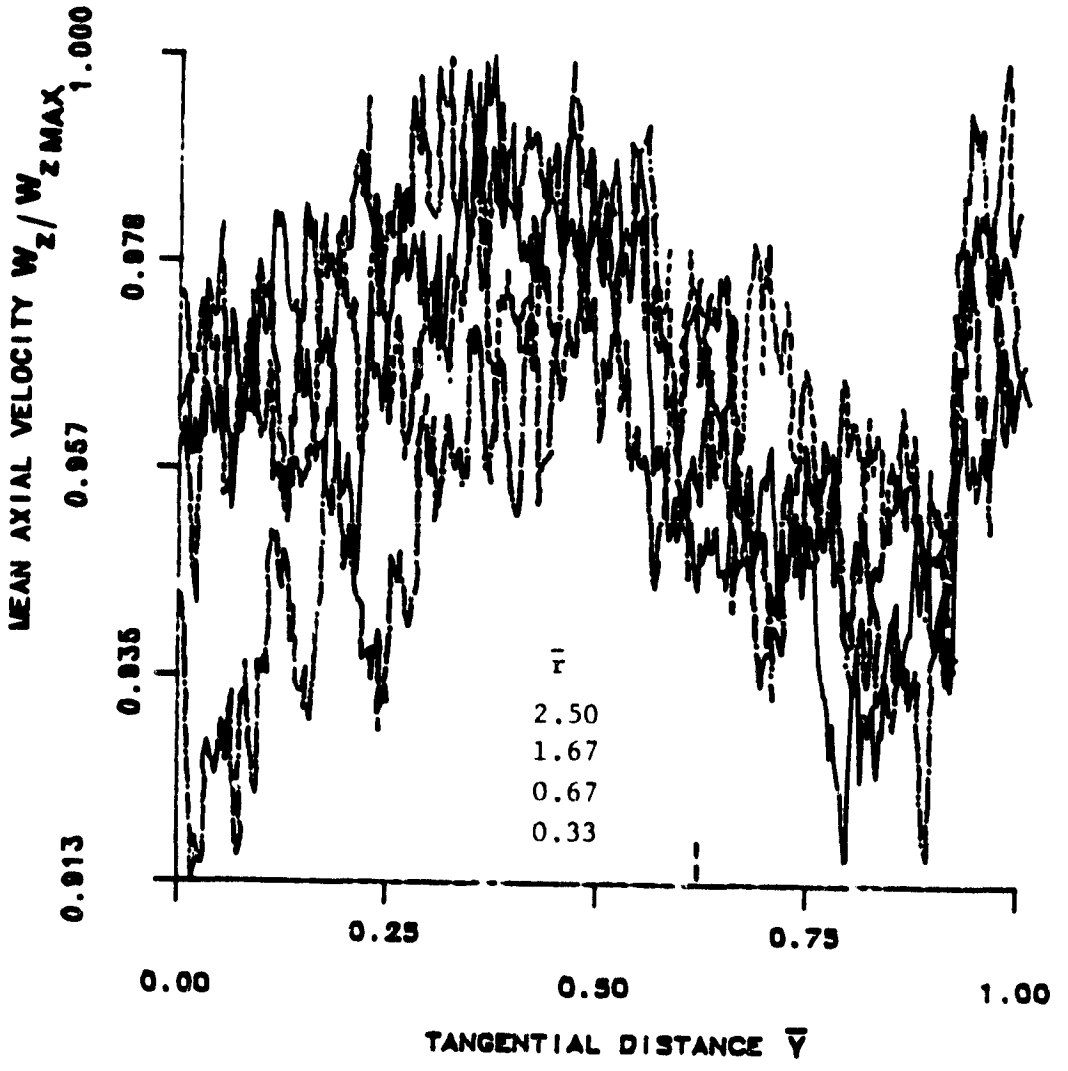

Figure 4.7 Variation of Mean Axial Velocity (Z = 1.593) at Off-Design Condition

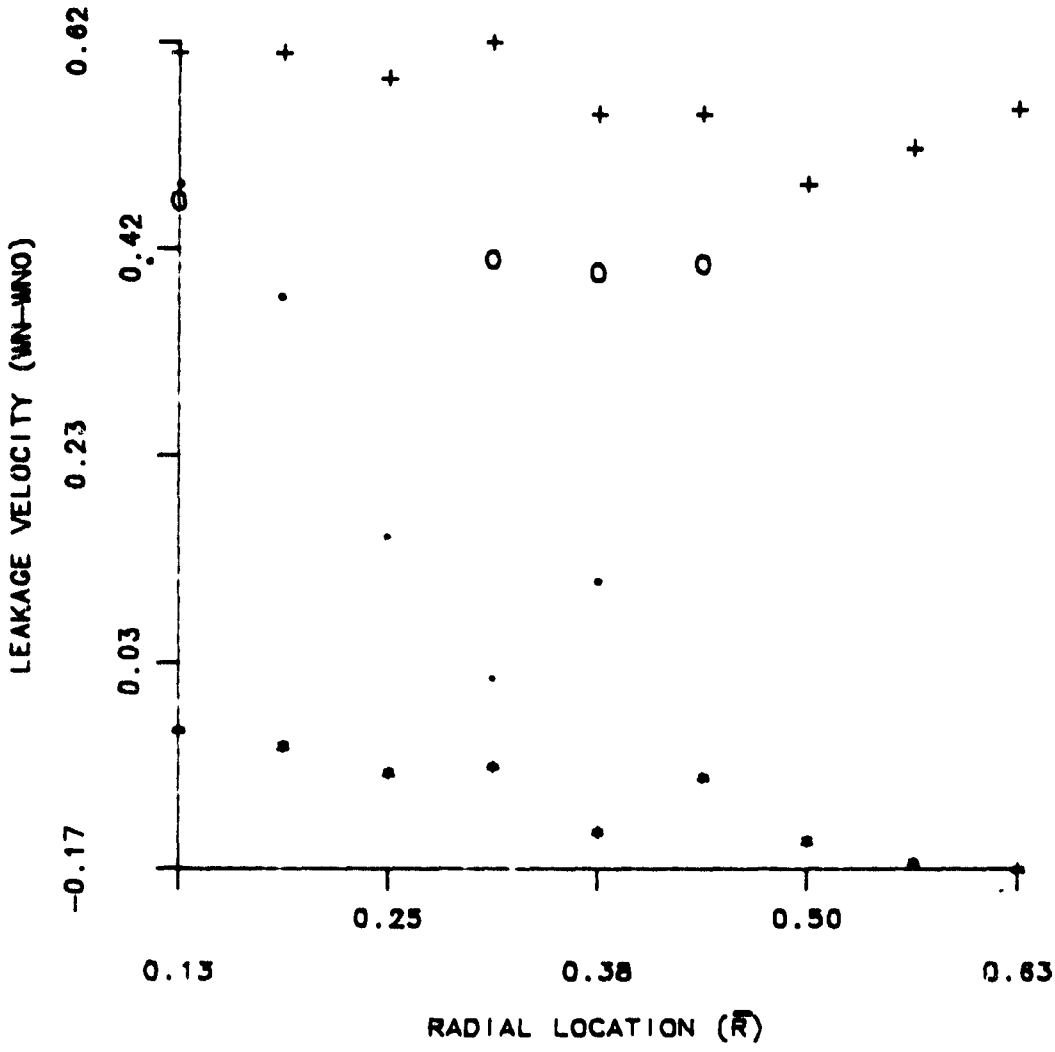

Z	
*	0.003
+	0.5
O	0.75
•	0.979

Figure 4.8 Variation of the Leakage Velocity at Suction Surface at Off-Design Condition

of the blade. A similar behavior is shown by the leakage velocities at the pressure surface (Figure 4.9).

4.1.4 Velocity Vector Plots and Boundary Layer Development

Figures 4.10 and 4.11 show the relative velocity vectors in z-θ plane at $\bar{R}$ = 0.3125 and $\bar{R}$ = 0.125, respectively. These figures present an overall picture of the flow in the clearance region. In comparison with similar plots at design condition, the flow at the inlet of the rotor is slightly more underturned for both the radii. At Z = 0.003, the velocity vectors don't follow the blade contour as observed in Figures 3.12 and 3.13. A large underturning of the flow at Z = 0.50 is observed. The flow is almost along the tangential direction at both the radii. At Z = 0.75 the underturning has reduced considerably for $\bar{R}$ = 0.3125. The magnitude of the velocity vectors is smaller than that at the design conditions.

The radial variation of the axial and the absolute tangential velocities averaged over the passage at various axial locations is plotted in Figure 4.12. The main difference in the boundary layer development at ϕ = 0.60 is observed in the boundary layer at the inlet. $\bar{V}_\theta$ is considerably larger than $\bar{W}_z$, and the boundary layer is highly skewed. At ϕ = 0.55 both the components of the velocity in the incoming boundary layer are approximately of the same order. The effect of the skewed boundary layer entering the rotor passage is propagated downstream and can be observed in terms of a very high level of $\bar{V}_\theta$ at Z = 0.003 and 0.5. As the flow leaves the rotor passage a continuous redistribution of energy takes place, and at Z = 1.731, where the flow is almost uniform, the annulus-wall boundary layer has

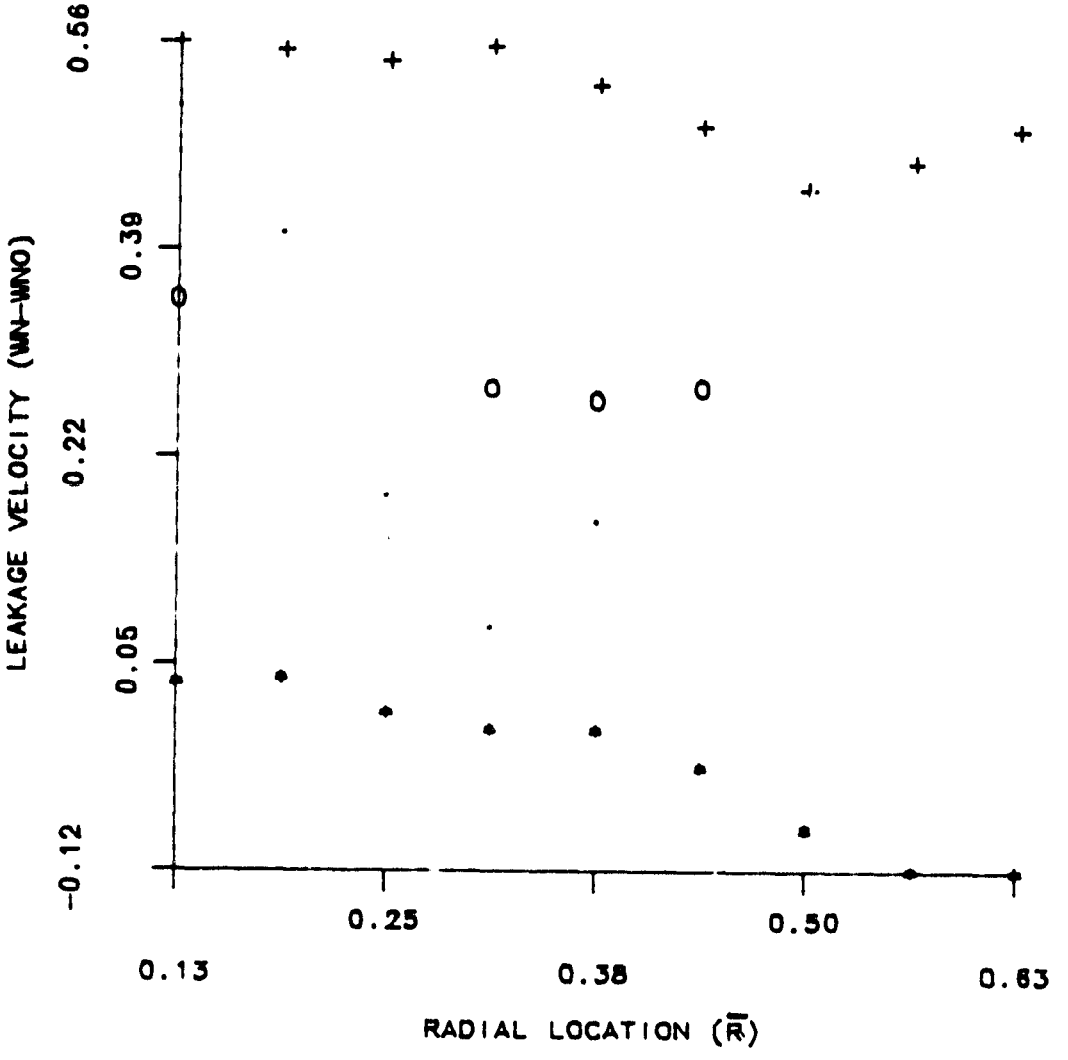

(Refer to Figure 4.8 for notations.)

Figure 4.9 Variation of the Leakage Velocity at Pressure Surface at Off-Design Condition

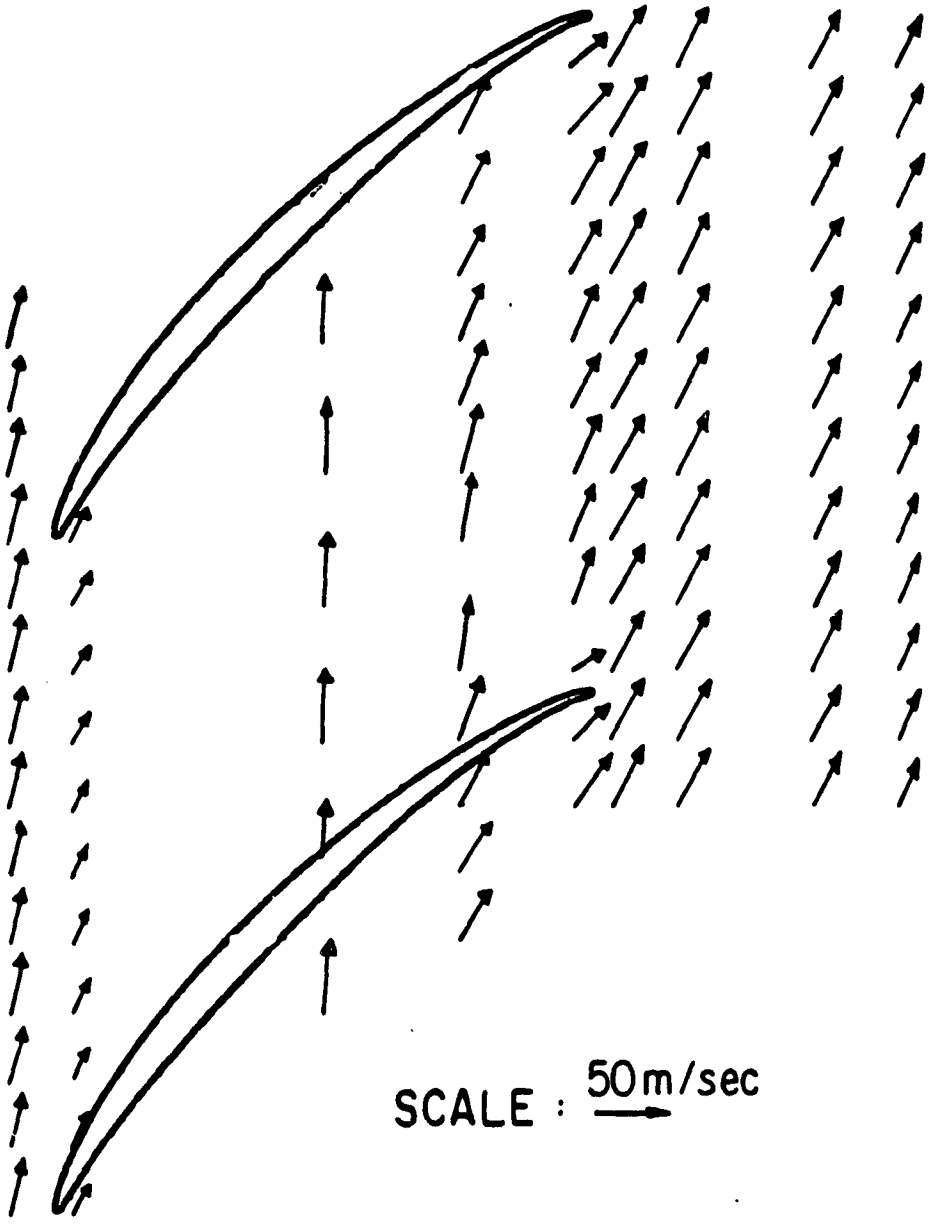

Figure 4.10 Relative Velocity Vectors Inside the Clearance Region ($\bar{R}$ = 0.3125) at Off-Design Condition

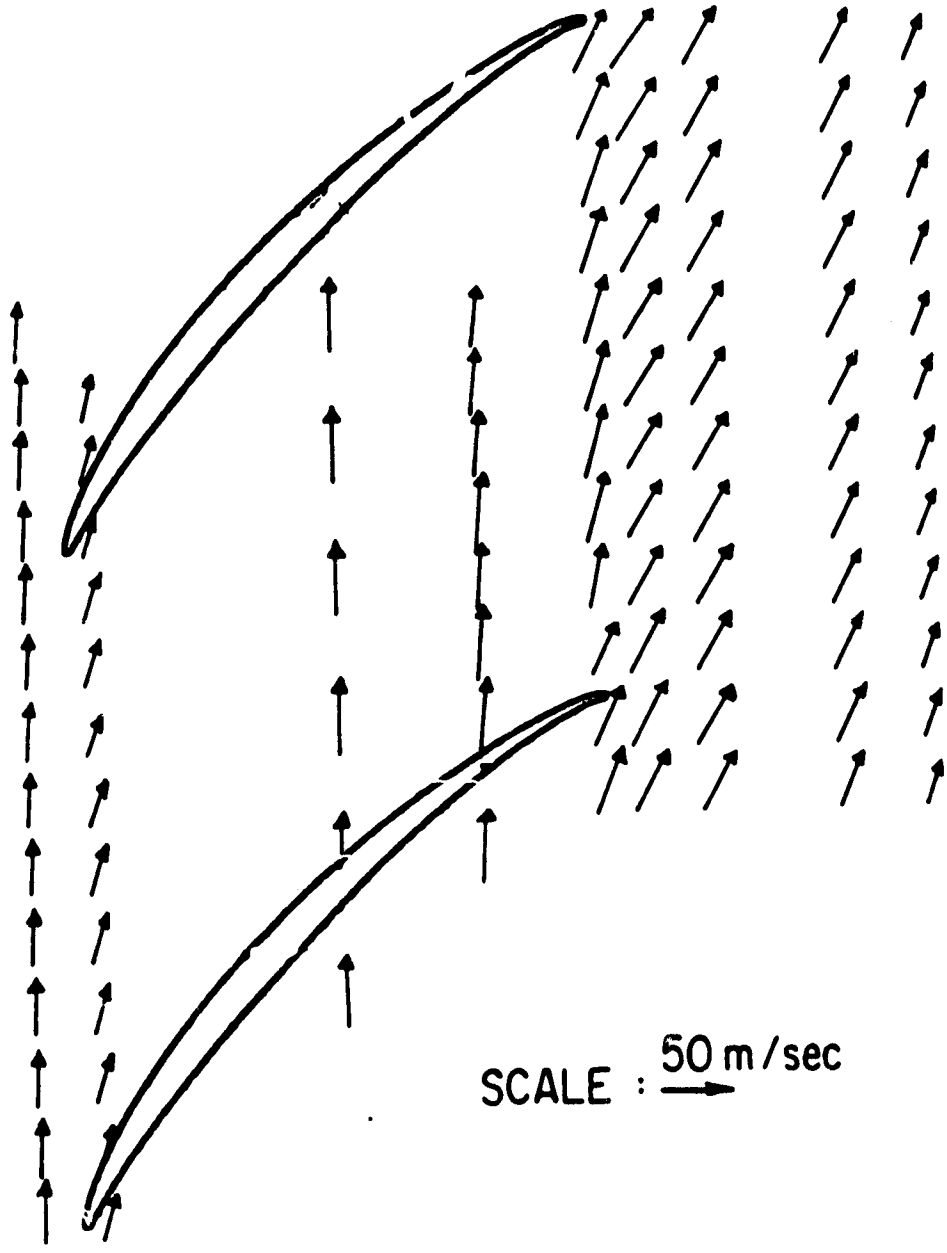

Figure 4.11 Relative Velocity Vectors Inside the Clearance Region ($\bar{R}$ = 0.125) at Off-Design Condition

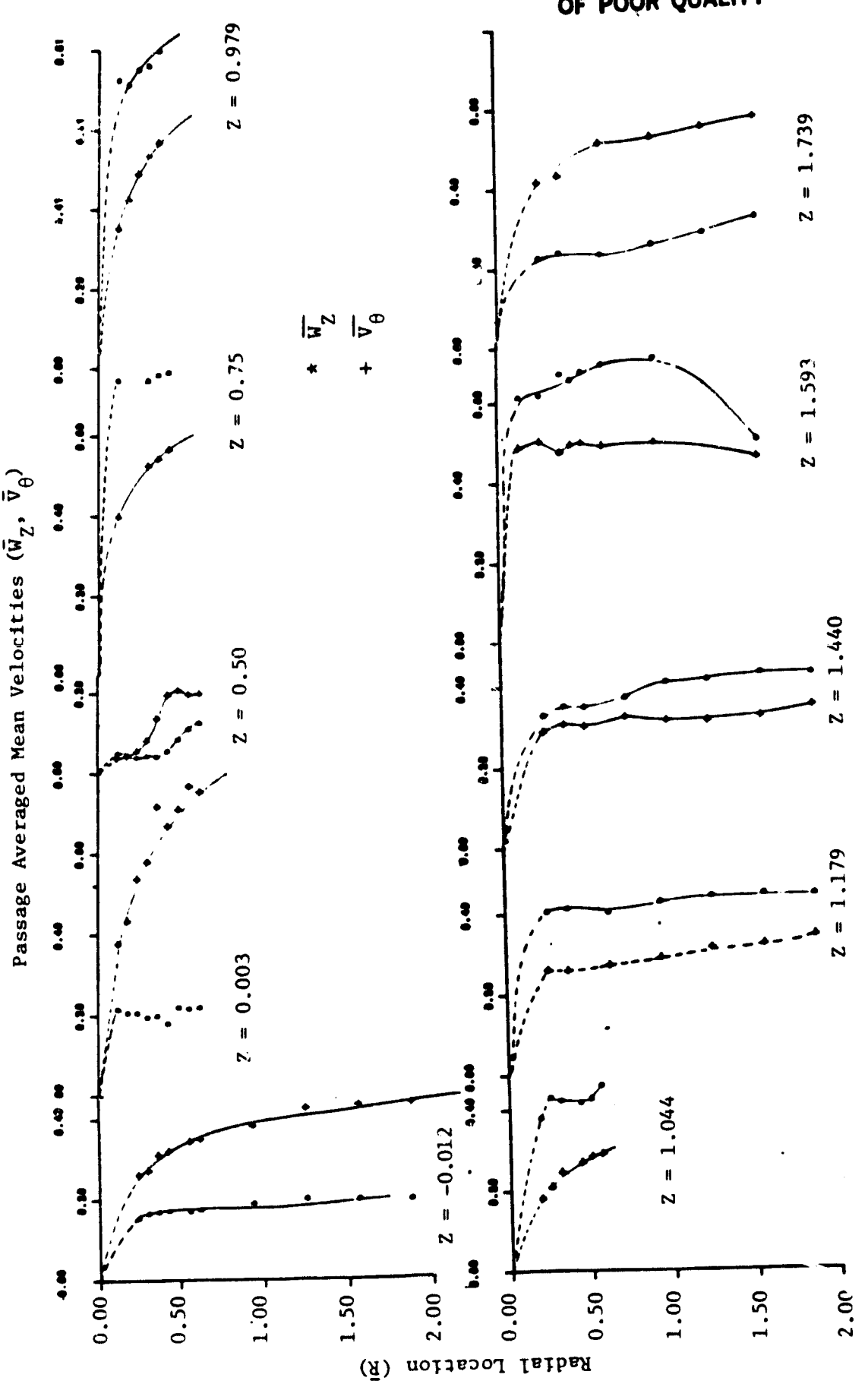

Figure 4.12 Measured Development of the Annulus-Wall Boundary Layer at Off-Design Condition

achieved the same order of skewness as observed in the incoming boundary layer.

4.2 Turbulence Properties

The turbulence intensity profiles at off-design condition are shown in Figures 4.13-4.15. Both T_z and T_θ are normalized with respect to the local maximum total velocity. The normalizing velocities at various axial and radial stations are listed in Table 4.1. Measurements were taken at all the stations listed in Table 2.2, but only the turbulence intensity profiles which significantly differed from those at the design condition are included in the thesis.

The turbulence intensity profiles at the inlet to the rotor and at the axial location near the leading edge inside the rotor passage (figures not included here) show very little blade to blade variation in the intensities. But, the level of T_θ is higher than that at the design condition.

Figure 4.13 shows the variation of T_z and T_θ at the mid-chord location. It can be observed from Figure 4.13(a,b) that at $\bar{r} = 0.57$ the turbulence intensities T_z and T_θ decrease in the clearance region. The level of T_θ continues to decrease up to a short distance away from suction surface of the blade and then increases gradually. This region near $\bar{Y} = 0.29$ indicates the rolling up of the leakage flow as soon as it leaves the tip clearance passage. However, the vortex indicated here is very weak. These results support the conclusion drawn from the mean velocities that the leakage flow does not travel as far as it does at design condition before rolling up. It can also be observed that the level of turbulence intensities at $\bar{r} = 0.46$, 0.29 and 0.12 is

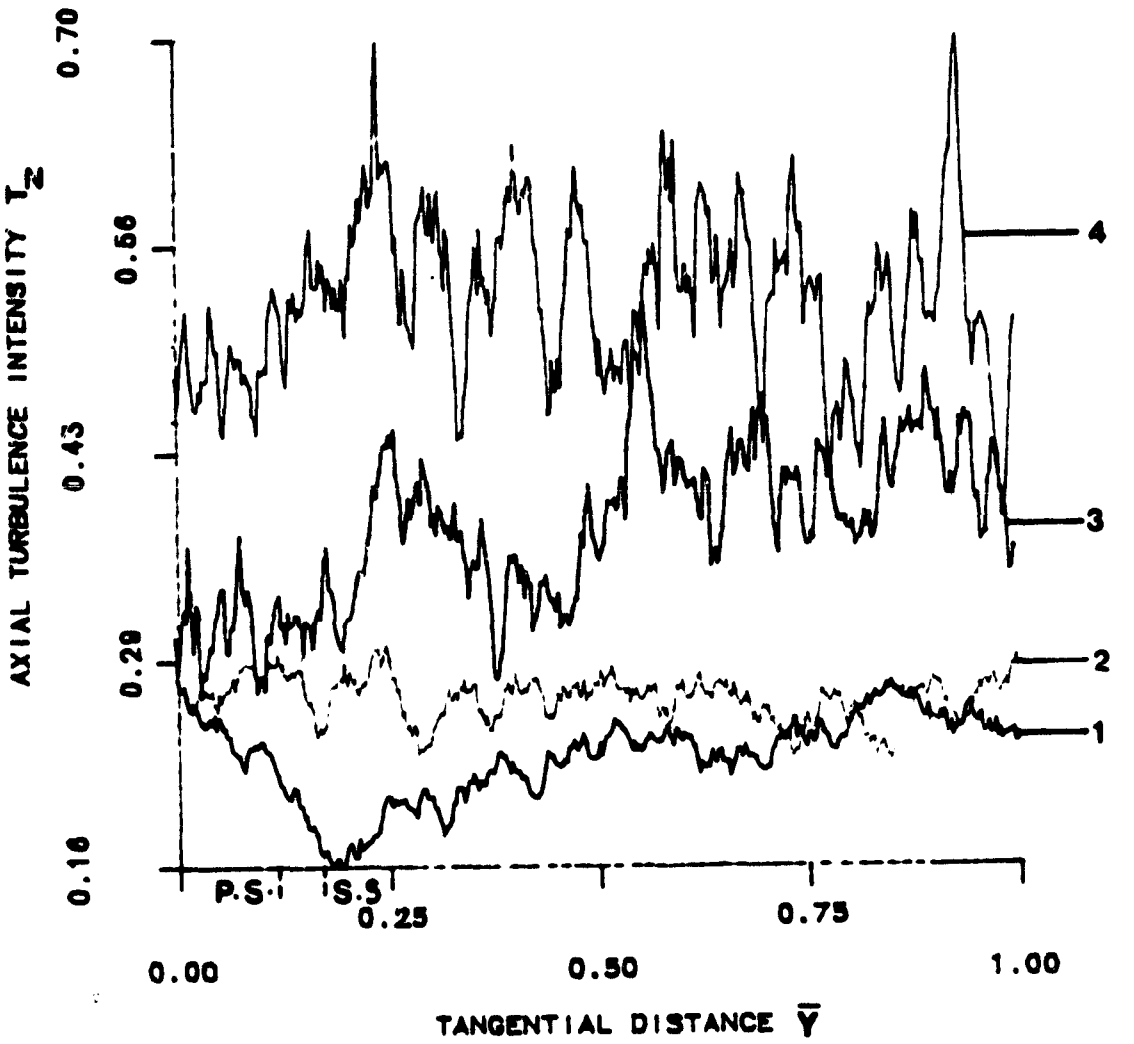

	$\bar{r}$
1	0.57
2	0.46
3	0.29
4	0.12

Figure 4.13a Variation of Axial Turbulence Intensity (Z = 0.50) at Off-Design Condition

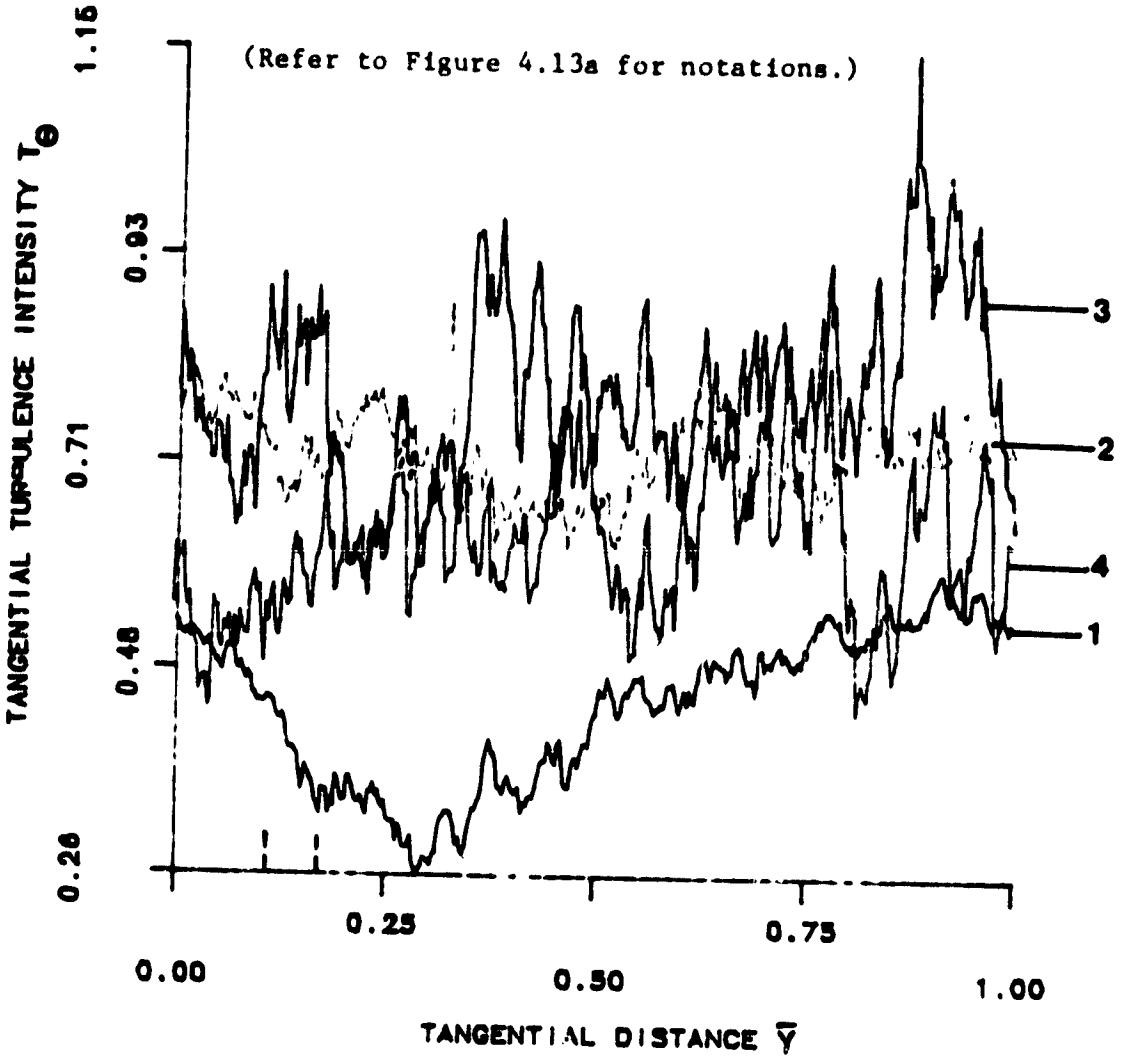

Figure 4.13b Variation of Tangential Turbulence Intensity (Z = 0.50) at Off-Design Condition

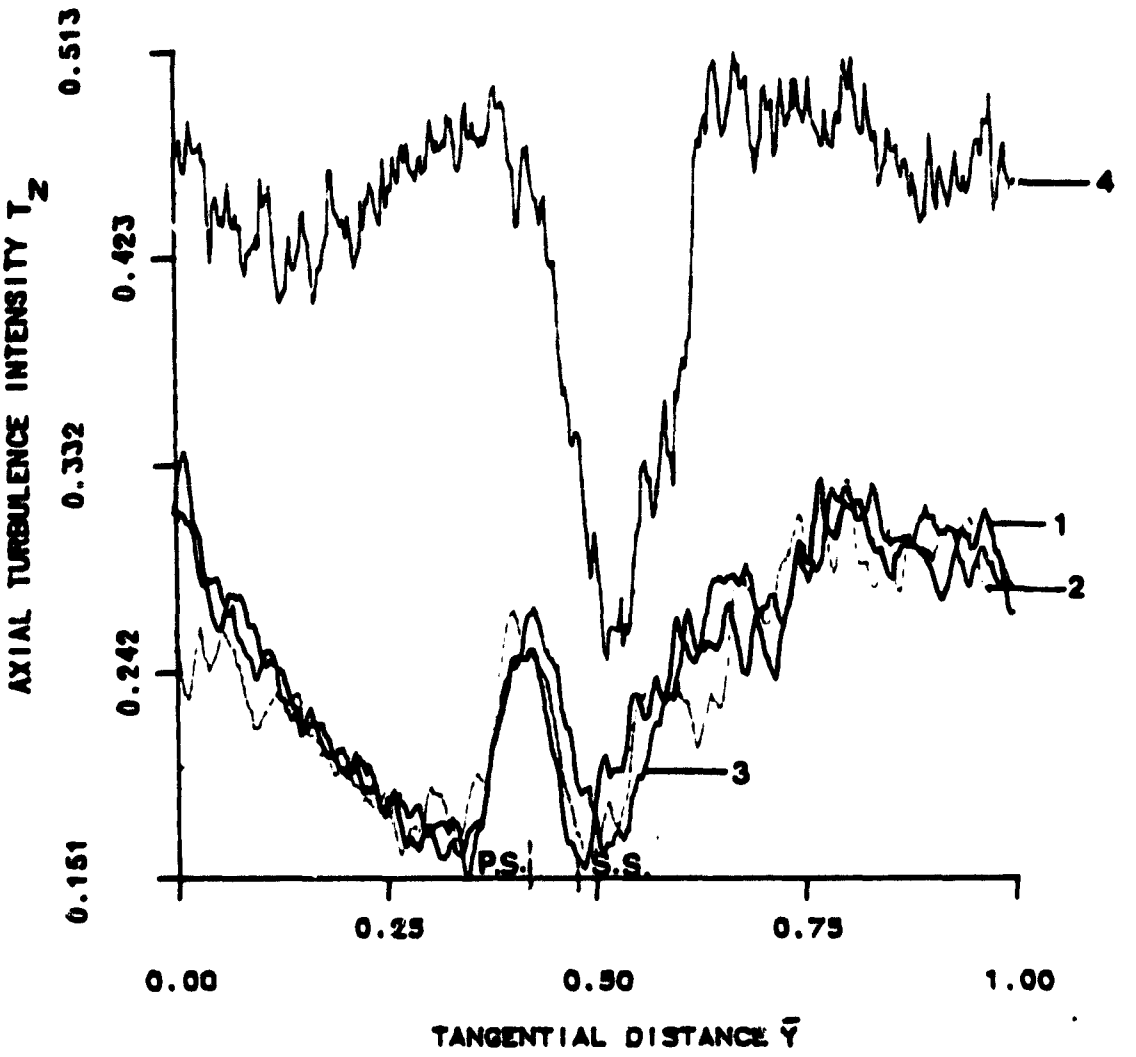

	$\bar{r}$
1	0.67
2	0.42
3	0.25
4	0.16

Figure 4.14a Variation of Axial Turbulence Intensity ($Z = 0.75$) at Off-Design Condition

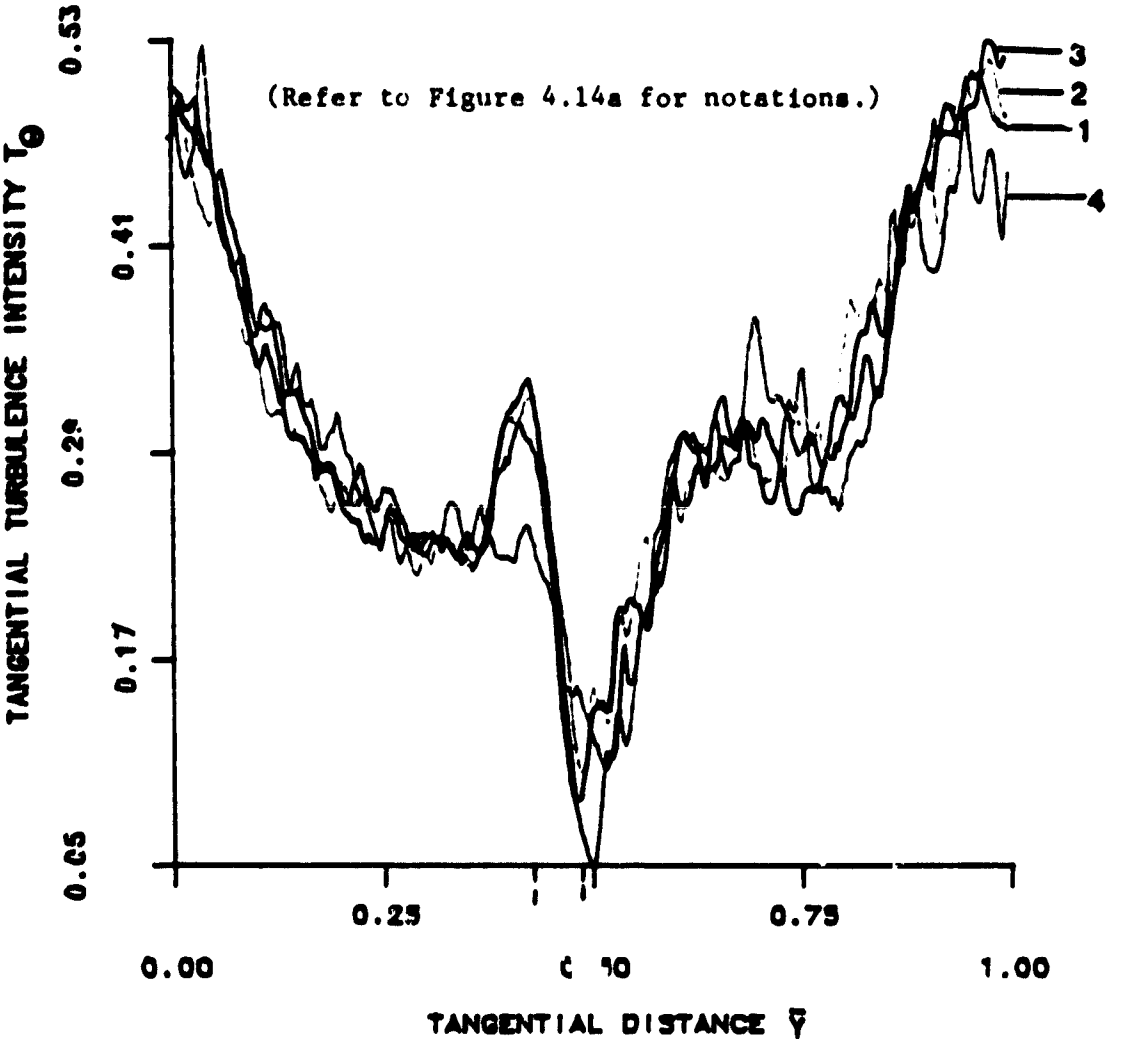

Figure 4.14b Variation of Tangential Turbulence Intensity (Z = 0.75) at Off-Design Condition

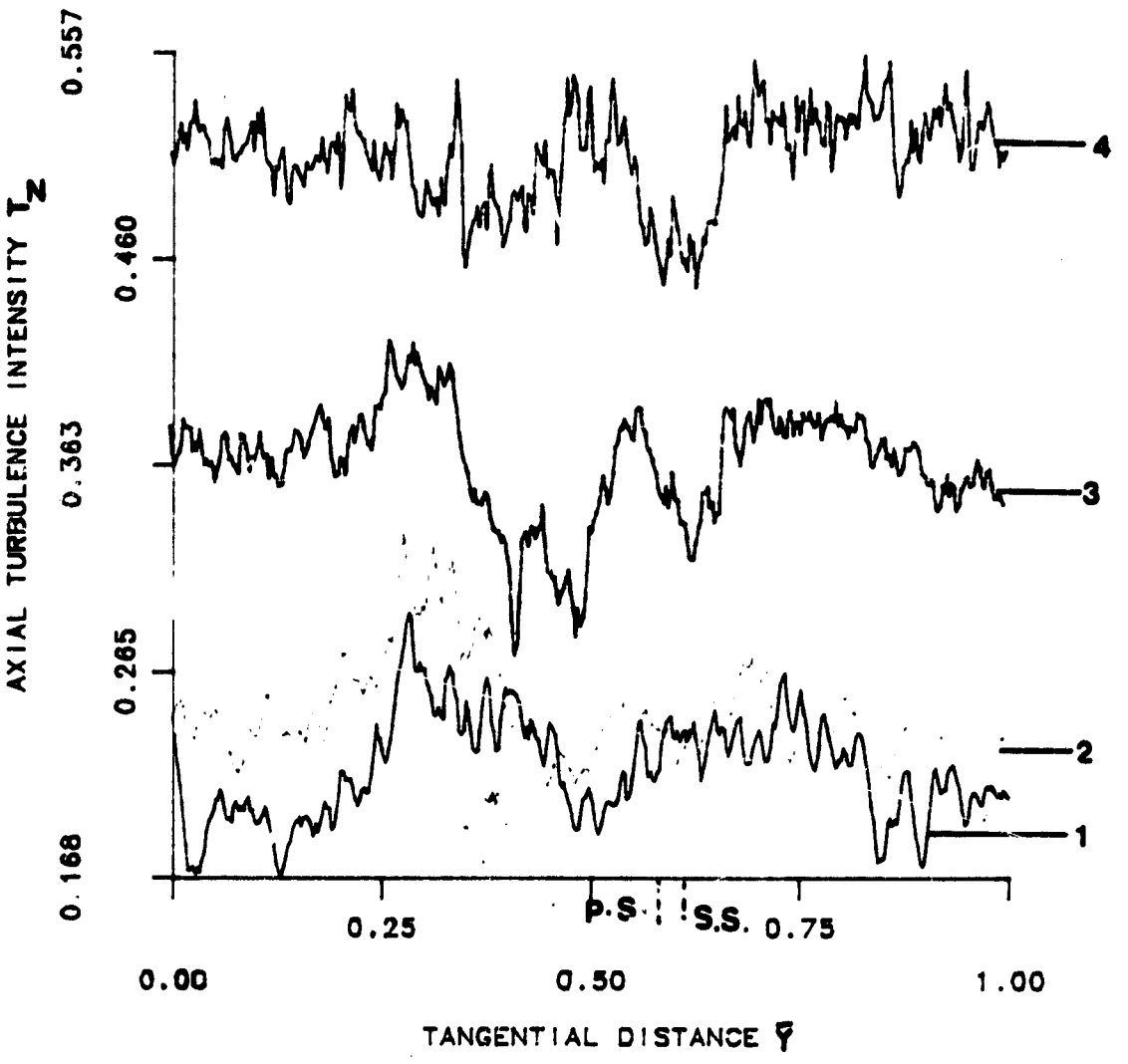

	$\bar{r}$
1	0.50
2	0.42
3	0.25
4	0.167

Figure 4.15a Variation of Axial Turbulence Intensity (Z = 0.979) at Off-Design Condition

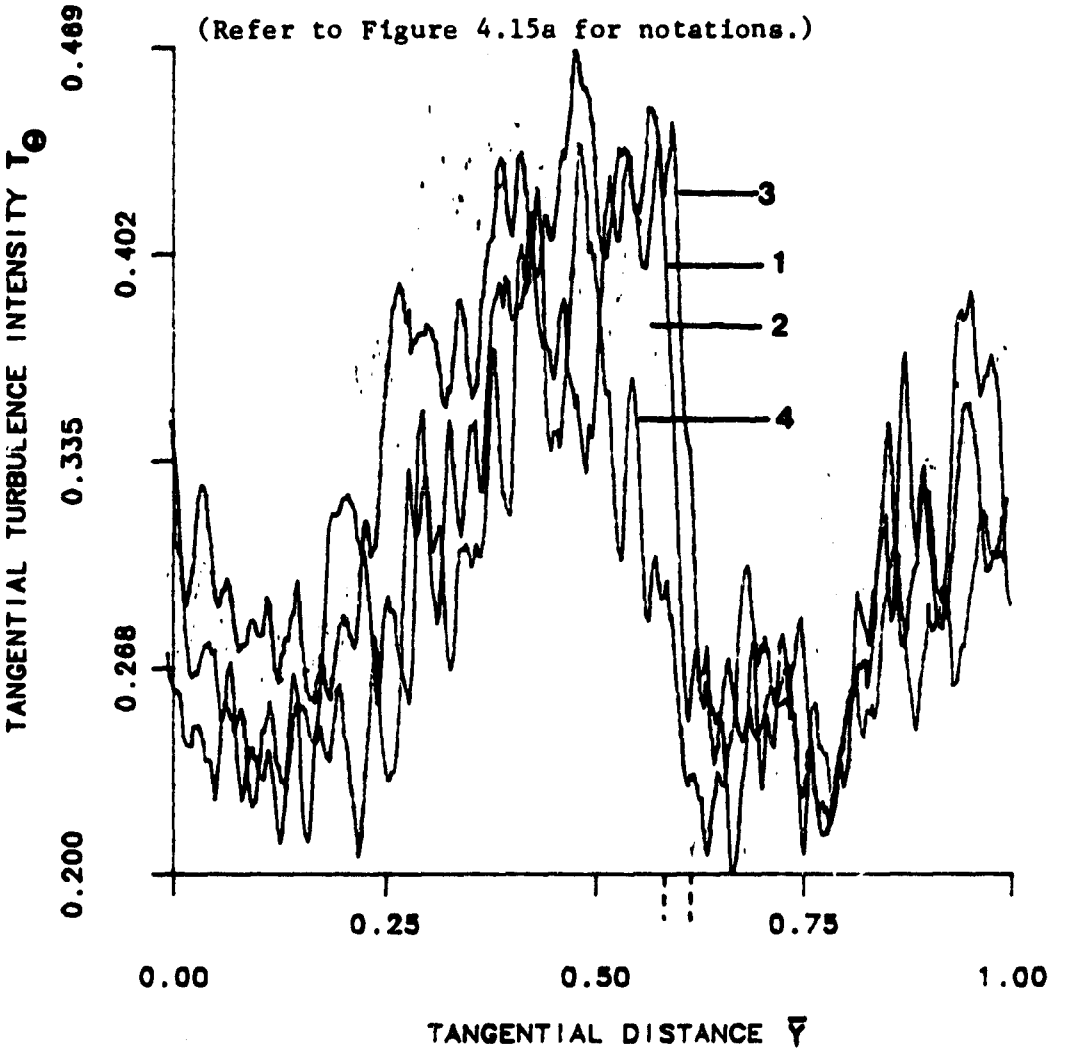

Figure 4.15b Variation Tangential Turbulence Intensity (Z = 0.979) at Off-Design Condition

Table 4.1

Maximum Total Velocities* at the Radial and the Axial Stations of Measurement at ϕ=0.60

R \ Z	-0.012	0.003	0.50	0.75	0.979	1.055	1.179	1.440	1.593	1.731
1.875	0.487	-	-	-	-	-	0.565	0.572	-	-
1.5625	0.476	-	-	-	-	-	0.557	0.553	0.683	0.710
1.25	0.465	-	-	-	-	-	0.546	0.525	0.631	-
1.0	-	-	-	-	-	-	-	0.519	-	-
0.9375	0.420	-	-	-	-	-	0.524	-	0.590	0.874
0.75	-	-	-	-	-	-	-	0.499	-	-
0.625	0.393	0.873	0.315	-	-	-	0.504	-	0.575	0.866
0.5625	0.385	0.797	0.260	-	-	0.560	-	-	-	-
0.5	-	0.718	0.246	-	-	0.515	-	0.465	0.496	0.841
0.4375	0.364	0.711	0.219	0.385	-	0.490	-	-	-	0.830
0.375	0.351	0.741	0.125	0.398	0.715	-	0.496	0.464	0.497	0.813
0.3125	0.311	0.629	0.105	0.390	0.803	0.488	-	-	-	-
0.25	0.298	0.626	0.104	-	0.678	0.468	0.496	0.443	0.477	0.802
0.1875	-	0.469	0.065	-	0.539	0.419	-	-	-	-
0.125	-	0.411	0.066	0.311	0.453	-	-	-	-	-

*All the velocities are normalized by the blade tip speed (150 ft/sec).

very high. Due to the high velocity gradient in the annulus-wall boundary layer, mixing is high near the wall and hence the turbulence intensities are expected to be high. But the very high level indicated from these results may be because of the error involved in the estimation of the turbulence intensities. It was assumed that the turbulence intensity in the radial direction is small compared to the mean velocities in the axial and the tangential directions. Table 4.1 shows that the maximum total velocities at these stations are very small which implies that the axial and the tangential components of these velocities are also very small. It is likely that the fluctuations in the radial direction are comparable to the fluctuations in the other two orthogonal directions which will introduce error in the estimation of T_z and T_θ as discussed in Appendix A.

Figure 4.14(a,b) shows the T_z and T_θ variations at Z = 0.75. It indicates a sudden decrease in the turbulence intensities across the blade implying that the flow becomes almost laminar inside the tip clearance. A similar behavior can be observed at Z = 0.979 as shown in Figure 4.15. An interesting feature of the flow at Z = 0.75 and 0.979 is that the intensities increase suddenly near the pressure surface before the marked decrease across the blade takes place. This may be due to the scraping effect on the annulus-wall boundary layer or because of the blade boundary layer interaction with the leakage flow and the annulus-wall boundary layer.

The blade to blade variation at the exit of the rotor is almost uniform at all the stations. The maximum variation for a given radius is less than 5 percent. Hence, the figures are not included. An

overall picture of the level of turbulence intensities at these stations can be obtained from the iso-contours of the tangential, the axial turbulence intensities, shown in Figures 4.16-4.19.

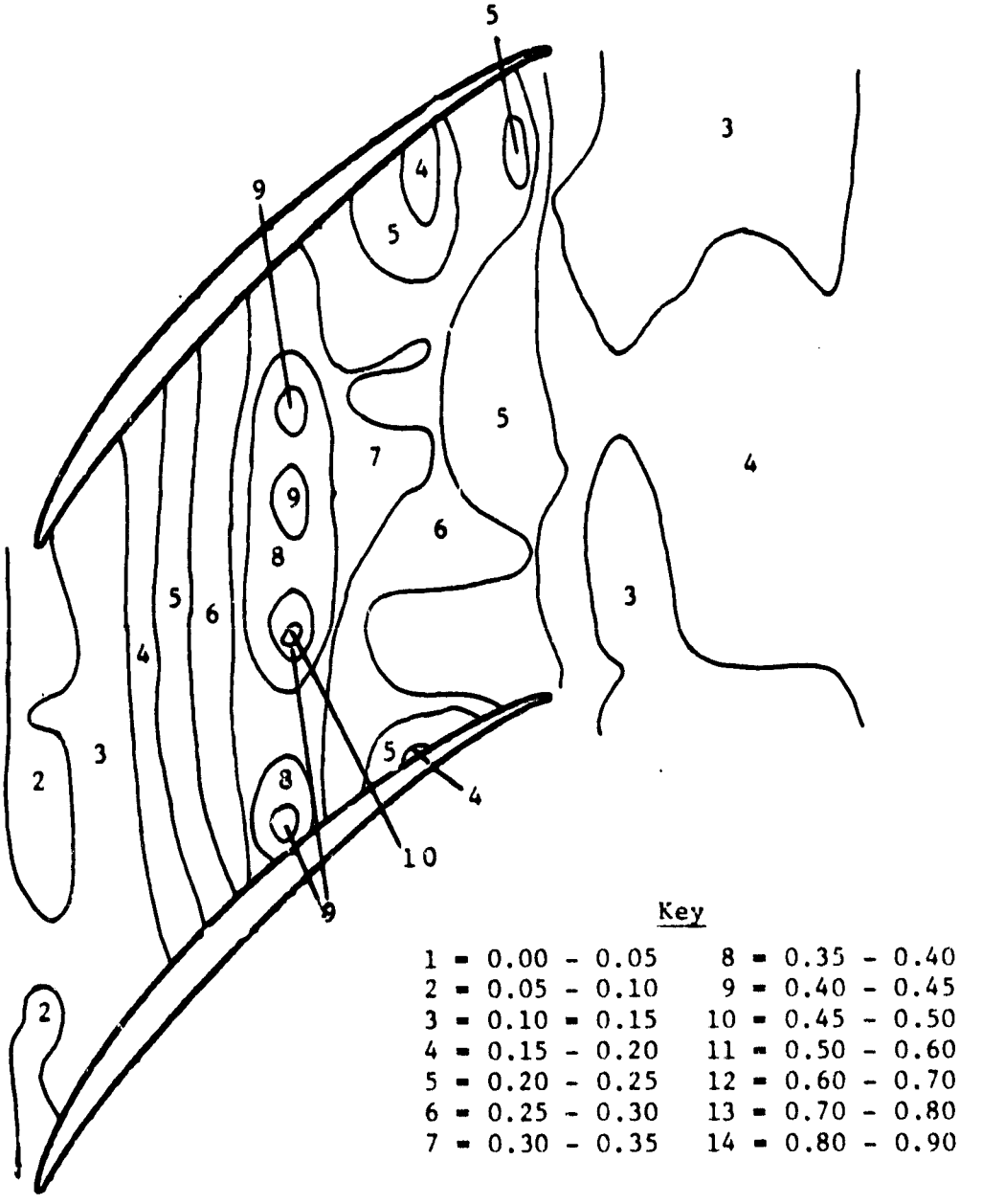

Figure 4.16 Iso-Contours for Axial Turbulence Intensity ($\bar{R}$ = 0.3125) at Off-Design Condition

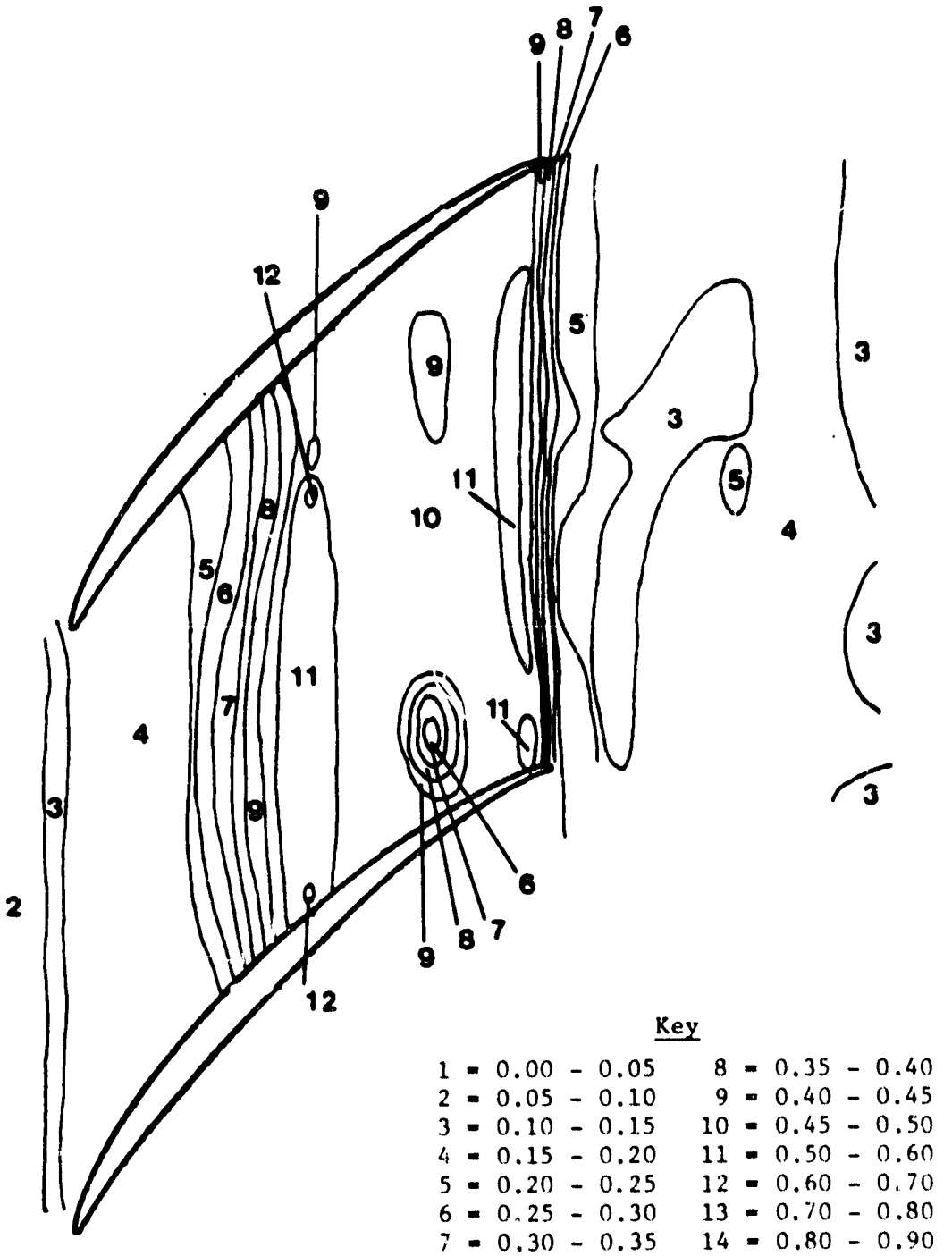

Figure 4.17 Iso-Contours for Axial Turbulence Intensity ($\bar{R}$ = 0.125) at Off-Design Condition

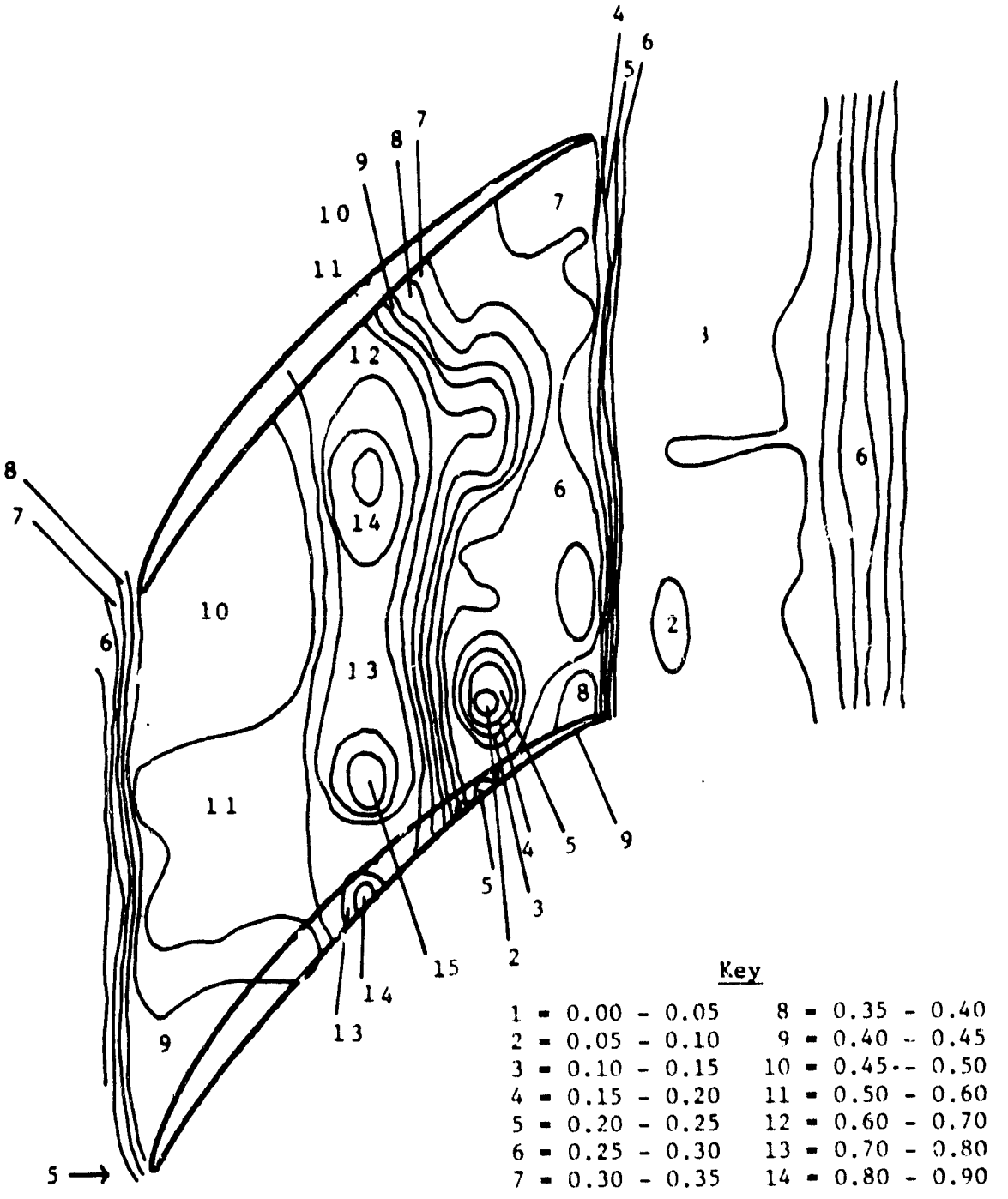

Figure 4.18 Iso-Contours for Tangential Turbulence Intensity ($\bar{R}$ = 0.125) at Off-Design Condition

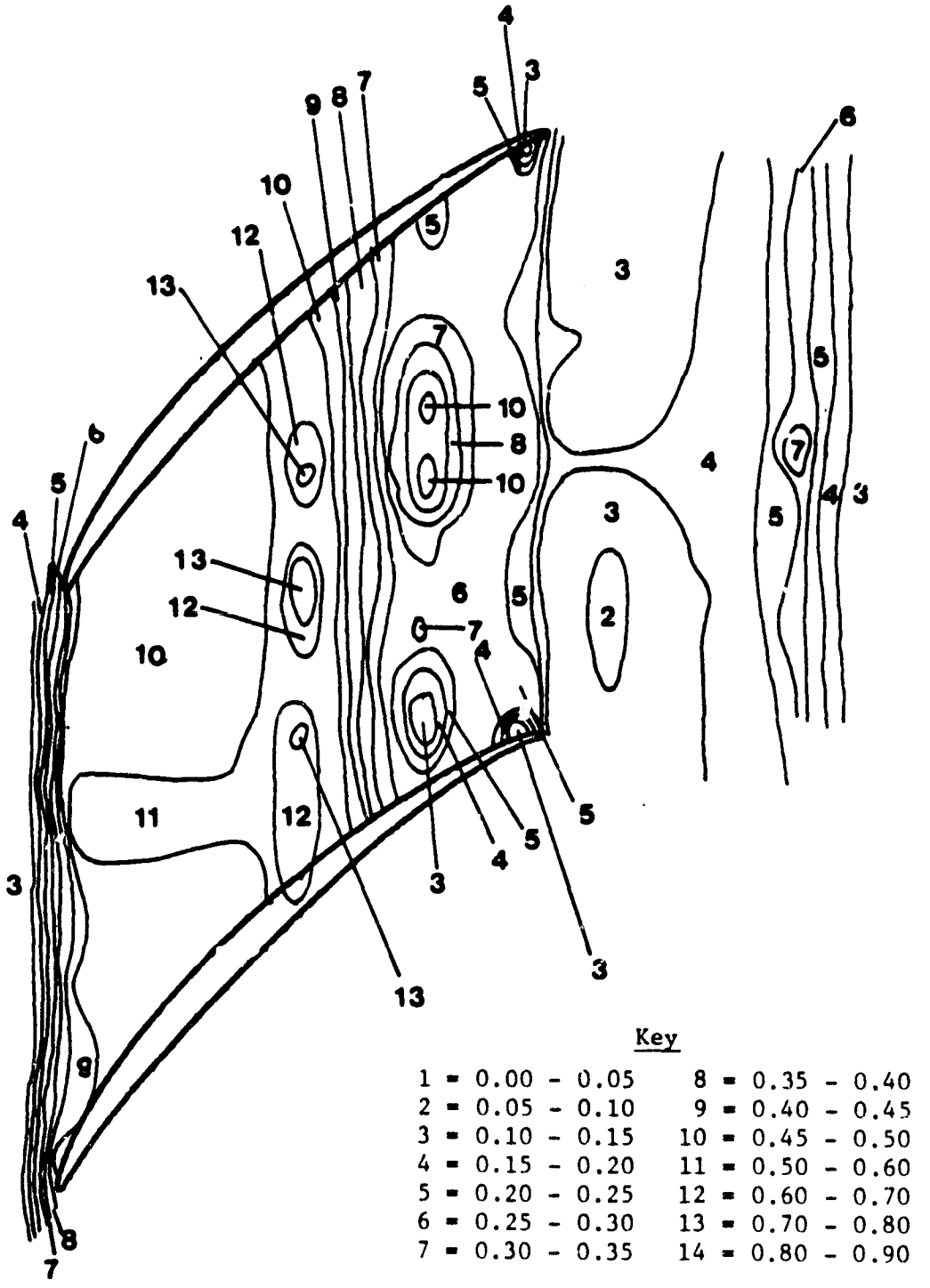

Figure 4.19 Iso-Contours for Tangential Turbulence Intensity ($\bar{R}$ = 0.3125) at Off-Design Condition

CHAPTER V

SUMMARY AND CONCLUSIONS

5.1 Conclusions

The following conclusions can be drawn from the detailed measurements carried out inside the tip clearance region of the rotor passage as well as the exit at the design condition.

1. The flow very near the leading edge shows the usual features of annulus-wall boundary layer, with perturbations caused by the scraping effect.

2. The presence and interaction of the leakage flow, annulus-wall boundary layer, and the scraping vortex is the dominant feature at mid-chord position. The rotation of the blade augments the leakage flow resulting in the movement of the leakage jet towards the mid passage. This feature is observed from the measurement.

3. The blade to blade distribution of properties is highly non-uniform, except in the downstream and upstream regions.

4. The leakage flow has developed considerably at 75 percent chord length. Leakage flow is the most predominant feature at this location, and the rolling up of the leakage flow to form a vortex takes place approximately midway between the passage. The flow at the trailing edge shows a similar trend. The measurements indicate the presence of separated regions near the suction side at mid-chord and the trailing edge locations.

5. A marked increase in the axial velocity and a considerable decrease in the tangential velocity characterizes the flow leaving the

rotor blade passage in the annulus-wall region. A weak wake profile in the axial velocity is observed near the blade tip but it rapidly decays as the flow approaches the annulus-wall.

6. A rapid decay of the wake profile takes place in the axial direction downstream of the blade and the flow becomes nearly uniform after 20 percent of the chord downstream of the rotor. A large difference between the values of the two components of the velocity still exists beyond 20 percent chord downstream. A continuous redistribution of the flow takes place up to 75 percent of the chord downstream where both the components of the velocity are found to be the same order of magnitude.

7. Leakage velocity derived from the data shows that it is very small at the leading edge and increases at mid-chord. At 75 percent chord the leakage velocity is slightly less than that at mid-chord but it is maximum at the trailing edge.

8. The vector plot indicates that the flow is underturned in most regions inside the passage. This underturning decreases drastically as the flow leaves the blade trailing edge.

9. The annulus-wall boundary layer profile, based on the passage averaged mean velocity, indicates substantial changes in the mid-chord and the exit regions.

10. The turbulence intensities increase towards the annulus-wall because the mean velocity gradients are high near the wall.

11. The turbulence intensity profiles at Z = 0.003 indicate the dragging effect of the blade on the flow. The flow separation near the blade surface and the presence of the blade boundary layer scraping are also evident from these profiles.

12. The high level of the turbulence intensities at Z = 0.50 indicates a strong interaction of the leakage flow with the annulus-wall boundary layer, the secondary flow and the vortex generated by the scraping of the annulus-wall boundary layer.

13. Both, the mean velocity profiles and the turbulence intensity distribution at Z = 0.50 indicate the presence of a strong leakage flow jet which washes away the annulus-wall boundary layer completely causing a very high level of mixing near the annulus-wall.

14. At Z = 0.75 and 0.979, the turbulence intensities drop suddenly in the tip clearance region. The leakage flow tends to becoming laminar in the clearance region at these locations.

15. The flow at the exit of the rotor is characterized by low turbulence in the tangential direction. A continuous redistribution of energy takes place up to 70 percent chord downstream of the rotor trailing edge where the turbulence is isotropic.

The results obtained from the experimental data at off-design condition indicate the following:

a. At the reduced loading and r.p.m., the effect of the unsteady flowfield due to the compressor rotor does not propagate upstream of the rotor.

b. As a result of the reduction in r.p.m. and the decreased loading the annulus-wall boundary layer entering the rotor is highly skewed. The effect of the skewed boundary layer propagates up to 70 percent chord downstream of the rotor.

c. The leakage velocities are reduced at all the axial locations. The effect of reduced leakage velocity is reflected in more regular

flow behavior compared to the flow behavior at the design condition at the mid-chord location.

d. The leakage jets at (Z = 0.50, 0.75) are not strong enough to travel up to the mid-passage before rolling up. They either roll up near the suction surface or merely diffuse in the mainstream.

e. At the rotor exit, characteristic wake profiles are observed up to 60 percent chord downstream of the trailing edge. The leakage flow is not strong enough to destroy the wake structure as it does in the experiments at the design condition.

g. The velocity vector plots indicate that over the entire region of measurement, the flow is more underturned compared to the underturning of the flow at the design condition.

5.2 Limitations of the Present Investigation and Suggestions for Future Work

All the flowfield measurements reported in the thesis were carried out using a two-sensor hot-wire probe, which presented a severe limitation. It is not possible to measure the radial component of the velocity with a two-sensor hot wire probe. Also, the radial component of the turbulence intensity introduces a large error in the calculation of the axial and the tangential components. Further, the clearance height is so small that neither an inclined wire probe nor three-sensor probe could be used. Also, it was not possible to measure the flowfield very close to the blade tip.

Another major drawback of these experiments was the difficulty in locating the exact position of the blade with respect to the pulse signal from the photocell. The hot-wire anemometer signals and the

tachometer pulse signal are recorded at the same time, but they pass through different electronic circuits. A time lag of 0.4 micro seconds in such circuit is not uncommon which may mean the displacement of one of the signals by almost 1/8 of the passage width.

The only way to overcome these limitations is to use a non-invasive flow measurement technique such as laser doppler velocimetry.

In order to gain fuller understanding of the results presented in this thesis, static pressure measurements on the annulus-wall and the flow visualization may be very useful.

REFERENCES

1. Dean, R. C., "Influence of Tip Clearance on Boundary Layer Characteristics in a Rectilinear Cascade," M.I.T., G.T.L. Report No. 27-3, 1954.

2. Lakshminarayana, B. and Horlock, J. H., "Leakage and Secondary Flows in Compressor Cascades," British ARC R and M 3483, Her Majesty's Stationary Office, London, 1967, pp. 1-58.

3. Lakshminarayana, B., "Methods of Predicting the Tip Clearance Effects in Axial Flow Turbomachinery," J. Basic Engineering, Vol. D92, September 1970, pp. 467-482.

4. Phillips, W. R. C. and Head, M. R., "Flow Visualization in the Tip Region of a Rotating Blade Row," Int. J. Mech. Sci., Vol. 22, January 1980, pp. 495-521.

5. Booth, T. C., Dodge, P. R. and Hepworth, H. R., "Rotor Tip Leakage Part I--Basic Methodology," ASME Paper 81-GT-71, December 1980.

6. Herzig, H. A., Hansen, A. G. and Costello, G. R., "A Visualization Study of Secondary Flows in Cascades," NACA T R 1163, 1953.

7. Davino, R. and Lakshminarayana, B., "Characteristics of Mean Velocity in the Annulus Wall Region at the Exit of Turbomachinery Rotor Passage," AIAA Paper 81-0068, 1981. (To be published in the AIAA Journal in 1982.)

8. Ravindranath, A., "Three Dimensional Mean and Turbulence Characteristics of the Near Wake of a Compressor Rotor Blade," M.S. Thesis, Department of Aerospace Engineering, The Pennsylvania State University, 1979.

9. Lakshminarayana, B., Davino, R. and Pouagare, M., "Three Dimensional Flow Field and Annulus Wall Boundary Layer Development in the Tip Region of a Compressor Rotor Passage." (To be presented at ASME Gas Turbine Conference, London, April 1982.)

10. Lakshminarayana, B., Davino, R. and Pouagare, M., "Turbulent Properties in the Tip Region of Compressor Rotor Passage." (To be presented at ASME Gas Turbine Conference, London, April 1982.)

11. Lakshminarayana, B. and Horlock, J., "Secondary Flows and Losses in Cascades and Axial Flow Turbomachines," Int. J. Mech. Sci., Vol. 5, 1963, pp. 287-307.

12. Reeder, J., "Tip Clearance Problems in Axial Compressors (A Survey of Available Literature)," AEC R and D Report K16, I, 1968.

13. Rains, D., "Tip Clearance Flow in Axial Flow Compressors and Pumps," Cal. Inst. Tech. Mech. Eng. Lab. Report 5, 1954.

14. Vavra, M., Aerothermodynamics and Flow in Turbomachines, John Wiley and Sons, New York, 1960, p. 381.

15. Betz, A., "The Phenomena at the Tips of Kaplan Turbines," Hydraulic Problems, 1925.

16. Wu, C. and Wu W., "Analysis of Tip Clearance Flow in Turbomachines," Poly. Inst., Brooklyn, Tech. Report, No. 1, 1954.

17. Niida, T., Yoshida, T. and Hirata, R., "Flow Rate Through the Clearance Between a Scraper Blade and the Outer Wall of an Annular Sector," Proceedings of the Society of Chemical Engineers, Japan), Vol. 3, No. 2, pp. 109-114, 1977.

18. Gearhart, W., "Tip Clearance Flow in Turbomachines," M.S. Thesis, The Pennsylvania State University, 1966.

19. Boyce, M., Schiller, R. and Desai, A., "Study of Casing Treatment Effects in Axial Flow Compressors," Journal of Engineering for Power, Paper No. 74-GT-89, November 1973.

20. Lakshminarayana, B., "An Axial Flow Research Compressor Facility Designed for Flow Measurements in Rotor Passages," Proc. ASME Symp. on Measurement Methods in Rotating Components of Turbomachinery, New Orleans, 1980, pp. 31-42.

21. Smith, L. H., "Three Dimensional Flow in an Axial Flow Turbomachinery," WADC Tech. Report No. 55-348, Vol. II, John Hopkins University, March 1956.

22. Poncet, A. and Lakshminarayana, B., "Three Dimensional Analysis and Measurement of the Flow in a Three Bladed Rocket Pump Inducer," NASA-CR-2290, pp. 1-126, 1973.

23. Davino, R., "Three Dimensional Mean and Turbulence Characteristics in the Annulus Wall Region of an Axial Flow Compressor Rotor Blade Passage," M.S. Thesis, Department of Aerospace Engineering, The Pennsylvania State University, November 1980.

24. Reynolds, B. and Lakshminarayana, B., "Characteristics of Fully Loaded Fan Rotor Blade Wakes," NASA-CR-3188, October 1979, 180 pp.

25. Anand, A., "An Experimental and Theoretical Investigation of Three Dimensional Boundary Layers Inside the Passage of a Turbomachinery Rotor," Ph.D. Thesis, Department of Aerospace Engineering, The Pennsylvania State University, May 1976.

APPENDIX A

EXPERIMENTAL ERROR ANALYSIS

The errors involved in hot-wire probe measurements fall under three categories: probe errors, instrumentation errors and mechanical errors. A detailed discussion of these errors is given by Anand [25]. Only the major sources of the errors particular to the present investigation are discussed briefly.

In the case of measurements with two-sensor hot-wire probe in close proximity of the annulus-wall, the following sources of error may occur.

1. Inclination of the wire to the flow streamline (deviation from cosine law).
2. Finite distance between the wires (spatial resolution of the probe).
3. Finite dimensions of the individual wires.
4. Thermal inertia of the wires.
5. Aging, oxidation and contamination of the wires.
6. Ambient temperature drift.
7. Proximity of wire to the wall.
8. The radial component of the mean velocity and the turbulence intensity in the radial direction.

The errors due to the deviation from cosine law and the drift in the ambient temperature are eliminated using correction factors from available hot-wire literature. The probe and sensor errors are minimized by proper selection of the probe dimensions, support needles and sensors. The effect of the wall proximity was taken care of while

calibrating the probe. As discussed by Anand [25], a linear interpolation scheme can be used to eliminate the errors due to spatial resolution of the probe.

The major sources contributing to the errors in the present investigation are the radial components of the mean velocity and the turbulence intensity. These errors could not be eliminated. An estimation of the errors in the calculation of the mean velocities and the turbulence intensities in the axial and the tangential directions is given here.

It is important to note that for the flow entering the compressor rotor, the turbulence is isotropic. Inside the rotor passage in the clearance region, mixing is very high in the tangential direction due to the leakage flow. Hence, the turbulence intensities in the tangential direction are expected to be higher than those in the axial and the tangential directions. The intensities in the axial and the radial directions are assumed to be of the same order of magnitude. Therefore, the error involved in the calculation of T_z and W_z will be larger than that in the calculation of T_θ and V_θ. Errors in the calculation of T_z and W_z are estimated and the errors in T_θ and V_θ will always be smaller than or equal to these errors.

The total velocity sensed by the wire normal to the axial direction is given by

$$W'_{wz} = [(W'_z)^2 + (W'_r)^2]^{1/2}$$

$$W'_{wz} = [(W_z + w_z)^2 + (W_r + w_r)^2]^{1/2}$$

$$W'_{wz} = (W_z + w_z)\left[1 + \left(\frac{W_r+w_r}{W_z+w_z}\right)^2\right]^{1/2}$$

Expanding the right hand side of the above equation, we get

$$W'_{wz} = (W_z + w_z)\left[1 + \frac{1}{2}\left(\frac{W_r}{W_z+w_z} + \frac{w_r}{W_z+w_z}\right)^2 - \frac{1}{8}\left(\frac{W_r+w_r}{W_z+w_z}\right)^4 + \ldots\right]$$

neglecting the 4^{th} order and other higher order terms

$$W'_{wz} \approx (W_z + w_z)\left[1 + \frac{1}{2}\left(\frac{W_r}{W_z+w_z}\right)^2 + \frac{1}{2}\left(\frac{w_r}{W_z+w_r}\right)^2 + \frac{W_r w_r}{(W_z+w_z)^2}\right] \qquad \text{(i)}$$

It is reasonable to assume that in the clearance region, the mean radial velocity is not higher than 10 percent of the total velocity in the axial direction. Hence

$$\frac{W_r}{W_z+w_z} \approx 0.1 \qquad \text{(ii)}$$

Also assuming that w_r and w_z are of the same order of magnitude,

$$w_r \approx w_z \qquad \text{(iii)}$$

Substituting (ii) and (iii) in (i), we get

$$W'_{wz} = (W_z + w_z)\left[1 + .005 + \frac{1}{2}\frac{(w_z/W_z)^2}{(1+w_z/W_z)^2} + \frac{0.1(w_z/W_z)}{(1+w_z/W_z)}\right]$$

$$= 1.055\, W_z + 1.055\, w_z$$

If the radial components of the mean velocity and the turbulence intensity are assumed to be negligible

$$W'_{wz} = W_z + w_z$$

Hence, the errors in the mean axial velocity and the axial velocity and the axial turbulence intensity are approximately 5.5 percent when the axial turbulence intensity is 30 percent.

APPENDIX B

FOTONIC SENSOR SPECIFICATIONS

The Fotonic sensor (Model KD-45A) used for the clearance measurements was manufactured by MTI Instruments Division. It is an optical device consisting of a probe, a remote cartridge, a control unit and a power supply unit. The probe and the remote cartridge contain fiber optic light guides consisting of thousands of precisely aligned glass fibers. This device can also be used for the surface reflectivity measurements of the engine components which are not easily accessible hence the probel dimensions are very small. The probe is 5 cms long and has a diameter of 2 mm.

The calibration curve for the clearance measurements is shown in Figure B1. The variation of the output voltage (percent of the maximum output voltage) versus the clearance in thousandths of an inch is plotted. The output increases from 0 to 100 percent as the clearance increases from 0 to 10 thousandth of an inch. As the clearance increases beyond 10 thousandths of an inch, the output gradually drops down. The maximum output voltage is 2 volts.

The frequency response of the probe is shown in Figure B2. As it can be observed from this figure, the frequency response is constant up to 40 kilo cycles per second.

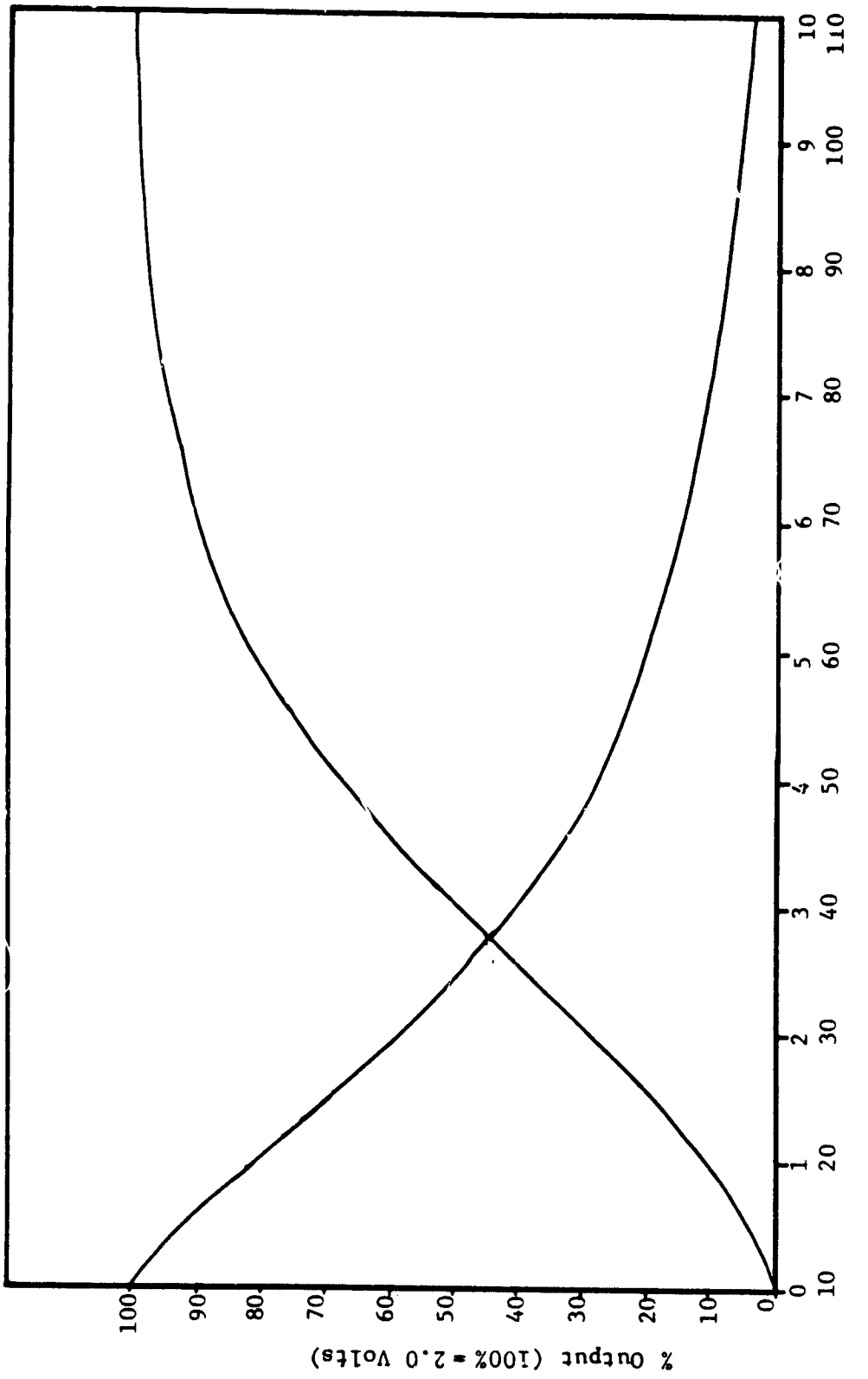

Figure B.1 Calibration Curve for the Fotonic Sensor

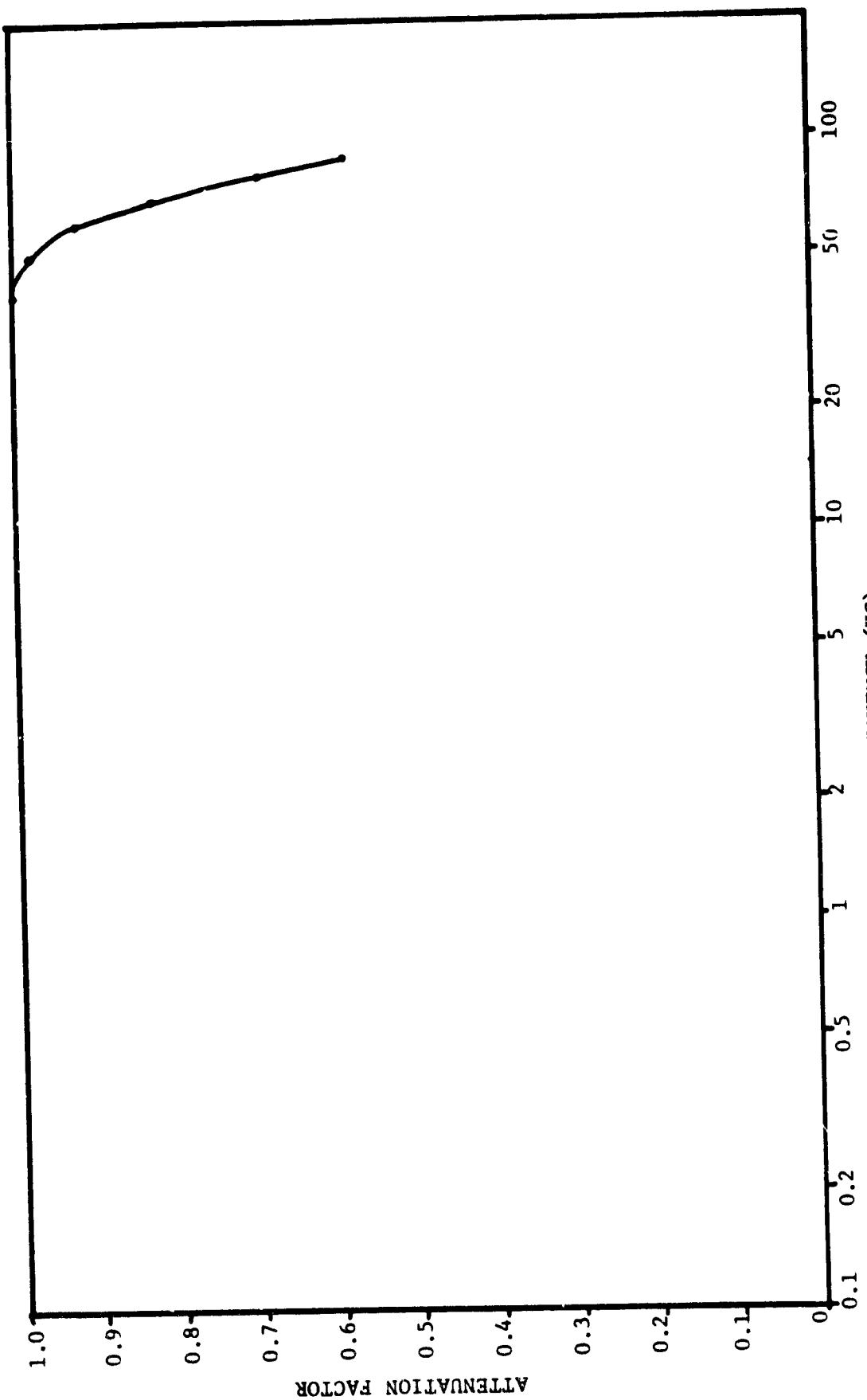

Figure B.2 Frequency Response for the Fotonic Sensor